NATURE OF THE ARGON-AMMONIA COMPLEX AND FREQUENCY DETERMINATION IN MOLECULAR DYNAMICS

45

by
Luhai Huang

A Thesis
Submitted to the Faculty of Graduate Studies
in Partial Fulfillment of the Requirements
for the Degree of
Master of Science

Department of Chemistry
University of Manitoba
Winnipeg, Manitoba

February, 1996

National Library
of Canada

Acquisitions and
Bibliographic Services Branch

395 Wellington Street
Ottawa, Ontario
K1A 0N4

Bibliothèque nationale
du Canada

Direction des acquisitions et
des services bibliographiques

395, rue Wellington
Ottawa (Ontario)
K1A 0N4

Your file *Votre référence*

Our file *Notre référence*

The author has granted an irrevocable non-exclusive licence allowing the National Library of Canada to reproduce, loan, distribute or sell copies of his/her thesis by any means and in any form or format, making this thesis available to interested persons.

L'auteur a accordé une licence irrévocable et non exclusive permettant à la Bibliothèque nationale du Canada de reproduire, prêter, distribuer ou vendre des copies de sa thèse de quelque manière et sous quelque forme que ce soit pour mettre des exemplaires de cette thèse à la disposition des personnes intéressées.

The author retains ownership of the copyright in his/her thesis. Neither the thesis nor substantial extracts from it may be printed or otherwise reproduced without his/her permission.

L'auteur conserve la propriété du droit d'auteur qui protège sa thèse. Ni la thèse ni des extraits substantiels de celle-ci ne doivent être imprimés ou autrement reproduits sans son autorisation.

ISBN 0-612-13198-X

Canada

Name _____

Dissertation Abstracts International and *Masters Abstracts International* are arranged by broad, general subject categories. Please select the one subject which most nearly describes the content of your dissertation or thesis. Enter the corresponding four-digit code in the spaces provided.

Chemistry
SUBJECT TERM

0494
SUBJECT CODE

UMI

Subject Categories

THE HUMANITIES AND SOCIAL SCIENCES

COMMUNICATIONS AND THE ARTS
Architecture 0729
Art History 0377
Cinema 0900
Dance 0378
Fine Arts 0357
Information Science 0723
Journalism 0391
Library Science 0399
Mass Communications 0708
Music 0413
Speech Communication 0459
Theater 0465

EDUCATION
General 0515
Administration 0514
Adult and Continuing 0516
Agricultural 0517
Art 0273
Bilingual and Multicultural 0282
Business 0688
Community College 0275
Curriculum and Instruction 0727
Early Childhood 0518
Elementary 0524
Finance 0277
Guidance and Counseling 0519
Health 0680
Higher 0745
History of 0520
Home Economics 0278
Industrial 0521
Language and Literature 0279
Mathematics 0280
Music 0522
Philosophy of 0998
Physical 0523
Psychology 0525
Reading 0535
Religious 0527
Sciences 0714
Secondary 0533
Social Sciences 0534
Sociology of 0340
Special 0529
Teacher Training 0530
Technology 0710
Tests and Measurements 0288
Vocational 0747

LANGUAGE, LITERATURE AND LINGUISTICS
Language
- General 0679
- Ancient 0289
- Linguistics 0290
- Modern 0291

Literature
- General 0401
- Classical 0294
- Comparative 0295
- Medieval 0297
- Modern 0298
- African 0316
- American 0591
- Asian 0305
- Canadian (English) 0352
- Canadian (French) 0355
- English 0593
- Germanic 0311
- Latin American 0312
- Middle Eastern 0315
- Romance 0313
- Slavic and East European 0314

PHILOSOPHY, RELIGION AND THEOLOGY
Philosophy 0422
Religion
- General 0318
- Biblical Studies 0321
- Clergy 0319
- History of 0320
- Philosophy of 0322

Theology 0469

SOCIAL SCIENCES
American Studies 0323
Anthropology
- Archaeology 0324
- Cultural 0326
- Physical 0327

Business Administration
- General 0310
- Accounting 0272
- Banking 0770
- Management 0454
- Marketing 0338

Canadian Studies 0385
Economics
- General 0501
- Agricultural 0503
- Commerce-Business 0505
- Finance 0508
- History 0509
- Labor 0510
- Theory 0511

Folklore 0358
Geography 0366
Gerontology 0351
History
- General 0578
- Ancient 0579
- Medieval 0581
- Modern 0582
- Black 0328
- African 0331
- Asia, Australia and Oceania 0332
- Canadian 0334
- European 0335
- Latin American 0336
- Middle Eastern 0333
- United States 0337

History of Science 0585
Law 0398
Political Science
- General 0615
- International Law and Relations 0616
- Public Administration 0617

Recreation 0814
Social Work 0452
Sociology
- General 0626
- Criminology and Penology 0627
- Demography 0938
- Ethnic and Racial Studies 0631
- Individual and Family Studies 0628
- Industrial and Labor Relations 0629
- Public and Social Welfare 0630
- Social Structure and Development 0700
- Theory and Methods 0344

Transportation 0709
Urban and Regional Planning 0999
Women's Studies 0453

THE SCIENCES AND ENGINEERING

BIOLOGICAL SCIENCES
Agriculture
- General 0473
- Agronomy 0285
- Animal Culture and Nutrition 0475
- Animal Pathology 0476
- Food Science and Technology 0359
- Forestry and Wildlife 0478
- Plant Culture 0479
- Plant Pathology 0480
- Plant Physiology 0817
- Range Management 0777
- Wood Technology 0746

Biology
- General 0306
- Anatomy 0287
- Biostatistics 0308
- Botany 0309
- Cell 0379
- Ecology 0329
- Entomology 0353
- Genetics 0369
- Limnology 0793
- Microbiology 0410
- Molecular 0307
- Neuroscience 0317
- Oceanography 0416
- Physiology 0433
- Radiation 0821
- Veterinary Science 0778
- Zoology 0472

Biophysics
- General 0786
- Medical 0760

EARTH SCIENCES
Biogeochemistry 0425
Geochemistry 0996
Geodesy 0370
Geology 0372
Geophysics 0373
Hydrology 0388
Mineralogy 0411
Paleobotany 0345
Paleoecology 0426
Paleontology 0418
Paleozoology 0985
Palynology 0427
Physical Geography 0368
Physical Oceanography 0415

HEALTH AND ENVIRONMENTAL SCIENCES
Environmental Sciences 0768
Health Sciences
- General 0566
- Audiology 0300
- Chemotherapy 0992
- Dentistry 0567
- Education 0350
- Hospital Management 0769
- Human Development 0758
- Immunology 0982
- Medicine and Surgery 0564
- Mental Health 0347
- Nursing 0569
- Nutrition 0570
- Obstetrics and Gynecology 0380
- Occupational Health and Therapy 0354
- Ophthalmology 0381
- Pathology 0571
- Pharmacology 0419
- Pharmacy 0572
- Physical Therapy 0382
- Public Health 0573
- Radiology 0574
- Recreation 0575
- Speech Pathology 0460
- Toxicology 0383

Home Economics 0386

PHYSICAL SCIENCES
Pure Sciences
Chemistry
- General 0485
- Agricultural 0749
- Analytical 0486
- Biochemistry 0487
- Inorganic 0488
- Nuclear 0738
- Organic 0490
- Pharmaceutical 0491
- Physical 0494
- Polymer 0495
- Radiation 0754

Mathematics 0405
Physics
- General 0605
- Acoustics 0986
- Astronomy and Astrophysics 0606
- Atmospheric Science 0608
- Atomic 0748
- Electronics and Electricity 0607
- Elementary Particles and High Energy 0798
- Fluid and Plasma 0759
- Molecular 0609
- Nuclear 0610
- Optics 0752
- Radiation 0756
- Solid State 0611

Statistics 0463

Applied Sciences
Applied Mechanics 0346
Computer Science 0984
Engineering
- General 0537
- Aerospace 0538
- Agricultural 0539
- Automotive 0540
- Biomedical 0541
- Chemical 0542
- Civil 0543
- Electronics and Electrical 0544
- Heat and Thermodynamics 0348
- Hydraulic 0545
- Industrial 0546
- Marine 0547
- Materials Science 0794
- Mechanical 0548
- Metallurgy 0743
- Mining 0551
- Nuclear 0552
- Packaging 0549
- Petroleum 0765
- Sanitary and Municipal 0554
- System Science 0790

Geotechnology 0428
Operations Research 0796
Plastics Technology 0795
Textile Technology 0994

PSYCHOLOGY
General 0621
Behavioral 0384
Clinical 0622
Developmental 0620
Experimental 0623
Industrial 0624
Personality 0625
Physiological 0989
Psychobiology 0349
Psychometrics 0632
Social 0451

THE UNIVERSITY OF MANITOBA

FACUTY OF GRADUATE STUDIES

COPYRIGHT PERMISSION

NATURE OF THE ARGON-AMMONIA COMPLEX AND FREQUENCY DETERMINATION IN MOLECULAR DYNAMICS

BY

LUHAI HUANG

A Thesis/Practicum submitted to the Faculty of Graduate Studies of the University of Manitoba in partial fulfillment of the requirements for the degree of

MASTER OF SCIENCE

Luhai Huang © 1996

Permission has been granted to the LIBRARY OF THE UNIVERSITY OF MANITOBA to lend or sell copies of this thesis/practicum, to the NATIONAL LIBRARY OF CANADA to microfilm this thesis/practicum and to lend or sell copies of the film, and to UNIVERSITY MICROFILMS INC. to publish an abstract of this thesis/practicum..

This reproduction or copy of this thesis has been made available by authority of the copyright owner solely for the purpose of private study and research, and may only be reproduced and copied as permitted by copyright laws or with express written authorization from the copyright owner.

Acknowledgment

I am indebted to my supervisor, Dr. Robert Wallace for his encouragement and assistance in preparing this thesis.

To my parents

TABLE OF CONTENTS

Part Two

FREQUENCY DETERMINATION IN MOLECULAR DYNAMICS

Part One

INTERPRETATION OF THE MICROWAVE SPECTRA AND POTENTIAL ENERGY SURFACES OF Ar-AMMONIA COMPLEX

Abstract

The ground state potential energy surfaces of the van der Waals complex, argon-ammonia, are computed for intracomplex rotation and inversion of the ammonia molecule. Every surface is given analytically in the form of a spherical harmonic expansion through $l = 7$, where the expansion coefficients are expressed in terms of the Eulerian angles of ammonia which describe the orientation of the molecule relative to the atom Ar. The barrier to threefold internal rotation of ammonia is about 26.63 cm^{-1}. The potential is applied to the calculation of intracomplex rotation spectra.

List of Figures

List of Tables

1. INTRODUCTION

The complex $Ar-NH_3$ is an interesting complex and a good model system for experimental and theoretical investigation. It is not only a prototype of weak bonding of ammonia, but it is also true that the ammonia nearly undergoes free rotation and inversion. Therefore it is an ideal model for developing theoretical methods for treating several large amplitude motions.

To investigate and understand thermodynamic and kinetic properties of the complex $Ar-NH_3$, for example, the interpretation of the rovibrational spectra, transport properties, etc., the first and most important task is to get the detailed potential energy surfaces of the complex. The potential interaction energy should be expressed as a function of coordinates that describe every possible configuration of the complex. Some potential surfaces are obtained by ab initio calculation and from spectroscopic data.[1,2] However, all of these potentials are not suitable for describing large amplitude motion of the complex. In this thesis a potential form is proposed to investigate the large amplitude motions: intracomplex rotation and intracomplex inversion; strictly speaking, the motions are the large amplitude vibrations. The potential surface is given analytically in the form of a spherical harmonic expansion through $l = 7$, where the expansion coefficients are expressed in terms of the Eulerian angles of ammonia which describe the orientation of the molecule relative to the atom Ar. The $N-H$ bond distance for the potential surface is kept constant since the frequency of the $N-H$ bond vibration is much higher than rotational and version frequency of ammonia. From the potential, the barrier to internal rotation of ammonia is about 26.63 cm^{-1} by calculation; the calculated barrier is consistent with the barrier obtained by experiments.

The potential is used to investigate the large amplitude motions of the complex: the intracomplex rotation and intracomplex inversion. It is shown by the potential that

the interaction between ammonia and argon is very weak, the ammonia undergoes almost free rotation and inversion. Hence the motions of the intracomplex rotation and intracomplex inversion are treated as if the molecule ammonia undergoes rotation and inversion in the potential field imposed by argon atom. For the intracomplex rotational spectra of the complex, they are obtained by three steps: first step, the free ammonia molecular rotational spectra are obtained by the traditional method[3] ; second step, the influence of the ammonia inversion to the free ammonia molecular rotational spectra is calculated by the method suggested by Dr. R. Wallace[4] , every single free ammonia rotational spectroscopic line is split into a pair; third step, the influence of the interaction between ammonia and argon is calculated by perturbation theory, the complicated intracomplex rotation spectra are obtained.

2. HAMILTONIAN $\hat{H}(\mu,\theta,\chi)$ OF AMMONIA IN The COMPLEX

For any system if we know its rotational Hamiltonian, then we can calculate the rotation energy levels and understand the rotation spectra.[3] However, the complex is not a rigid rotation system since there exists large amplitude intracomplex rotation and inversion; in order to deal with this system, we use a model Hamiltonian derived by Wallace[4] which provides a good description of inversion-rotational motion in NH_3 in terms of a single internal variable which is the polar angle of three equivalent symmetric Jacobi vectors which are themselves derived from three bond vectors.

In order to form the quantum-mechanical Hamiltonian operator, we establish the two coordinate systems shown in Fig.2.1. One is the complex-fixed axes X, Y, and Z; the other is the ammonia molecule-fixed axes a, b, c; and their origins O are all at the mass center of molecule. OZ axis is along the vector R from the N atom to the Ar

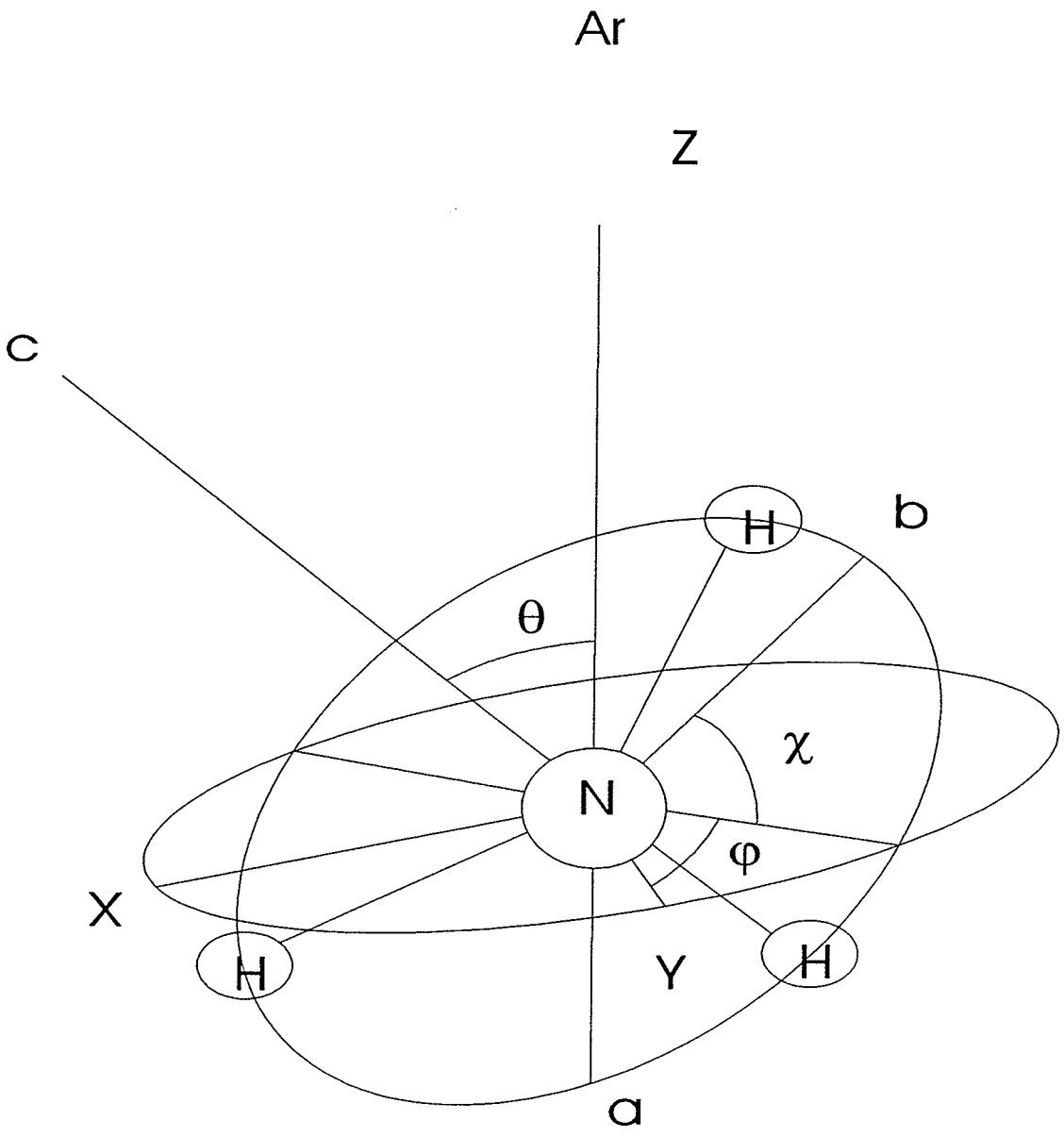

Figure 2.1 The Eulerian angles. X, Y, and Z is the complex-fixed axes; a, b, c is the ammonia molecule-fixed axes; and their origins O(which is overlapped by N) are all at the mass center of molecule. OZ axis is along the vector R from the N atom to the Ar atom; Oc is along the 3-fold rotation axis of the ammonia molecule; the θ refers to the angle between OZ and Oc, and is the angle of rotation about ON(which is the line of intersection of between the planes XY and ab); the φ angle of rotation about OZ; the χ is the angle of rotation about Oc axis.

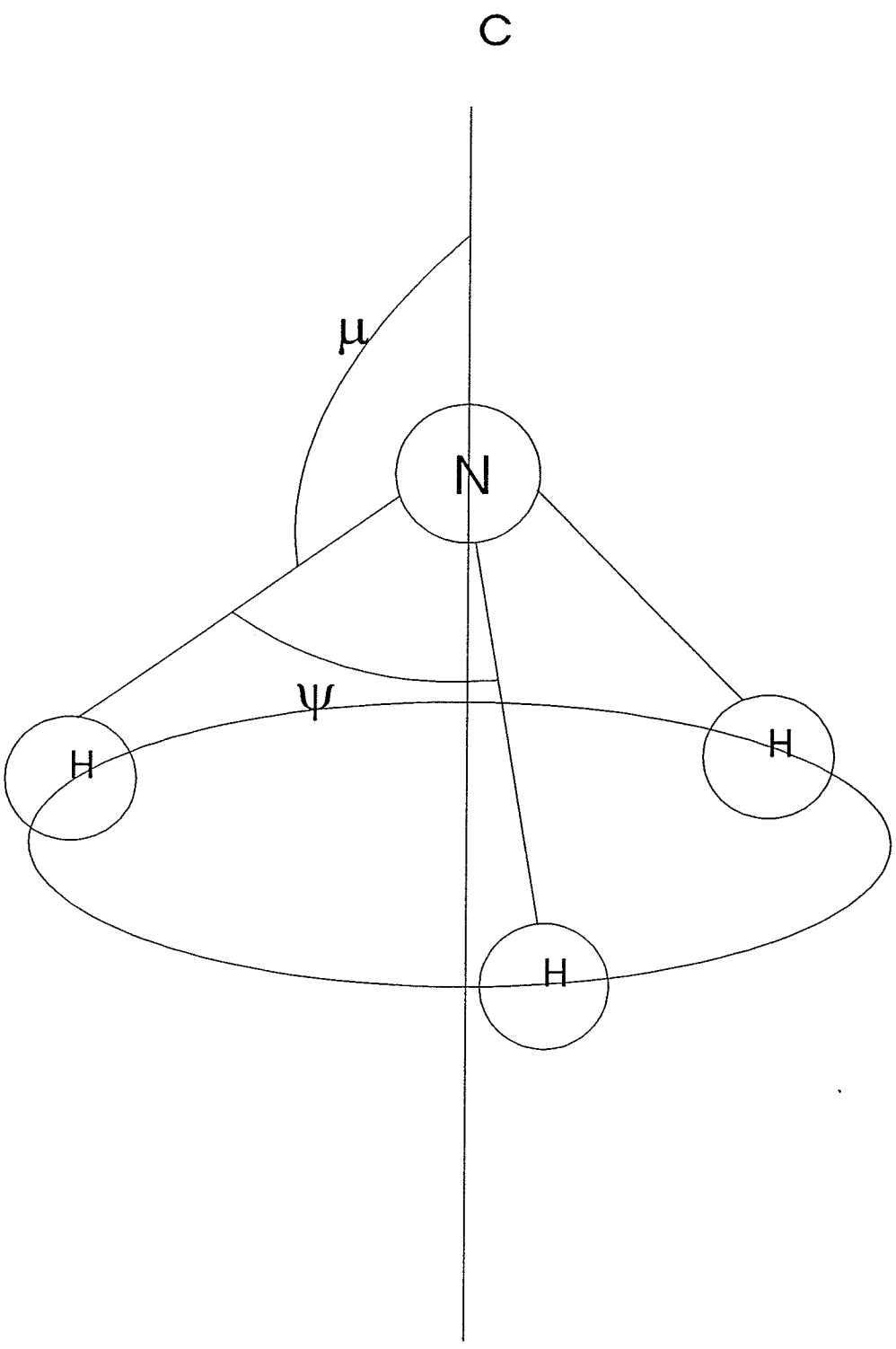

Figure 2.2 The relationship between alternative descriptions of inversion ψ and μ on ammonia molecule.

atom; Oc is along the 3-fold rotation axis of the ammonia molecule; the θ refers to the angle between OZ and Oc, and is the angle of rotation about ON(which is the line of intersection of between the planes XY and ab); φ is the angle of rotation about OZ; χ is the angle of rotation about Oc axis.

It is assuming that the Hamiltonian of the complex system depends on the conformation of the molecule ammonia described by the angle ψ as shown in Fig.2.2. For convenience, choose the variable μ instead of ψ to specify the conformation of the molecule ammonia. The relationship between μ and of ψ is shown in Fig.2.2. Hence the Hamiltonian the complex system is written as

$$\hat{H}_N = \hat{T}_{trans} + \hat{T}_{rot} + \hat{T}_{vib} + \hat{T}_{vib-rot} + V(R,\mu,\theta,\chi) \qquad (2.1)$$

$\hat{T}_{vib}$ is only umbrella motion because the $N-H$ bond distance is assumed constant.

Group it as

$$\hat{H}_N = \hat{H}_1 + \hat{H}_2 \qquad (2.2)$$

in which $\hat{H}_1 = \hat{T}_{vib} + V(R,\mu,\theta,\chi)$, $\hat{H}_2 = \hat{T}_{trans} + \hat{T}_{rot} + \hat{T}_{vib-rot}$

Van der Waals interaction is a long range interaction and calculations shown in Fig.2.3 under different distances between Ar and atom N from 1.0 to 30.0 atomic units

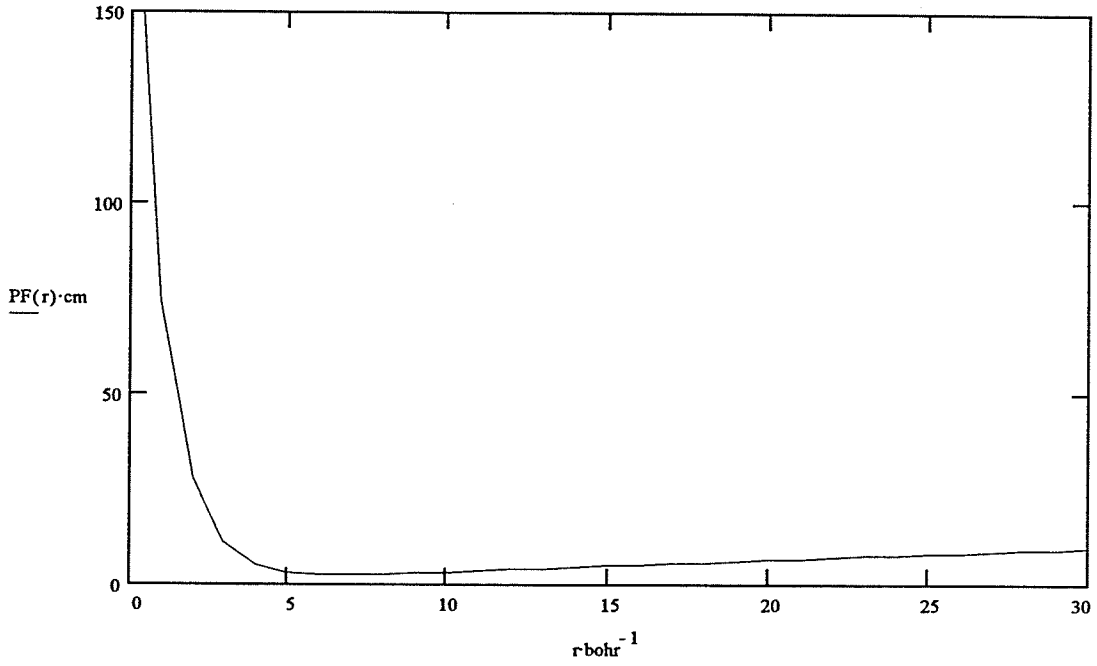

Figure 2.3 The *ammonia – Ar* potential change with respect to the distance between ammonia and *Ar* .

show that the interaction energy is so small from Bulski et al.[16] ab initio calculations of *Ar* -ammonia potential surfaces that we need only consider ammonia rotation being perturbed. Hence it is reasonable to only consider intracomplex rotation of ammonia under the interaction imposed by *Ar* and neglect the overall rotation of the complex. For example, the symmetric top of ammonia is rotating and inverting in the potential field imposed by *Ar* and its complex Hamiltonian $\hat{H}_1$ is expressed as

$$\hat{H}_1 = \hat{T}(R) + \hat{T}(\mu,\theta,\chi) + V(R,\mu,\theta,\chi) = \hat{H}_R + \hat{H}(\mu,\theta,\chi) \qquad (2.3)$$

$$V(R,\mu,\theta,\chi) = V(R) + V_{inter}(\mu,\theta,\chi) \qquad (2.4)$$

$$\hat{H}(\mu,\theta,\chi) = \hat{T}(\mu,\theta,\chi) + V_{inter}(\mu,\theta,\chi) \qquad (2.5)$$

in which $\hat{T}(\mu,\theta,\chi)$ is free ammonia rotation energy operator, $V_{inter}(\mu,\theta,\chi)$ is the internal potential of ammonia itself plus the potential imposed on ammonia by *Ar* . $\hat{H}(\mu,\theta,\chi)$ is Hamiltonian of ammonia in the complex. What we do now is to find the kinetic energy operator and analytical potential form.

3. KINETIC ENERGY OPERATOR $\hat{T}(\mu,\theta,\chi)$

Since the ammonia is not a rigid rotor, it is difficult to establish a kinetic energy operator. We use the model Hamiltonian established by Wallace[4] for the free ammonia system.

The basis for this model Hamiltonian arises from consideration of the metric properties of the configuration space. By taking account of coordinate scaling, in general[5]

$$\hat{T} = -\frac{\hbar^2}{2}\Delta \qquad (3.1)$$

The kinetic energy operator $\hat{T}$ for free ammonia expressed by Wallace[4] in terms of the polar angle μ as shown in Fig.2.2 becomes

$$\hat{T} = -\frac{\hbar^2}{2}\left[\frac{1}{3}\frac{\partial^2}{\partial Q^2}+\frac{2}{Q^2}\frac{\partial}{\partial Q}\right]-\frac{\hbar^2}{2}\left\{\frac{1}{Q^2}\frac{\partial^2}{\partial \mu^2}+\frac{1}{Q^2}\left[\cot\mu-\sin 2\mu\left(\frac{1}{1+\cos^2\mu}+\frac{1}{1+3\cos^2\mu}\right)\right]\frac{\partial}{\partial \mu}\right\}$$
$$+\frac{1}{2}\left(\frac{2}{3Q^2}\frac{1}{1+\cos^2\mu}\left[\hat{P}^2-\hat{P}_z^2\right]+\frac{1}{3Q^2\sin^2\mu}\hat{P}_z^2\right)$$
$$-\frac{\hbar^2}{2}\left[\left(\frac{\partial}{\partial s^1}\right)^2+\left(\frac{\partial}{\partial s^2}\right)^2\right]-\frac{\hbar^2}{2Q^2}\frac{3-\frac{3}{2}\sin^2\mu}{2-\frac{3}{2}\sin^2\mu}\left[\left(\frac{\partial}{\partial s^3}\right)^2+\left(\frac{\partial}{\partial s^4}\right)^2\right]$$

(3.2a)

$$Q = 3^{-\frac{1}{2}}\left(Q^1+Q^2+Q^3\right) \qquad (3.2b)$$

As for the intracomplex rotation, the inversion of ammonia has much stronger effect on intrarotation than other movements like ammonia stretching. Therefore what is useful to us is the part of the Hamiltonian which is the rotation-inversion energy operator separated from that of Q-stretching,

$$H(\mu,\theta,\chi)=\frac{\hbar^2}{2Q}\left[-\left(\frac{\partial}{\partial\mu}\right)^2-F(\mu)\frac{\partial}{\partial\mu}+\hat{T}_R+V(\mu,\theta,\chi)\right] \qquad (3.3)$$

in which

$$F(\mu)=\cot\mu-\sin 2u\left(\frac{1}{1+\cos^2\mu}+\frac{1}{1+3\cos^2\mu}\right) \qquad (3.4)$$

$$\hat{T}_R=\frac{1}{2Q^2}\left(\frac{2}{3}\frac{1}{1+\cos^2\mu}\left[\hat{P}^2-\hat{P}_Z^2\right]+\frac{1}{3\sin^2\mu}\hat{P}_Z^2\right) \qquad (3.5)$$

4. POTENTIAL $V(\mu,\theta,\chi)$

We have separated the inversion-rotation movements from other movements; hence what we are looking for is the potential $V(\mu,\theta,\chi)$ which is only a function of inversion and rotation. Since the interaction between Ar and ammonia is much weaker than other interactions, we divide $V(\mu,\theta,\chi)$ into two parts.

$$V(\mu,\theta,\chi)=V_{inversion}(\mu)+V_{complex}(\mu,\theta,\chi) \qquad (4.1)$$

The first part of the potential is the pure molecular inversion potential which only depends on the variable μ [4]

$$V_{inversion}(\mu)=c_0+c_1\cos 2\mu+c_2\cos 4\mu+c_3\cos 6\mu+c_4\cos 8\mu \qquad (4.2)$$

in which $c_0=3950,\ c_1=5054,\ c_2=3549,\ c_3=558.6,\ c_4=89.46$

The intermolecular potential between Ar and ammonia $V_{inter}(m,q,c)$ is not only crucial to us but also the key to the interpretation of the phenomena related to the complex, such as microwave spectra, etc.. Some analytical forms of potential energy

surfaces have been obtained by ab initio calculation or fit of spectral data. One of them is derived from examining the lowest few rotation-inversion states of free NH_3 and fitting the spectroscopic data.[1,2] Another potential energy form is worked out with the aid of *ab initio* calculations by Bulski.[6] However none of these potentials fit our problem because they present their calculation results within a limited range of the inversion. We have to look for an appropriate interaction potential for large amplitude motion.

Clearly the interaction energy of the Ar atom and ammonia molecule depends on the angles θ, χ, and a vector R pointing from the N atom to the Ar atom as well as the inversion angle μ. In a range of R around the potential minimum of the $Ar - NH_3$ complex, the potential is only weakly dependent upon R. Therefore it is reasonable that the potential is expressed as

$$V_{\mathbf{complex}}(\mu,\theta,\chi) = \sum_{l} \sum_{m=-l}^{l} \upsilon_{lm}(\mu) Y_l^m(\theta,\chi) \qquad (4.3)$$

Due to the reflection symmetry in the $x-z$ plane, no sine type harmonic functions appear in this expansion. In addition, only the terms with $\cos m\chi$, $m = 0(\mathrm{mod}\,3)$, contribute to the interaction energy because of the three fold symmetry of ammonia. We take the form of potential as[6]

$$V_{complex}(\mu,\theta,\chi) = \sum_{l} \sum_{m=-l}^{l} \upsilon_{lm}(\mu) P_l^m(\theta) \cos(m\chi) \qquad (4.4)$$

$$V_{complex}(\mu,\theta,\chi)$$
$$= \sum_{l=0}^{7} \sum_{3m=0}^{l} \left(D_{0,lm} + D_{1,lm}\cos(\mu) + D_{2,lm}\cos(2\mu) + D_{3,lm}\cos(3\mu) + D_{4,lm}\cos(4\mu)\right) P_l^m(\theta)\cos(m\chi) \qquad (4.5)$$

The coefficients of $D_{n,lm}$ are obtained by computations using Guassian program and shown in table 4.1.

Table 4.1 The Coefficients of $D_{n,lm}$

l	$m(\mathbf{mod}\,3)$	$D^0_{lm}(cm^{-1})$	$D^1_{lm}(cm^{-1})$	$D^2_{lm}(cm^{-1})$	$D^3_{lm}(cm^{-1})$	$D^4_{lm}(cm^{-1})$
0	0	-14.5348	0.01800	-2.1320	0.00210	0.4564
1	0	0.9634	31.8410	-0.2627	-1.4198	0.3100
2	0	-9.9776	0.0342	-4.0808	0.0041	0.8848
3	0	1.0684	25.0417	-0.4825	-3.3092	0.4722
	3	1.5200	0.0441	-5.2485	0.0053	1.1301
4	0	-13.9827	0.0340	-4.0387	0.0041	0.8663
	3	0.6687	16.2991	-0.2894	-1.9440	0.2873
5	0	0.1564	2.7838	-0.0869	-0.6304	0.0801
	3	-10.836	0.0267	-3.1927	0.0032	0.6975
6	0	-3.2006	0.0071	-0.8493	0.0008	0.1904
	3	-0.1010	-2.3728	0.0453	0.3081	-0.0445
	6	-1.1871	0.0058	-0.6868	0.0007	0.1483
7	0	0.0590	2.9405	0.0039	0.1182	0.0058
	3	-1.7188	0.0038	-0.4528	0.0004	0.1026
	6	0.0482	1.2061	-0.0205	-0.1393	0.0204

The potential $V_{complex}(\mu,\theta,0) = V1$ is shown in Fig.4.1

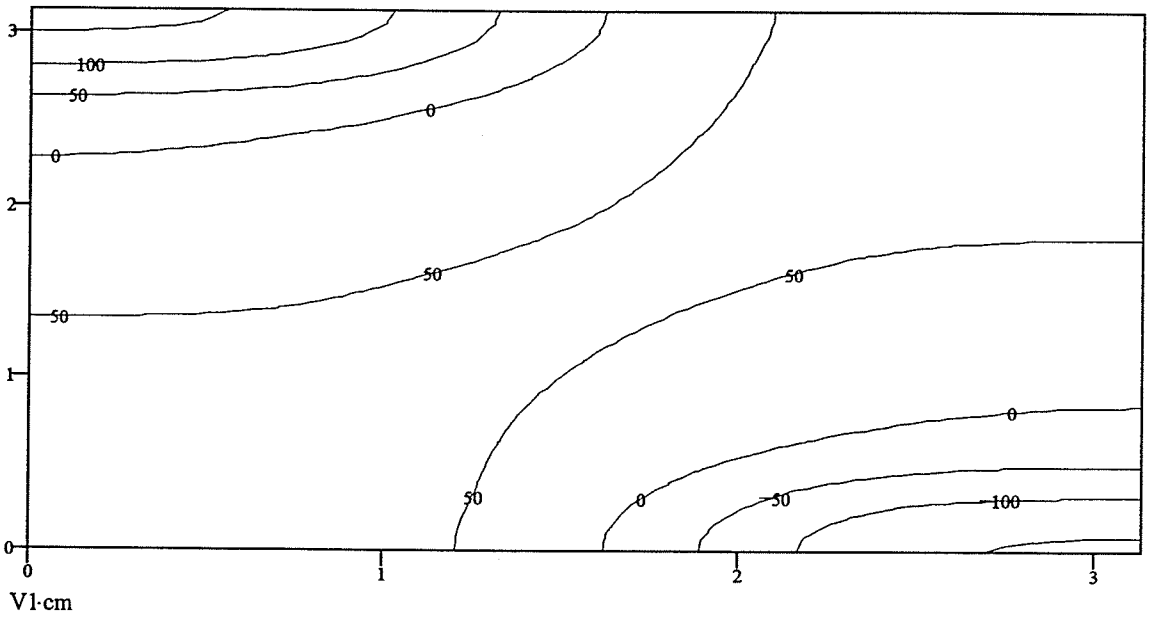

Figure 4.1 The contour plot of the potential $V_{complex}(\mu,\theta,0) = V1$

in which the x axis is μ and the y axis is θ.

Fig. 4.1 shows that the potential surface under the conformations both $(\mu = 0, \theta = 0, \chi = 0)$ and $(\mu = \pi, \theta = \pi, \chi = 0)$, the potentials are at a maximum since the three hydrogen atoms are closest to Ar; under the conformations $(\mu = \pi, \theta = 0, \chi = 0)$ and $(\mu = 0, \theta = \pi, \chi = 0)$, the potentials are at a minimum since the three hydrogen atoms are farthest away from the Ar atom.

The potential $V_{complex}\left(\mu,\theta,\frac{\pi}{2}\right)=V2$ is shown in Fig.4.2

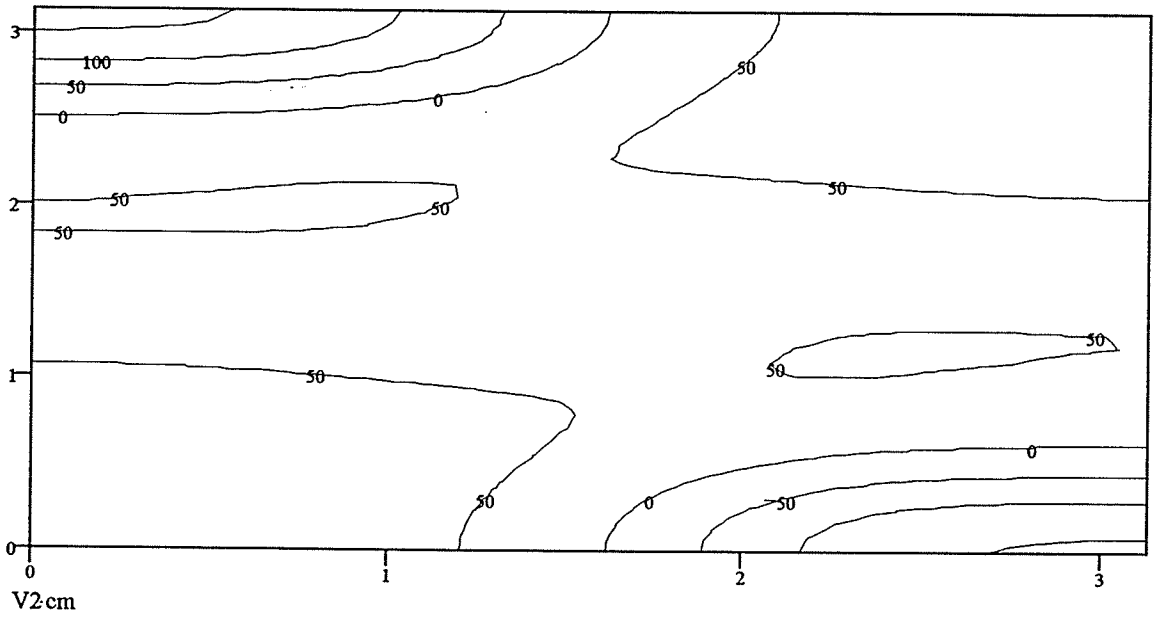

Figure 4.2 The contour plot of the potential $V_{complex}\left(\mu,\theta,\frac{\pi}{2}\right)=V2$

in which the x axis is μ and the y axis is θ.

When the variable χ changes from 0 to $\frac{\pi}{2}$, the shape of the potential surface is changed. However, the conformations of maximum and minimum potential surfaces do not change: the conformations of maximum potential surfaces are both $(\mu=0,\theta=0,\chi=0)$ and $(\mu=\pi,\theta=\pi,\chi=0)$,and the conformations of minimum potentials are both $(\mu=\pi\ ,\theta=0,\chi=0)$ and $(\mu=0,\theta=\pi,\chi=0)$.

The potential $V_{complex}(\mu,0,\chi) = V5$ is shown in Fig.4.3.

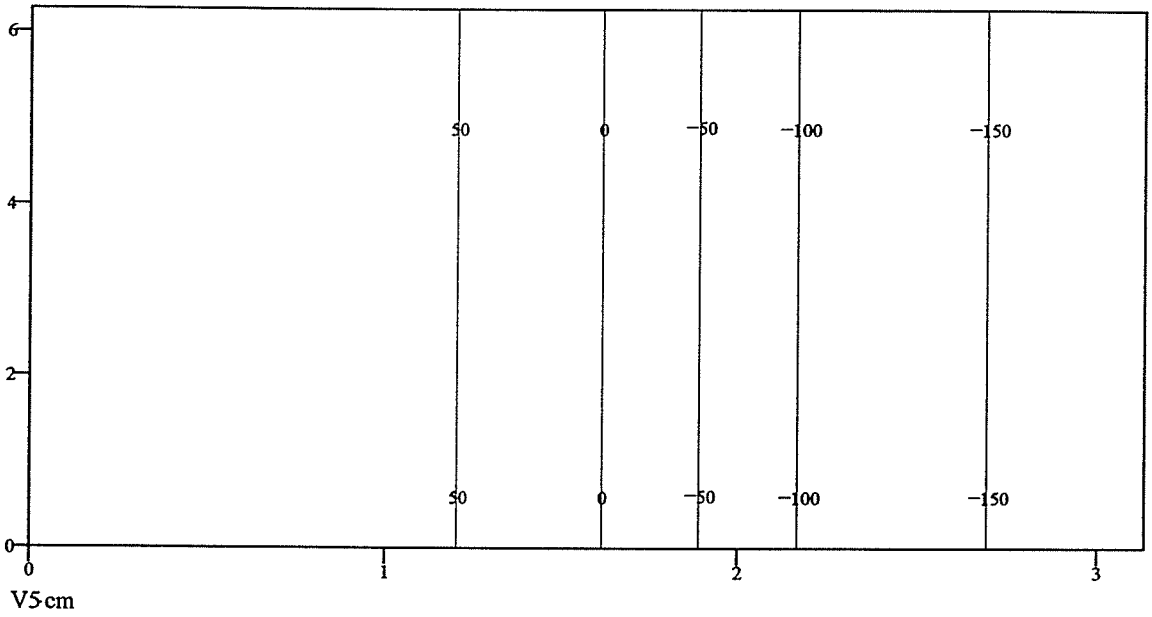

Figure 4.3 The contour plot of the potential $V_{complex}(\mu,0,\chi) = V5$

in which the x axis is μ and the y axis is χ.

Fig. 4.3 shows that the potential $V_{complex}(\mu,0,\chi)$ is independent of the variable χ. The conformations of the maximum and minimum potential surfaces are $(\mu = 0\ ,\theta = 0,\chi)$ and $(\mu = \pi,\theta = 0,\chi)$, respectively, because under the conformation $(\mu = 0\ ,\theta = 0,\chi)$, the three hydrogen atoms are closest to Ar; under the conformation $(\mu = \pi,\theta = 0,\chi)$, the three hydrogen atoms are farthest away from the Ar atom.

The potential $V_{complex}\left(\mu,\frac{\pi}{2},\chi\right)=V6$ is shown in Fig.4.4.

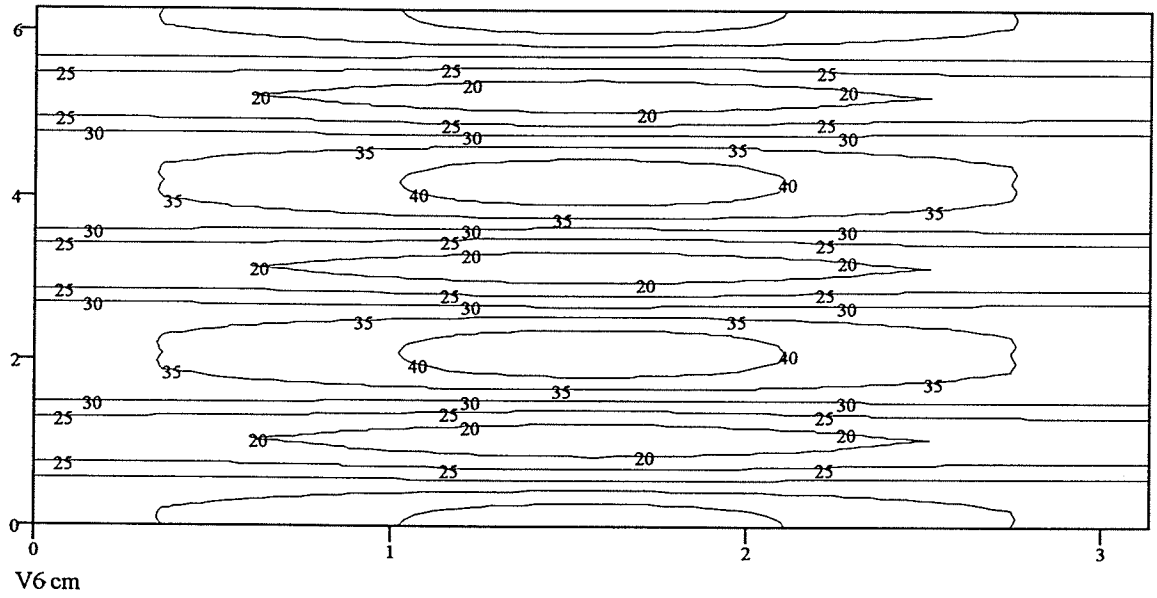

Figure 4.4 The contour plot of the potential $V_{complex}\left(\mu,\frac{\pi}{2},\chi\right)=V6$

in which the x axis is μ and the y axis is χ.

Fig.4.4 shows that when $\theta=\frac{\pi}{2}$,the potential surface has three maximum and minimum points. The conformations of the three maximum potential points are $\left(\mu=\frac{\pi}{2},\theta=\frac{\pi}{2},0\right)$, $\left(\mu=\frac{\pi}{2},\theta=\frac{\pi}{2},\frac{2\pi}{3}\right)$ and $\left(\mu=\frac{\pi}{2},\theta=\frac{\pi}{2},\frac{4\pi}{3}\right)$ since under these conformations one of the three hydrogen atoms is closest to Ar. The conformations of the three minimum potential points are $\left(\mu=\frac{\pi}{2},\theta=\frac{\pi}{2},\frac{\pi}{3}\right)$, $\left(\mu=\frac{\pi}{2},\theta=\frac{\pi}{2},\frac{4\pi}{3}\right)$ and $\left(\mu=\frac{\pi}{2},\theta=\frac{\pi}{2},\frac{5\pi}{3}\right)$ since under these conformations one of the three hydrogen atoms is farthest away from the Ar atom.

The potential $V_{complex}(\mu, \pi, \chi) = V7$ is shown in Fig.4.5

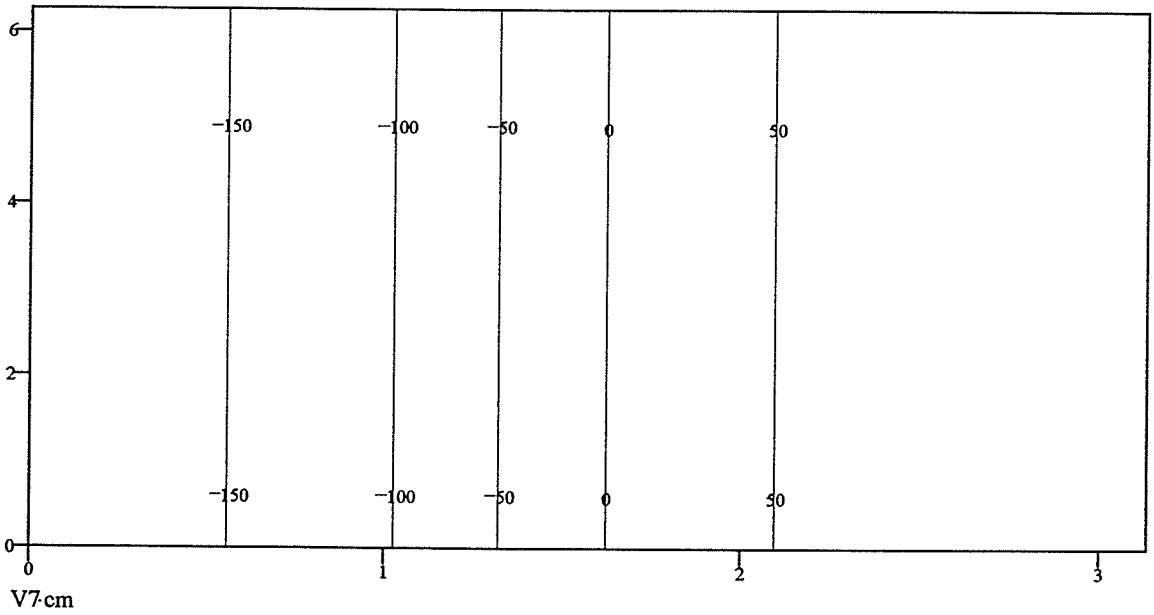

Figure 4.5 The contour plot of the potential $V_{complex}(\mu, \pi, \chi) = V7$

in which the x axis is μ and the y axis is χ.

Fig. 4.5 shows that the potential $V_{complex}(\mu, \pi, \chi)$ is independent of the variable χ. The conformation of the maximum is $(\mu = \pi\ , \theta = \pi, \chi)$ since under the conformation $(\mu = \pi\ , \theta = \pi, \chi)$ the three hydrogen atoms are closest to Ar; and that of the minimum potential surface is $(\mu = 0\ , \theta = \pi, \chi)$ since under the conformation $(\mu = 0\ , \theta = \pi, \chi)$ the three hydrogen atoms are farthest away from the Ar atom.

The potential $V_{complex}(0.2,\theta,\chi) = V8$, the X axis is θ and the Y axis is χ, is shown in Fig.4.6

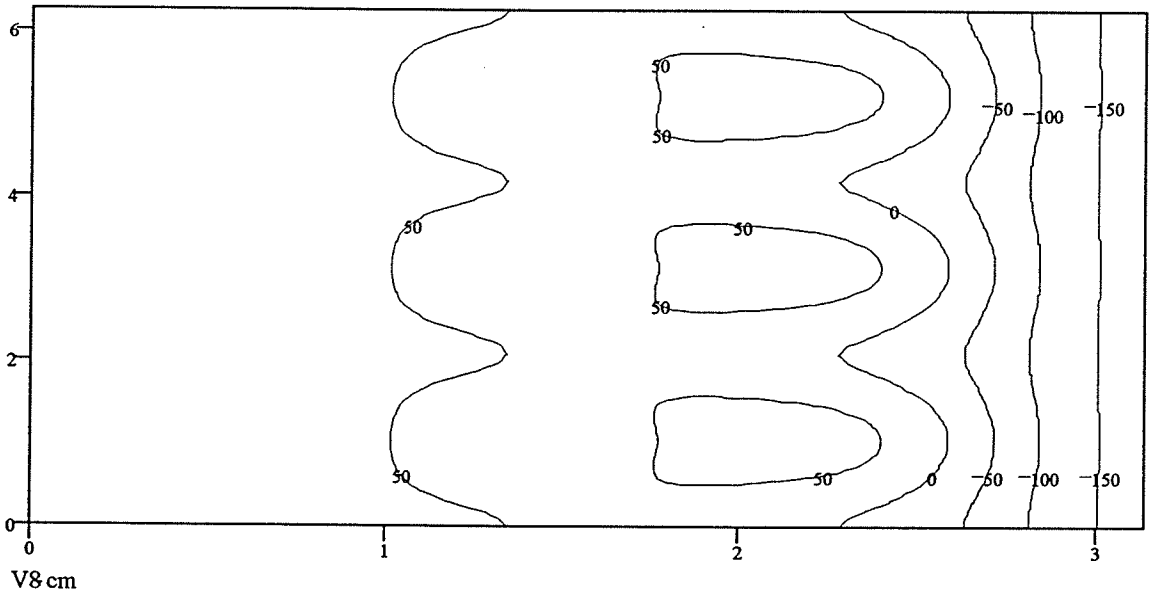

Figure 4.6 The contour plot of the potential $V_{complex}(0,\theta,\chi) = V8$

in which the x axis is θ and the y axis is χ.

Fig. 4.6 shows that the potential $V_{complex}(0.2,\theta,\chi)$ is slightly dependent on the variable χ and the $V_{complex}\left(0.2,\theta,\frac{\pi}{2}\right)$ is shown in Fig.4.7. The conformation of the maximum is $(\mu = 0.2\ ,\theta = 0,\chi)$ since under the conformation $(\mu = 0.2\ ,\theta = 0,\chi)$ the three hydrogen atoms are closest to Ar; and that of the minimum potential surface is $(\mu = 0.2\ ,\theta = \pi,\chi)$ since under the conformation $(\mu = 0.2\ ,\theta = \pi,\chi)$ the three hydrogen atoms are farthest away from the Ar.

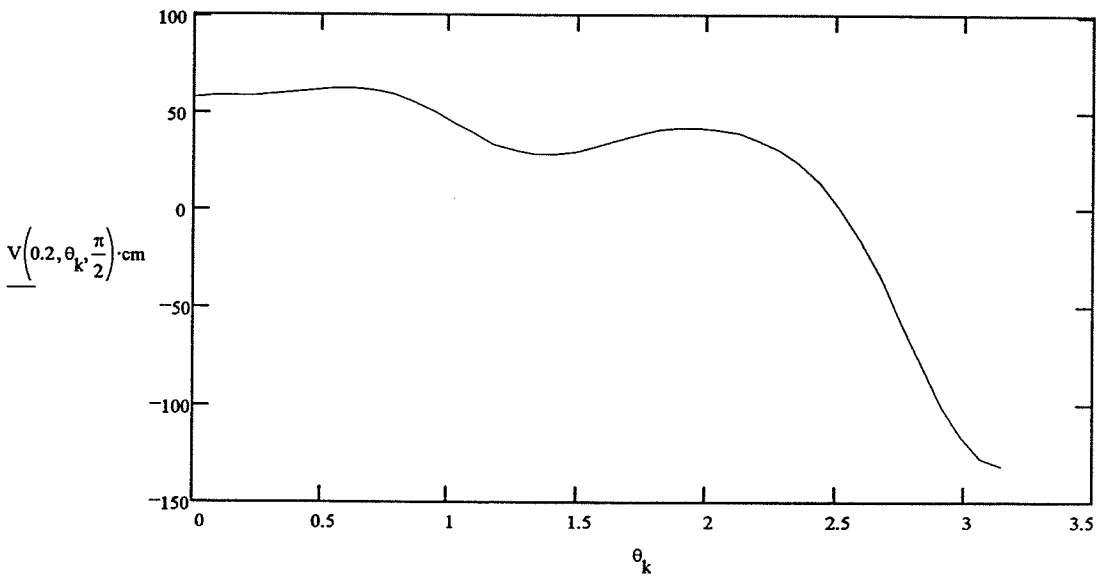

Figure 4.7 The potential change with respect to the angle θ

when the conformation is $\left(\mu = 0.2 \quad , \theta, \chi = \frac{\pi}{2}\right)$

The potential $V_{complex}\left(\frac{\pi}{2}, \theta, \chi\right) = V9$ is shown in Fig.4.8

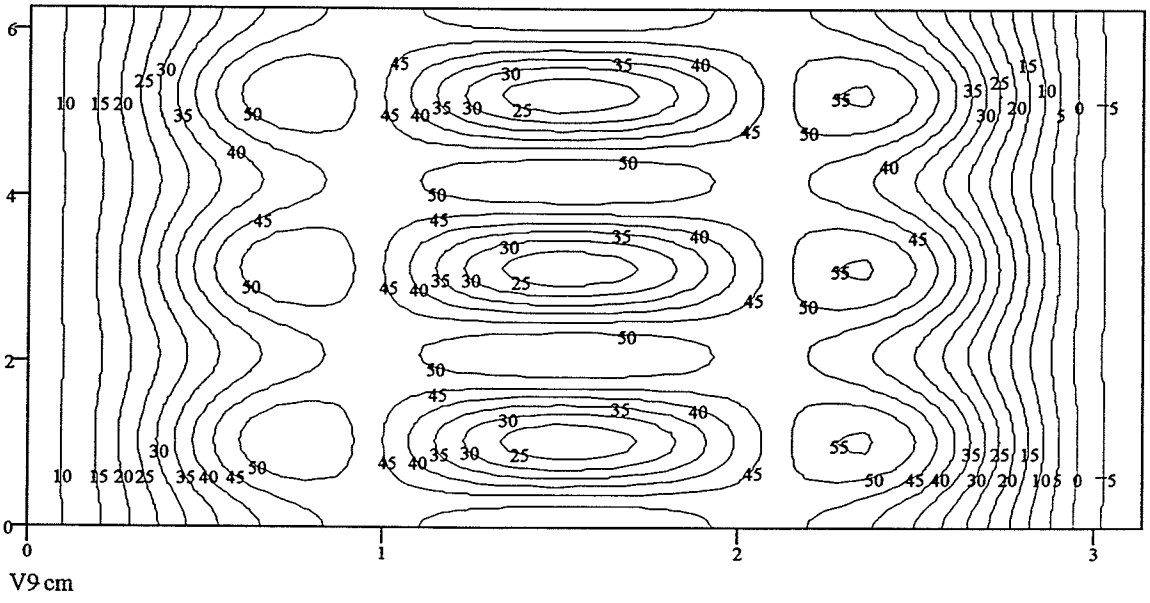

Figure 4.8 The contour plot of the potential $V_{complex}\left(\frac{\pi}{2}, \theta, \chi\right) = V9$

in which the x axis is θ and the y axis is χ.

Fig.4.8 shows that the potential surface of $V_{complex}\left(\frac{\pi}{2},\theta,\chi\right)$ has three maximum and minimum points. The conformations of the three maximum potential points are $\left(\mu=\frac{\pi}{2},\theta=\frac{\pi}{2},0\right)$, $\left(\mu=\frac{\pi}{2},\theta=\frac{\pi}{2},\frac{2\pi}{3}\right)$ and $\left(\mu=\frac{\pi}{2},\theta=\frac{\pi}{2},\frac{4\pi}{3}\right)$ since under these conformations one of the three hydrogen atoms is closest to Ar. The conformations of the three minimum potential points are $\left(\mu=\frac{\pi}{2},\theta=\frac{\pi}{2},\frac{\pi}{3}\right)$, $\left(\mu=\frac{\pi}{2},\theta=\frac{\pi}{2},\frac{4\pi}{3}\right)$ and $\left(\mu=\frac{\pi}{2},\theta=\frac{\pi}{2},\frac{5\pi}{3}\right)$ since under these conformations one of the three hydrogen atoms is farthest away from the Ar atom.

The potential $V_{complex}(\pi,\theta,\chi)=V10$ is shown in Fig.4.9

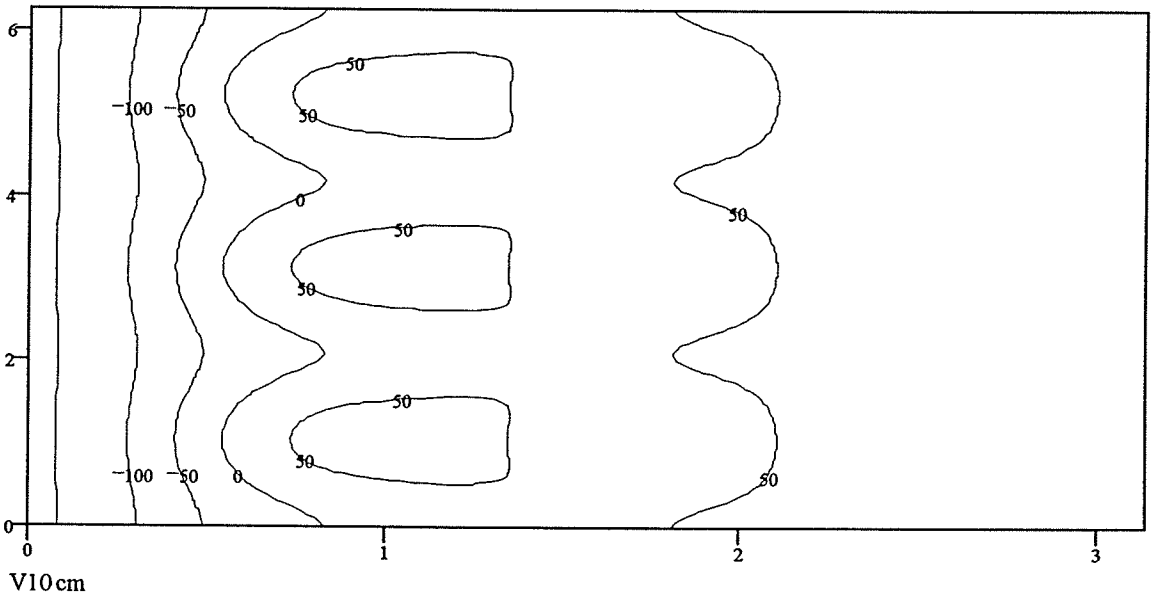

Figure 4.9 The contour plot of the potential $V_{complex}(\pi,\theta,\chi)=V10$

in which the x axis is θ and the y axis is χ.

Fig. 4.9 shows that the potential $V_{complex}(\pi,\theta,\chi)$ is slightly dependent on the variable χ. The conformation of the maximum is $(\mu=0\ ,\theta=\pi,\chi)$ since under the conformation $(\mu=0\ ,\theta=\pi,\chi)$ the three hydrogen atoms are closest to Ar; and that of the minimum potential surface is $(\mu=0\ ,\theta=0,\chi)$ since under the conformation $(\mu=0\ ,\theta=0,\chi)$ the three hydrogen atoms are farthest away from the Ar.

5. INVERSION ENERGY LEVELS

From the previous discussion, the Hamiltonian of internal complex motion is written as

$$H_v(\mu, J, K) = H_v^0(\mu, J, K) + V_{complex} \qquad (5.1)$$

$$H_v^0(m, J, K) = \frac{\hbar^2}{2Q^2}\left[-\frac{\partial^2}{\partial m^2} - F(m)\frac{\partial}{\partial m} + \frac{2}{3}\frac{1}{1+\cos^2(m)}\left[J(J+1) - K^2\right] + \frac{1}{3\sin^2(m)}K^2\right] + V_{inversion}(m) \qquad (5.2)$$

in which $|\mathbf{V}_{inversion}| >> |\mathbf{V}_{complex}|$. Under the influence of inversion potential $V_{inversion}$, the vibrational levels are drawn together in pairs. At the same time the vibrational energy levels are also dependent on rotational quantum numbers J and K.[4] From the Hamiltonian we see that the interaction energy potential $V_{complex}$ also has influence on the vibrational energy levels; however, since $|\mathbf{V}_{inversion}| >> |\mathbf{V}_{complex}|$, its influence can be neglected when calculating inversion eigenvalues and eigenfunctions. $V_{complex}$ is considered as a perturbation to inversion.

6. INTRACOMPLEX ROTATION ENERGY LEVELS

6.1 Free Rotation Energy Levels of Ammonia

If we neglect the interaction potential imposed by Ar, the rotation of the ammonia in the complex is a free rotor.

$$\hat{H}_R^0 = \frac{\hat{P}^2 - \hat{P}_Z^2}{2I_a} + \frac{\hat{P}_Z^2}{2I_c} = \frac{1}{2Q^2}\left(\frac{2}{3}\frac{\hat{P}^2 - \hat{P}_Z^2}{1+\cos^2\mu} + \frac{\hat{P}_Z^2}{3\sin^2\mu}\right) \qquad (6.1)$$

If I_a and I_c are constants, then

$$\hat{H}_R^0|JKM\rangle = E_R^0|JKM\rangle = \left[\frac{J(J+1) - K^2}{2I_a} + \frac{K^2}{2I_c}\right]|JKM\rangle \qquad (6.2)$$

in which $J = 0,\ldots\ldots,\ K = -J,-J+1,\ldots\ldots,J-1,J;\ M = -J,-J+1,\ldots\ldots,J-1,J.$ It is clear that the rotational energy depends only on J and $|K|$; hence the degeneracy of their energy levels is $2J+1$-fold.

Since eigenfunctions of a symmetric top are eigenfunctions of $\hat{P}_c$ and $\hat{P}_z$, they have the form

$$\frac{1}{2\pi} G_{JKM}(\theta) e^{iK\chi} e^{iM\varphi} \qquad (6.3)$$

The theta factor G can be obtained by direct solution.[7] Putting these eigenfunctions into Eq.(6.1), we get

$$\frac{d^2G}{d\theta^2} + \cot\theta \frac{dG}{d\theta} - \frac{(M - K\cos\theta)^2}{\sin^2\theta} G = -E_G G \qquad (6.4)$$

where

$$E_G = \frac{2I_a E_R^0}{\hbar^2} - \frac{I_a}{I_c} K^2 \qquad (6.5)$$

By the substitution

$$Y(\theta) = (\sin\theta)^{\frac{1}{2}} G(\theta). \qquad (6.6)$$

it can be obtained

$$\frac{d^2Y}{d\theta^2} - \left[\frac{(M-\frac{1}{2})\left(M+\frac{1}{2}\right) + K^2 - 2MK\cos\theta}{\sin^2\theta} \right] Y = -\left(E_G + K^2 + \frac{1}{4}\right) Y \qquad (6.7)$$

This differential equation has been solved by Burkhard[7] and the exact analytical solutions for $K = J$ are

$$Y_{JJM}(\theta) = \left[\frac{(2J+2)!}{(J-M+1)!(J+M+1)!} \right]^{\frac{1}{2}} \sin^{J-M+\frac{1}{2}} \frac{\theta}{2} \cos^{J+M+\frac{1}{2}} \theta \qquad (6.8)$$

$$G_{JJM}(\theta) = \frac{1}{\sin^{\frac{1}{2}}\theta} \left[\frac{(2J+2)!}{(J-M+1)!(J+M+1)!} \right]^{\frac{1}{2}} \sin^{J-M+\frac{1}{2}} \frac{\theta}{2} \cos^{J+M+\frac{1}{2}} \theta \qquad (6.9)$$

For $K \neq J$ solutions can be found using the recursion formula

$$G_{JKM}(\theta) = \frac{(K+1)\cot\theta - \frac{M}{\sin\theta} + \frac{d}{d\theta}}{\left[(J+K+1)(J-K+1)\right]^{\frac{1}{2}}} G_{JK+1M}(\theta) \qquad (6.10)$$

From the above recursion formula, we can get any analytical rotational eigenfunction of quantum number J, K, M.

Since the inversion of the molecule also has an effect on the rotational energy level; we compute the rotational energies by replacing μ-dependent items in the rotational Hamiltonian by their expectation values, yielding

$$\frac{1}{2I_a} = \frac{\hbar^2}{2Q^2}\frac{2}{3}\left\langle \frac{1}{1+\cos^2\mu} \right\rangle \qquad \frac{1}{2I_c} = \frac{\hbar^2}{2Q^2}\left\langle \frac{1}{3\sin^2\mu} \right\rangle$$

We notice that under specific J and K the expectation values depend on the symmetry of the eigenfunctions of inversion and not on the energy levels of eigenfunctions. This means that as the inversion is introduced, every degenerate rotation level is split into two levels. Hence the rotation energy levels are

$$E_S^0(J,K) = \frac{1}{2Q^2}\left(\frac{2}{3}\left\langle \frac{1}{1+\cos^2\mu} \right\rangle_{\psi_S^V(n,\mu,J,K)} \left[J(J+1)-K^2\right] + \left\langle \frac{1}{3\sin^2\mu} \right\rangle_{\psi_S^V(n,\mu,J,K)} K^2 \right) \qquad (6.11)$$

$$E_A^0(J,K) = \frac{1}{2Q^2}\left(\frac{2}{3}\left\langle \frac{1}{1+\cos^2\mu} \right\rangle_{\psi_A^V(n,\mu,J,K)} \left[J(J+1)-K^2\right] + \left\langle \frac{1}{3\sin^2\mu} \right\rangle_{\psi_A^V(n,\mu,J,K)} K^2 \right) \qquad (6.12)$$

in which

$$H_V^0(\mu,J,K)\psi_S^V(n,\mu,J,K) = E_S^V(n,J,K)\psi_S^V(n,\mu,J,K) \qquad (6.13)$$

$$H_V^0(\mu,J,K)\psi_A^V(n,\mu,J,K) = E_A^V(n,J,K)\psi_A^V(n,\mu,J,K) \qquad (6.14)$$

6.2 Intracomplex Rotation Levels of Ammonia

If we consider the rotation of ammonia in the complex under the influence of the interaction potential between Ar and ammonia, the rotation Hamiltonian of the ammonia is

$$\mathrm{H_R}(\mu,\theta,\chi) = \mathrm{H_R^0}(\mu,\theta,\chi) + \mathrm{V_{complex}}(\mu,\theta,\chi) \qquad (6.15)$$

$$H_R^0(\mu,\theta,\chi) = \frac{1}{2Q^2}\left(\frac{2}{3}\frac{1}{1+\cos^2\mu}\left[\hat{P}^2 - \hat{P}_Z^2\right] + \frac{1}{3\sin^2\mu}\hat{P}_Z^2\right) \qquad (6.16)$$

Under the influence of inversion the Hamiltonian becomes

$$\mathrm{H_R^S}(\theta,\chi,\varphi) = \mathrm{H_s^0}(\theta,\chi,\varphi) + \mathrm{V_{complex}^s}(\theta,\chi) \qquad (6.17)$$

in which the rotation operator's μ variable is substituted by its expectation value on ammonia's symmetrical inversion functions, i.e.

$$H_S^0(\theta,\chi,\varphi) = \left\langle H_R^0(\mu,\theta,\chi,\varphi)\right\rangle_{\psi_S^V(n,\mu,J,K)} \qquad (6.18)$$

$$\mathrm{V_{complex}^S}(\theta,\chi) = \left\langle \mathrm{V_{complex}}(\mu,\theta,\chi)\right\rangle_{\psi_S^V(\mathrm{n,\mu,J,K})} \qquad (6.19)$$

Hence we can calculate rotation eigenvalues and eigenfunctions as follows

$$H_R^S(\theta,\chi,\varphi)\left|\psi_S(J,K,M)\right\rangle = E_S(J,K,M)\left|\psi_S(J,K,M)\right\rangle \qquad (6.20)$$

$$E_S(J,K,M) = E_S^0(J,K) + E_S^{(1)}(J,K,M) \qquad (6.21)$$

in which

$$\mathrm{H_S^0}(\theta,\chi,\varphi)\left|\psi_S^0(\mathrm{J,K,M})\right\rangle = \mathrm{E_S^0}(\mathrm{J,K})\left|\psi_S^0(\mathrm{J,K,M})\right\rangle \qquad (6.22)$$

$$\left|\psi_S^0(\mathrm{J,K,M})\right\rangle = \frac{1}{2\pi}\mathrm{G_{JKM}}(\theta)e^{\mathrm{iK}\chi}e^{\mathrm{iM}\varphi} \qquad (6.23)$$

For antisymmetric inversion eigenfunctions, in the same manner, we get

$$\mathrm{H_R^A}(\theta,\chi,\varphi) = \mathrm{H_A^0}(\theta,\chi,\varphi) + \mathrm{V_{complex}^A}(\theta,\chi,\varphi) \qquad (6.24)$$

$$H_A^0(\theta,\chi,\varphi) = \left\langle H^0(\mu,\theta,\chi,\varphi)\right\rangle_{\psi_A^V(n,\mu,J,K)} \qquad (6.25)$$

$$V_{inter}^{A}(\theta,\chi,\varphi) = \left\langle V_{complex}(\mu,\theta,\chi)\right\rangle_{\psi_A^V(n,\mu,J,K)} \quad (6.26)$$

$$H_R^A(\theta,\chi,\varphi)\left|\psi_A(J,K,M)\right\rangle = E_A(J,K,M)\left|\psi_A(J,K,M)\right\rangle \quad (6.27)$$

$$E_A(J,K,M) = E_A^0(J,K) + E_A^{(1)}(J,K,M) \quad (6.28)$$

$$H_A^0(\theta,\chi,\varphi)\left|\psi_A^0(J,K,M)\right\rangle = E_A^0(J,K)\left|\psi_A^0(J,K,M)\right\rangle \quad (6.29)$$

$$\left|\psi_A^0(J,K,M)\right\rangle = \frac{1}{2\pi}G_{JKM}(\theta)e^{iK\chi}e^{iM\varphi} \quad (6.30)$$

It is easy to calculate $E_s^0(J,K)$ and $E_A^0(J,K)$

$$H_s^0(\theta,\chi,\varphi)\left|\psi_s^0(J,K,M)\right\rangle = E_s^0(J,K)\left|\psi_s^0(J,K,M)\right\rangle \quad (6.31)$$

$$H_A^0(\theta,\chi,\varphi)\left|\psi_A^0(J,K,M)\right\rangle = E_A^0(J,K)\left|\psi_A^0(J,K,M)\right\rangle \quad (6.32)$$

To calculate $E_{s,or,A}^1(J,K,M)$ introduced by the interaction between ammonia and the atom Ar, we consider the perturbation treatment of an energy level $\left(J,|K|\right)$ that is $2J+1$ fold degenerate.

For $\left(J,|K|\right)$ since there are equations

$$\frac{1}{2\pi}G_{JKM}(\theta)e^{iK\chi}e^{iM\varphi} = cons\tan t * \frac{1}{2\pi}G_{J-KM}(\theta)e^{iK\chi}e^{iM\varphi} \quad (6.33)$$

we have only $2J+1$ linearly independent unperturbed wave functions $\frac{1}{2\pi}G_{J|K|M}(\theta)e^{iK\chi}e^{iM\varphi}$ corresponding to the degenerate energy levels;

$$\hat{H}_{S,or,A}^0\frac{1}{2\pi}G_{JKM}(\theta)e^{iK\chi}e^{iM\varphi} = E_{S,or,A}^0(M)\frac{1}{2\pi}G_{JKM}(\theta)e^{iK\chi}e^{iM\varphi} \quad (6.34)$$

$$E_{S,or,A}^0(M=-J) = E_{S,or,A}^0(M=-J+1) = \ldots = E_{S,or,A}^0(M=J-1) = E_{S,or,A}^0(M=J).$$

For specific J and |K|, there are two situations corresponding to the μ-variable's expectation values with respect to symmetrical and anti symmetrical inversion eigenfunctions:

A) The μ-variable's expectation value on symmetrical inversion eigenfunctions

$$\hat{H}_R^S\psi_j = E_{j,S}\psi_j \quad (6.35)$$

$$E_{j,S} = E^0_{j,S}(J,|K|) + E^{(1)}_{j,S}(J,|K|) \qquad j = -J, -J+1, \ldots\ldots, J-1, J$$

$$\psi_j = \sum_N C_j^M \phi_M^{(0)} = \sum_{M=-J}^{J} C_j^M \frac{1}{2\pi} G_{J|K|M}(\theta) e^{iK\chi} e^{iM\varphi} \qquad (6.36)$$

and $E^{(1)}_{j,S}(J,|K|)$ are determined by

$$\det(H'_{mp,S} - \delta_{mp} E^{(1)}_{j,S}) = 0 \qquad (6.37)$$

$$H'_{mp,S}(J,|K|) = \left\langle \frac{1}{2\pi} G_{J|K|m}(\theta) e^{i|K|\chi} e^{im\varphi} \left| V^S_{\text{inter}}(\theta,\chi,\varphi) \right| \frac{1}{2\pi} G_{J|K|p}(\theta) e^{i|K|\chi} e^{ip\varphi} \right\rangle \qquad (6.38)$$

B) Similarly the μ-variable's expectation value on antisymmetrical inversion eigenfunctions

$$\hat{H}^A_R \psi_j = E_{j,A} \psi_j \qquad (6.39)$$

$$E_{j,A} = E^0_{j,A}(J,|K|) + E^{(1)}_{j,A}(J,|K|) \qquad j = -J, -J+1, \ldots\ldots, J-1, J$$

$$\psi_j = \sum_N C_j^M \phi_M^{(0)} = \sum_{M=-J}^{J} C_j^M \frac{1}{2\pi} G_{J|K|M}(\theta) e^{iK\chi} e^{iM\varphi} \qquad (6.40)$$

and $E^{(1)}_{j,S}(J,|K|)$ are determined by

$$\det(H'_{mp,A} - \delta_{mp} E^{(1)}_{j,A}) = 0 \qquad (6.41)$$

$$H'_{mp,A}(J,|K|) = \left\langle \frac{1}{2\pi} G_{J|K|m}(\theta) e^{i|K|\chi} e^{im\varphi} \left| V^A_{\text{inter}}(\theta,\chi,\varphi) \right| \frac{1}{2\pi} G_{J|K|p}(\theta) e^{i|K|\chi} e^{ip\varphi} \right\rangle \qquad (6.42)$$

Therefore the interaction between Ar and ammonia has split the $2J+1$-fold degenerate unperturbed level into $2J+1$ different perturbed levels

$$E^0_{S,or,A}(J,|K|) + E^{(1)}_{-J,S,or,A}(J,|K|),\ E^0_{S,or,A}(J,|K|) + E^{(1)}_{-J+1,S,or,A}(J,|K|),\ \ldots,$$
$$E^0_{S,or,A}(J,|K|) + E^{(1)}_{J-1,S,or,A}(J,|K|),\ E^0_{S,or,A}(J,|K|) + E^{(1)}_{J,S,or,A}(J,|K|)$$

The energy level scheme of $Ar-ammonia$ states correlating with the free rotor NH_3 state $(J=1,|K|=1)$ is illustrated schematically in Fig.6.1.

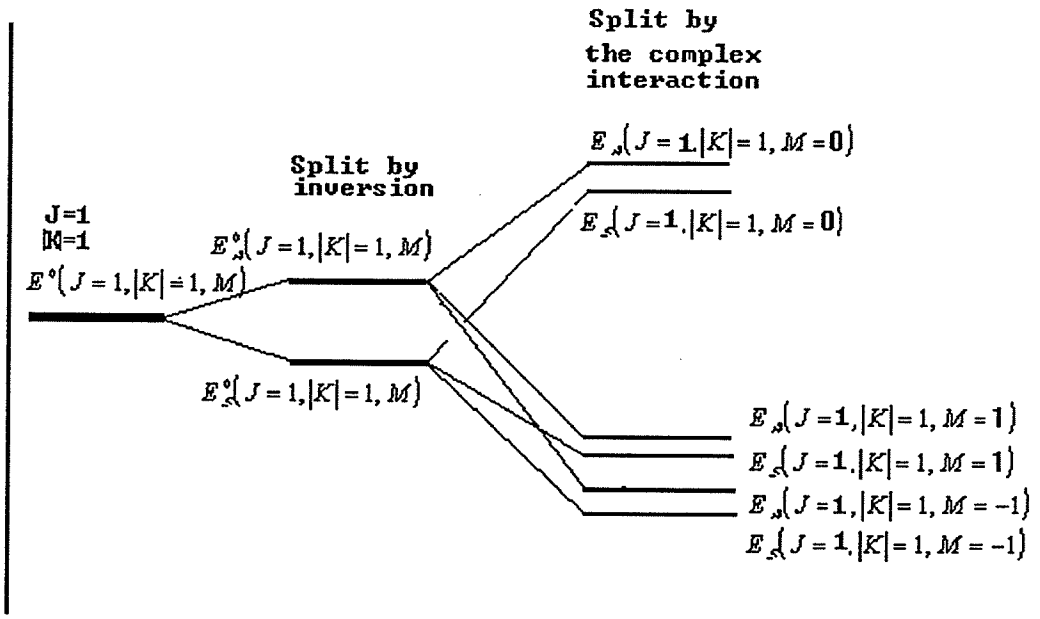

Figure 6.1 The energy level scheme of $Ar - NH_3$ states correlating with free ammonia $(J=1,|K|=1)$.

7. RESULTS OF CALCULATION

For different J and K, we use numerov method[8] to solve eigenfunctions of ammonia's inversion Hamiltonian; then compute the μ-variable's expectations on ammonia inversion eigenfunctions needed in calculating intracomplex rotation eigenvalues using inversion eigenfunctions. After obtaining the expectations, we calculate the intrarotational energy levels using the method described in Section 5 as in Table 7.1

Table 7.1 Comparison of calculated intracomplex rotation spectra with experiment.

States				$E(J,K,M)$ (cm^{-1})		
J	K	Symmetry	M	*Calc.*	$Exp^{1,2}$.	*Exp.−Calc.*
0	0		0	0	0	0
1	1	A	1	15.3842	15.2530	-0.1294
			0	22.4764	22.0853	-0.3911
			-1	13.9862	14.0456	0.0594
		S	1	15.0801	14.0456	1.0345
			0	22.1586	21.7053	-0.4533
			-1	13.6742	13.3027	-0.3715
1	0	A	1	24.1089		
			0	12.4149		
			-1	24.1089		
		S	1	25.4671		
			0	13.7862		
			-1	25.4671		
2	2	A	2	55.3899		
			1	45.2135		
			0	54.3867		
			-1	43.4533		
			-2	55.1160		
		S	2	52.7816		
			1	42.6194		
			0	51.7802		
			-1	40.8559		
			-2	52.5073		

8. DISCUSSION

8.1 Asymmetry of the Interaction Energy Potential

From our calculation of interaction potential, there exists some asymmetry in the potential about two mirror configurations as shown in Fig 4. This reflects the ammonia in the complex is not completely freely rotating and inverting. The binding force between the atom Ar and ammonia, although the force is very weak, restricts the motion of the ammonia in the complex. From calculation we see that the height and the asymmetry of the potential are responsible for the splitting of rotation energy levels. The height of the potential is about 26.63 cm^{-1} as shown in Fig 4.

8.2 Rotational Selection Rules

The rotational selection rules for a symmetric top require that $\Delta J = 0, \pm 1$ and $\Delta K = 0$. The intensity of a transition depends on the behavior of the dipole matrix element

$$\langle i|\bar{\mu}|j\rangle$$

For a pure inversion transition, $\Delta J = 0$ and the eigenfunctions are just the inversion wave functions. For the matrix element $\langle i|\bar{\mu}|j\rangle$ to be non zero, the integral must be totally symmetric with respect to an inversion of the coordinates. Because the dipole moment is restricted to lie along the symmetry axis of a symmetric top, it changes direction during the inversion, and the dipole moment is antisymmetric with respect to this operation. Therefore, the inversion functions must be of opposite symmetry to make $\langle i|\bar{\mu}|j\rangle$ totally symmetric and a pure inversion transition is allowed in a symmetric rotor.

$+ \leftarrow\!\!\rightarrow -$; $\pm \leftarrow\!|\rightarrow \pm$

However, for rotation and inversion of the ammonia in the complex, since the potential is not completely symmetric, the rotational wave function is not symmetric if K is even and not antisymmetric if K is odd. Therefore, the above selection rules do not hold for symmetric top transitions involving rotation and inversion in the complex. We can predict that the intracomplex rotational and inversional transition spectra are much more complicated than those of pure rotation and inversion of free ammonia.

9. REFERENCES

1 *E. Zwart, H. Linnartz, W. L. Mertz, G. T. Fraser, D. D. Nelson, Jr and W. Klemperer, J. Chem. Phys. 95, 793(1991).*

2 *C. A. Schmuttenmaer, R.C. Cohen, J. G. Loeser, and R. J. Saykally, J. Chem. Phys. 95, 9(1991).*

3 *Ira N. Levine, Quantum Chemistry, vol.2, 1970.*

4 *R. Wallace and C.Chu, Chem. Phys. 161(1992) 155*

5 *J.P. Leroy, H. Rabitz and R. Wallace, Chem. Phys. 154(1991) 395.*

6 *M. Bulski, P. E. S. Wormer, and A. van der Avoird, J. Chem. Phys. 94(1),491(1991).*

7 *D. G. Burkhard, J. Mol. Spectry., 2, 187(1958).*

8 *J. P. Leroy and R. Wallace, J. Phys. Chem., 89, 1928(1985).*

Part Two

FREQUENCY DETERMINATION

IN

MOLECULAR DYNAMICS

Abstract

Three potential systems: the harmonic and Morse potential systems of the molecule *HCl* as well as the multiminimum potential system of n_butane intramolecular rotation, are investigated by classical and quantum mechanical methods. The dynamical property, vibrational frequency of the systems, is obtained by classical and quantum mechanical methods. The quantum mechanical methods are mainly stationary and dynamical quantum mechanical methods. The classical methods are the phase portrait and fast Fourier transform methods. Both of them use the computation results of molecular dynamics simulation. Since the use of computer simulations to study the internal dynamics of macromolecules has attracted a great deal of attention in the recent years and these simulations constitute the most detailed theoretical approach available for studying internal motions and structural flexibility of molecules, the fundamentals of molecular dynamics simulations will be introduced. The fast Fourier transform is very important analytical tool and it saves a lot of computer time, its basic principle will be presented in the paper. The comparison of the results obtained by different methods show that they have the almost comparable results.

List of Figures

1 Introduction

To investigate molecular motion, there exist two methods, quantum and classical mechanical methods. Although quantum mechanics can give a perfect description of molecular motion, it can only be used in small molecular systems. For macromolecular systems it is impossible to probe their dynamic properties by quantum mechanics; consequently classical mechanical method is the sole choice to investigate macromolecular dynamic properties.

Quantum mechanics gives the eigenvalues and eigenfunctions of a molecular system obtained by solving its Schrodinger equation; some Schrodinger equations have analytical solutions; some Schrodinger equations can only be solved by numerical methods; but most of them are intractable. However, classical mechanics can give the position and momentum change of *every* individual atom in every molecular system with respect to time; usually the positions and momenta are obtained by molecular dynamics simulations.

The classical mechanical methods which will be used to portray the dynamical properties of a molecular system in this thesis are the phase portrait and fast Fourier transform method. Both of them are directly based on the molecular dynamics simulation calculations of a molecular system. From the calculations, the vibrational frequency can be obtained by the fast Fourier transform of atom's positional change with respect to time or through the phase-space portrait by calculating its period. Since the use of computer simulations to study the internal dynamics has attracted a great deal of attention in recent years and these simulations constitute the most detailed theoretical approach available for studying internal motions and structural flexibility, the fundamentals of simulations will be introduced in this thesis. At the same time the essential basics of the fast Fourier transform will be presented because the fast Fourier

transform is a principal analytical tool in diverse fields and it saves a lot of computation time of molecular dynamical simulation calculations.

The methods of quantum mechanics are divided into stationary and dynamical quantum methods. Stationary quantum mechanics gives the time-independent eigenvalues and eigenfunctions of a molecular system. Any molecular dynamical properties, including vibrational frequency, can be obtained from the eigenvalues and eigenfunctions. Dynamical quantum mechanics depicts the motion of a state under a specific potential field with respect to time. The vibrational frequency can be picked up from the movement of a state by calculating the time spent by a period of the motion.

It does not matter which method is used; a potential surface form which reasonably describes the interaction among the atoms in a system is necessary to probe the motion of a molecular system. Since it is difficult to find a precise, universal potential surface for a molecular system, there exist many potential forms which approximately reflect the interaction potential of the system.

In this thesis the vibration properties of three potential interaction systems will be studied by quantum and classical mechanics: the harmonic and Morse potential surface forms of *HCl* molecular bond interaction as well as the multiminimum potential form of **n – butane** intramolecular rotation.

2. FUNDAMENTALS

2.1 Molecular Dynamics Simulation

Molecular dynamics simulations compute the changes of momentum and position of every single atom in a molecular system with respect to time. The internal motion of a molecule is very important since molecular dynamics constitutes a motion picture that follows molecules as they dart to and fro, twist, turn, collide with one another.

Although the method is very old in science, it is very useful because of its simplicity. Now systems can be computed a with up to 250 million particles and up to nanosecond time intervals by a super computer.

Simulation calculations can provide fundamental understanding of the propagation of microcracks and fracture in solids. It is optimistic or possible that computational molecular dynamics simulate or predict the properties of materials which are essential to new material design.

Chemical engineers can use dynamics simulation methods to conceptualize problems and approach solutions. For example, it is now realistic to imagine mathematical models of fundamental phenomena beginning to replace laboratory and field experiments. Such computations increasingly allow chemical engineers to bypass the long costly step of producing process and product prototypes, and permit the design of products and processes that better utilize scarce resources, are significantly less polluting, and are much safer.

Recently an exciting development in molecular dynamics simulations is direct dynamics method. Direct dynamics computations are the calculation of rates or other dynamical observables directly from electronic structure information, without the intermediary of fitting the electronic energies in the form of a potential energy function[1] .

For a $n-$atom system in three dimensions, a molecular dynamics simulation produces $3n$ values of positions and velocities every time when the equations of motion are integrated forward one step. Usually this huge amount of data can be grappled by a phase-space portrait. First the portrait is calculated using classical mechanics and then the features of the portrait are described in terms of classical nonlinear dynamics. Analyzing the portrait and position change with time by kinetic theory, and using the fast Fourier transform theory, one can obtain their dynamical properties. The portrait is tested by probing constraints imposed by periodic boundary conditions as well as conservation principles.

2.2 Newtonian dynamics

In Newtonian dynamics the translational motion of a point particle j is caused by a force F_j exerted by an external field. The motion and the applied force are expressed as

$$\boldsymbol{F}_j = m_j \ddot{\boldsymbol{r}}_j = -\frac{\partial V}{\partial r_j} \qquad (2.1)$$

The corresponding acceleration is given by

$$\boldsymbol{a}_j = \ddot{\boldsymbol{r}}_j = \frac{d^2 \boldsymbol{r}_j}{dt^2} \qquad (2.2)$$

For an isolated system there exists an energy conservation law

$$E = \sum E_j + V = \sum \frac{1}{2} m_k \dot{\boldsymbol{r}}_k^2 + V = \boldsymbol{constant} \qquad (2.3)$$

Theoretically the portrait for any system whose potential is known can be obtained from the Newtonian dynamical equations (2.1) to (2.3).

2.3 Hamiltonian Dynamics

From the Newtonian dynamics it is known that molecular forces, positions and velocities change with time; however the functional form of Newton's second law (2.1) is time independent. Therefore it is reasonable to guess that there is a function of the positions and velocities whose value is constant in time; this function is called the Hamiltonian H,

$$H(\boldsymbol{r}^N, \boldsymbol{p}^N) = constant \qquad (2.4)$$

For an isolated system, it is known that one conserved quantity is the total energy E; therefore, the total energy is identified as a Hamiltonian. For N particle system H takes the form

$$H(\boldsymbol{r}^N, \boldsymbol{p}^N) = \sum \frac{1}{2} m_k \dot{\boldsymbol{r}}_k^2 + V(\boldsymbol{r}^N) = E \qquad (2.5)$$

To obtain equations of motion, consider the total time derivative of the Hamiltonian Eq.(2.5)

and get for each particle j

$$\dot{\boldsymbol{r}}_j = \frac{\boldsymbol{p}_j}{m_j} = \frac{\partial H}{\partial \boldsymbol{p}_j} \qquad (2.6)$$

and

$$\dot{\boldsymbol{p}}_j = -\frac{\partial H}{\partial \boldsymbol{r}_j} \qquad (2.7)$$

Equations (2.6) and (2.7) are Hamilton's equations of motion. For a system of N point particles, these two equations represent $6N$ first order differential equations that are equivalent to Newton's $3N$ second-order equations (2.1).

Newtonian and Hamiltonian dynamics represent different views on motion. In the Newtonian view motion is a response to an applied force. However, in the

Hamiltonian view forces do not appear explicitly; instead, motion occurs in such a way as to preserve the Hamiltonian function.

2.4 Phase-space portrait

The first objective of a molecular dynamics simulation is to generate a molecular motion portrait over a finite time. It is necessary to extend the idea of the portrait to include not only positions but also atomic momenta. Consider a collection of N spherical atoms that interact through a prescribed potential function. The center of each atom is located by a position vector $\boldsymbol{r}_j$. For an isolated system, the atoms move in accordance with Newton's law, trace out trajectories that can be represented by time-dependent position vectors $\boldsymbol{r}_j(t)$. As an atom follows its trajectory, its momentum also changes in response to interactions with other atoms; thus, we also have time-dependent momentum vectors $\boldsymbol{p}_j(t)$.

At one instant, imagine plotting the positions and momenta of the N atoms in a $6N$-dimensional hyperspace. Such a space, called phase space, is composed of two parts: a $3N$-dimensional configuration space, in which the coordinate axes are the components of the position vectors $\boldsymbol{r}_j(t)$, and a $3N$-dimensional momentum space, in which the coordinate axes are the momenta of the entire N-atom system represented by one point in this space. As the positions and momenta change with respect to time, the point moves, describing a trajectory or portrait in phase space. We may now restate the first objective of a molecular dynamics simulation: compute the phase-space trajectory or portrait. The trajectory is obtained by numerically solving Newton's second law (2.1) or, equivalently, Hamilton's equation (2.6) and (2.7).

Features of the phase-space portrait can be used to classify the motion of objects in dynamical systems[3,4]. The classification takes a hierarchical level. The first level, systems having recurrent trajectories are separated from those having nonrecurrent

trajectories. Recurrent systems obey Poincare's recurrence theorem[3,4]: for a phase space of finite volume, the phase point will pass, arbitrarily closely and indefinitely often, to almost every accessible configuration on the trajectory. However, for systems of more than a few objects, the time required for a Poincare recurrence is huge--it can exceed the age of the universe[5,6].

Whether recurrent trajectories are Hamiltonian or non-Hamiltonian depends on whether an explicit Hamiltonian governs their motion. Non-Hamiltonian systems can be studied by nonequilibrium molecular dynamics methods. In such cases, particle trajectories are generated from equations of motion; however, those equations are not consistent with any Hamiltonian function.

In Hamiltonian systems the trajectory is constrained in phase space to the hypersurface of constant H. Hamiltonian systems can be further divided into integrable and nonintegrable systems. Integrable systems are those for which the number of constants of the motion equals the number of degrees of freedom. In most situations the number of conserved quantities is small, the equations of motion contain nonlinear terms, and so systems containing even a very few objects are usually nonintegrable.

Integrable systems can be subdivided into those that have periodic motion and those that can have either periodic or quasiperiodic motion. Quasiperiodic motion results from integrable Hamiltonian systems that are not periodic. In such systems the phase space trajectory is confined to the surface of a torus. Periodic motion means that within a finite time the phase trajectory will intersect itself. Because the motion of the phase point is completely determined by differential equations, once the phase point encounters its own trajectory, that trajectory is repeated indefinitely. All Hamiltonian systems having one degree of freedom are integrable and periodic.

From the phase space portrait of integrable periodic systems, it is easy to pick up the periodic time of the motion.

Another approach to picking up the vibrational frequency of a molecular system is to transform the time domain of positional change into frequency domain by the fast Fourier transform.

2.5 The fast Fourier transform

As shown in Figs.2.1, the Fourier transform of a waveform is to separate the waveform into a sum of sinusoids of different frequencies. The example waveform consists of the two sinusoids which add to yield the waveform. As shown, the Fourier transform diagrammatically displays both the amplitude and frequency of every sinusoid.

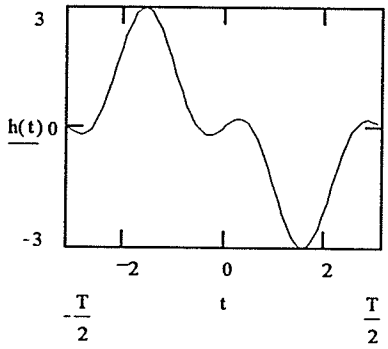

Figure 2.1-(a)

Figure 2.1-(a) defines a waveform $h(t)$ from $-\infty$ to $+\infty$

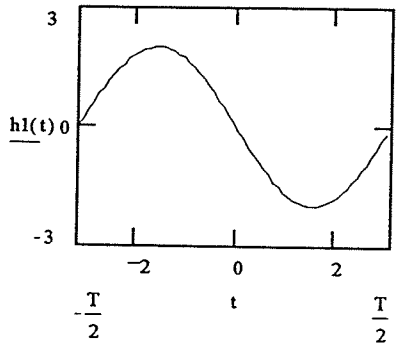

Figure 2.1-(b)

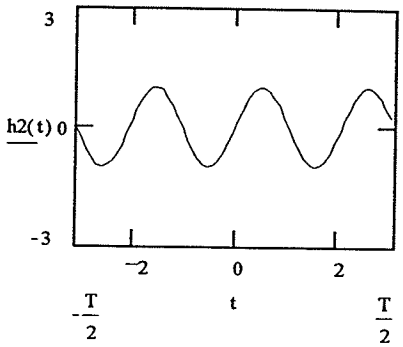

Figure 2.1-(c)

Synthesize a summation of sinusoids $h1(t)$, $h2(t)$ which add to give the waveform Figure 2.1-(a)

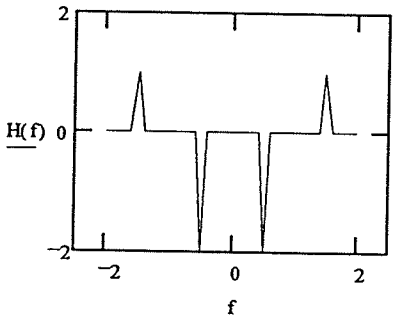

Figure 2.1-(d)

From the Fourier transform of $h1(t)$-(b) and $h2(t)$-(c), construct a diagram which displays amplitude and frequency of each sinusoid

Figure 2.1 Interpretation of the Fourier transform

Mathematically, the Fourier transform is defined as

$$H(f) = \int_{-\infty}^{\infty} h(t) e^{-i2\pi ft} dt \qquad (2.8)$$

where $h(t)$ is the waveform to be decomposed into a sum of sinusoids, $H(f)$ is the Fourier transform of $h(t)$.

From the definition of Eq.(2.8) the Fourier transform seems useless for solving problems since it requires transforming a function of a variable from $-\infty$ to ∞ to the function of another variable also from $-\infty$ to ∞. However it is reasonable to extend Eq.(2.8) as a numerical integration

$$H(f_k) = \sum_{i=0}^{N-1} h(t_i) e^{-i2\pi f_k t_i} (t_{i+1} - t_i) \qquad k = 0,1,\ldots\ldots,N-1 \qquad (2.9)$$

Usually $h(t_i)$ is the result of molecular dynamics simulation calculations, for example, the positional change with respect to time. It is known that molecular dynamics simulation calculations are very time consuming and it is clear that if the N is too large, it can not be calculated by a computer. Fortunately the computation time can be reduced by the fast Fourier transform developed in 1965 by Cooley and Tukey[2]. In order to get the vibration frequency from a simulation calculation, it only necessary to compute one period of the motion. Hence it is necessary to introduce the basic principle of the fast Fourier transform.

The fast Fourier transform is developed from the Fourier transform. The Fourier transform has two important properties: convolution and correlation. The convolution integral is defined as

$$y(t) = \int_{-\infty}^{\infty} x(\tau) h(t-\tau) d\tau = x(t) * h(t) \qquad (2.10)$$

Function $y(t)$ is said to be the convolution of the functions $x(t)$ and $h(t)$. It is not easy to clearly define the meaning of the mathematical operation of Eq. (2.10); hence the procedure of the convolution integral is graphically shown in Figure 2.2 as: folding,

displacement, multiplication, and integration.

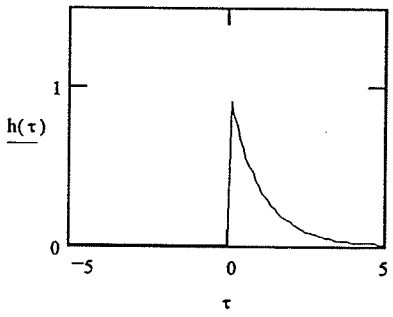

Figure 2.2-(a)

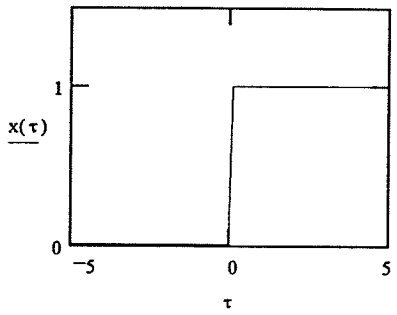

Figure 2.2-(b)

fold Figure 2.2-(a) $h(\tau) = e^{-\tau}$ to produce Figure 2.2-(c) $h1(\tau) = h(-\tau) = e^{\tau}$

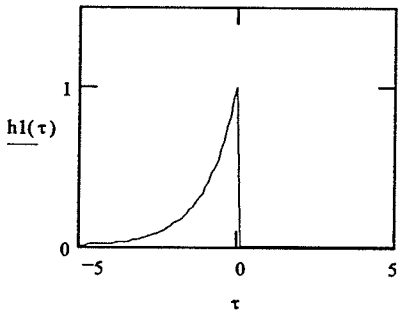

Figure 2.2-(c)

Displace Figure 2-(c) to get Figure 2.2-(d) $h2(\tau) = h(t-\tau) = e^{-(t-\tau)}$

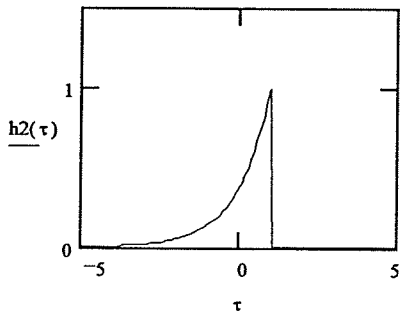

Figure 2.2-(d)

multiply Figure 2.2-(d) by $x(\tau)$ to yield Figure 2.2-(e) $h3(\tau) = x(\tau)h(t-\tau)$

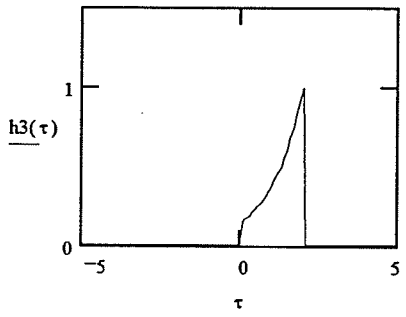

Figure 2.2-(e)

Integrate Figure 2.2-(e) to obtain Figure 2.2-(f) $y(t)$

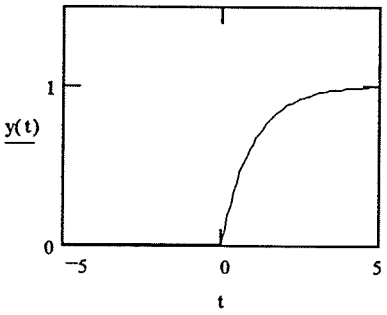

Figure 2.2-(f)

Figure 2.2 Convolution procedure: folding, displacement, multiplication, and integration

The result shown in Fig.2.2-(f) can be obtained directly from Eq.(2.10)

$$y(t) = \int_{-\infty}^{\infty} x(\tau)h(t-\tau)d\tau = x(t) * h(t) = \int (1)e^{-(t-\tau)}d\tau$$
$$= e^{-t}\left[e^{t} - 1\right] = 1 - e^{-t} \qquad (2.11)$$

The correlation integral is defined as

$$z(t) = \int_{-\infty}^{\infty} x(\tau)h(t+\tau)d\tau = x(t) \cdot h(t) \qquad (2.12)$$

A comparison of the above expression and the convolution integral (2.10) indicates that the two are closely related.

Considering now a periodic function $y(t)$ with period T_0, the preferred approach is to express it as a Fourier series.

$$y(t) = \frac{a_0}{2} + \frac{1}{2}\sum_{n=-\infty}^{\infty}(a_n - ib_n)e^{i2\pi f_n t} = \sum_{n=-\infty}^{\infty}\alpha_n e^{i2\pi f_n t} \qquad (2.13)$$

$$\alpha_n = \frac{1}{T_0}\int_{-\frac{T_0}{2}}^{\frac{T_0}{2}} y(t)e^{-i2\pi f_n t}$$

However, the Fourier series is only a special case of the Fourier integral and it can be proved that the Fourier series of a waveform is an infinite set of sinusoids determined directly from the Fourier integral. For the periodic triangular function shown in Fig 2.3-(e) it is known that the Fourier series of this waveform is an infinite set of sinusoids and it can be proved that an identical relationship can be obtained from the Fourier integral.

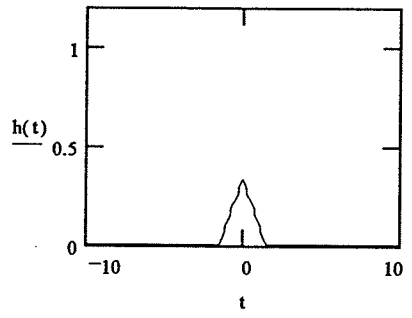

Figure 2.3-(a)

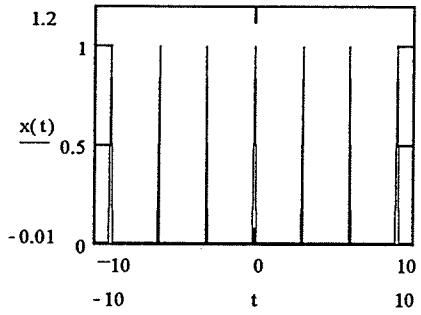

Figure 2.3-(b)

The convolution of 2.3-(a), $h(t)$ and (b), $x(t)$ is Figure 2.3-(e)

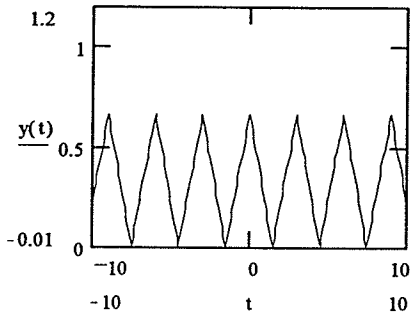

Figure 2.3-(e)

The Fourier transform of Figure 2.3-(e) is Figure 2.3-(f)

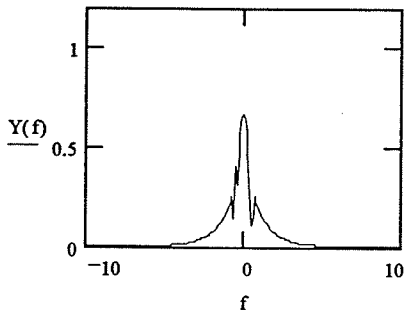

Figure 2.3-(f)

Figure 2.3-(f) can be obtained by multiplication of Figures 2.3-(c) and (d)

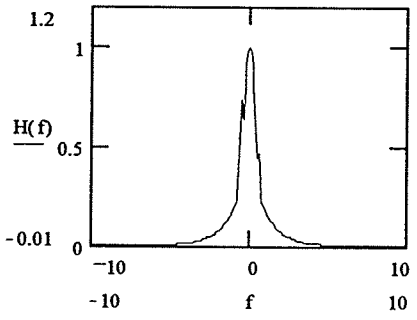

Figure 2.3-(c)

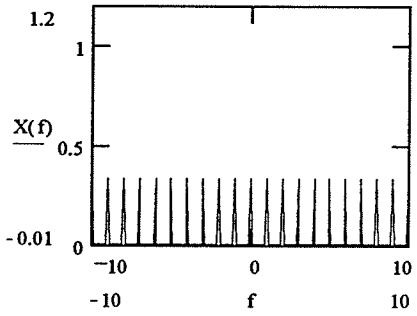

Figure 2.3-(d)

Figures 2.3-(c) and (d) are the Fourier transform of Figures 2.3-(a) and (b), respectively.

Figure 2.3 Graphical convolution theorem development of the Fourier transform of a periodic triangular waveform.

Note that the periodic triangular waveform is simply the convolution of the single triangle shown in Fig.2.3-(a), and the infinite sequence of equidistant impulses illustrated in Fig.2.3-(b). Periodic function $y(t)$ can be expressed by

$$y(t) = h(t) * x(t) \qquad (2.14)$$

Fourier transforms of both $h(t)$ and $x(t)$ have been determined and illustrated in Figs.2.3-(c) and (d), respectively. From the convolution theorem, the desired Fourier transform is the product of these two frequency functions

$$Y(f) = H(f)X(f) = H(f)\frac{1}{T_0}\sum_{n=-\infty}^{\infty}\delta\left(f-\frac{n}{T_0}\right) = \frac{1}{T_0}\sum_{n=-\infty}^{\infty}H\left(\frac{n}{T_0}\right)\delta\left(f-\frac{n}{T_0}\right) \tag{2.15}$$

The Fourier transform of the periodic function is then an infinite set of sinusoids with amplitudes of $H\left(\frac{n}{T_0}\right)$. But note that since

$$h(t) = y(t) \qquad -\frac{T_0}{2} < t < \frac{T_0}{2} \tag{2.16}$$

the function $y(t)$ can be replaced by $h(t)$

$$\alpha_n = \frac{1}{T_0}\int_{-T_0/2}^{T_0/2}h(t)e^{-i2\pi f_0 t}dt = \frac{1}{T_0}H(nf_0) = \frac{1}{T_0}H(\frac{n}{T_0}) \tag{2.17}$$

Thus the coefficients as derived by means of the Fourier integral and those of the conventional Fourier series are the same for a periodic function.

Now we have developed sufficient tools to investigate in detail the theoretical as well as the visual interpretations of sampled waveforms. If the function $h(t)$ is continuous at $t = T$, then the sample of $h(t)$ at time equal to T is expressed as

$$\hat{h}(t) = h(t)\delta(t-T) = h(T)\delta(t-T) \tag{2.18}$$

and the product must be interpreted in the sense of distribution theory. The impulse which occurs at time T has the amplitude equal to the function at time T. If $h(t)$ is continuous at $t = n \cdot T$ for $n = 0,....$

$$\hat{h}(t) = \sum_{n=-\infty}^{\infty}h(nT)\delta(t-nT) \tag{2.19}$$

is termed the sampled waveform $h(t)$ with sampled interval T. Sampled $h(t)$ is then an infinite sequence of equidistant impulses, each of whose amplitude is given by the value

of $h(t)$ corresponding to the time of occurrence of the impulse. Figure 2.4 illustrates graphically the sampling concept: the Fourier transform of the sampled waveform is a periodic function where one period is equal to the Fourier transform of the continuous function $h(t)$. However, the interval T has to be sufficient small.

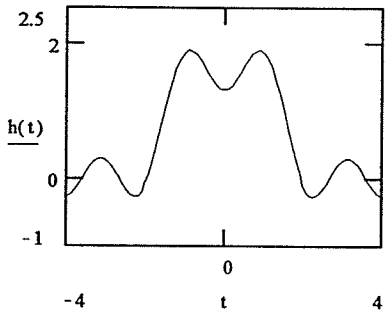

Figure 2.4-(a)

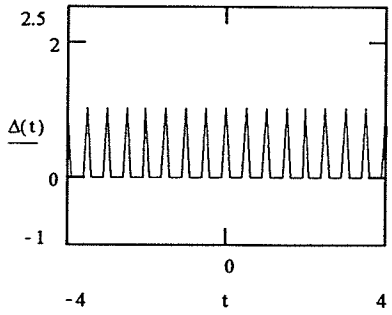

Figure 2.4-(b)

The sampled waveform $h(t)$ shown in Figure 2.4-(e) is obtained from multiplication of

Figure 2.4-(a) and (b)

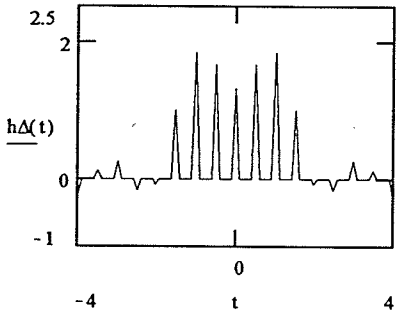

Figure 2.4-(e)

Fourier transform of Fig.2.4-(e) $h\Delta(t) = h(t) \cdot \Delta(t)$ is Figure 2.4-(f)

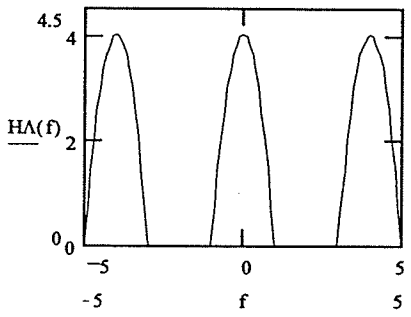

Figure 2.4-(f)

Figure 2.4-(f), $H\Lambda(f) = H(f) * \Lambda(f)$, can be obtained by multiplication of Figures 2.4-(c) and (d).

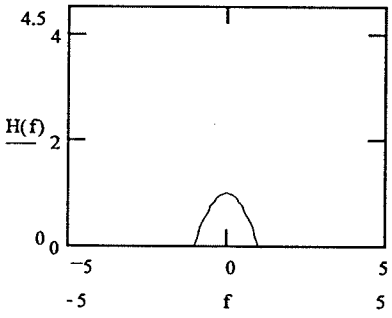

Figure 2.4-(c)

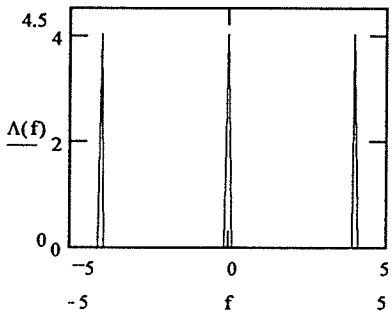

Figure 2.4-(d)

Figure 2.4-(c), $H(f)$, is the Fourier transform of Figure 2.4-(a), $h(t)$; 2.4-(d), $\Lambda(f)$ is the Fourier transform of Figure 2.4-(b), $\Delta(t)$.

Figure 2.4 Graphical frequency convolution theorem development of the Fourier transform of a sampled waveform.

If T is chosen too large, the results illustrated in Figs.2.5 are obtained. The distortion of the desired Fourier transform of a sampled function, the overlapping waveform illustrated in Fig. 2.5-(f), known as aliasing, occurs because the time function was not sampled at a sufficiently high rate, i.e., the sample interval T is too large. However, how can we guarantee that the Fourier transform of a sampled function is not aliased? An examination of Figs.2.5-(c) and (d) shows the fact that convolution overlap

will occur until the separation of the impulses of $\Lambda(f)$ is increased to $\frac{1}{T} = 2f_c$, where f_c is the highest frequency component of the Fourier transform of the continuous function $h(t)$. That is, *if the sample interval T is chosen equal to one half the reciprocal of the highest frequency component, aliasing will not occur*. This is an extremely important since that, if a waveform is sampled such that aliasing doesn't occur, these samples can be appropriately combined to reconstruct identically the continuous waveform. This is the statement of the sampling theorem which we will now investigate.

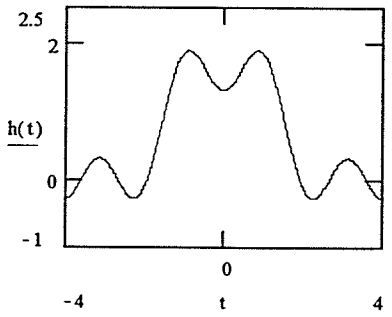

Figure 2.5-(a)

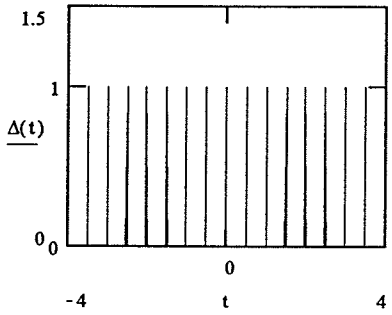

Figure 2.5-(b)

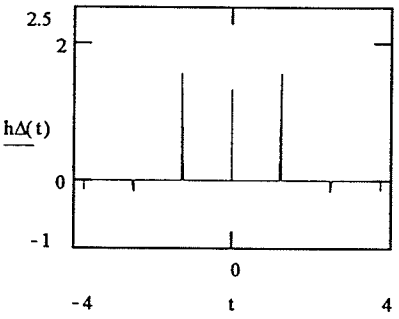

Figure 2.5-(e)

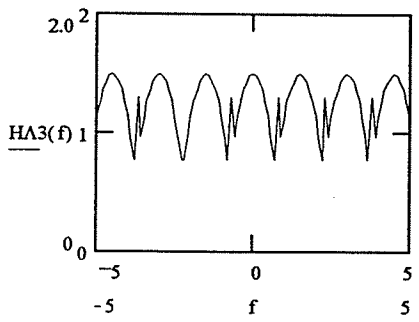

Figure 2.5-(f)

Aliased Fourier transform of a waveform at an insufficient rate

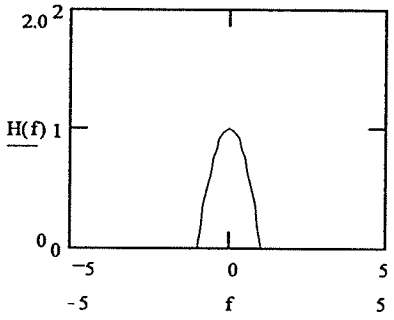

Figure 2.5-(c)

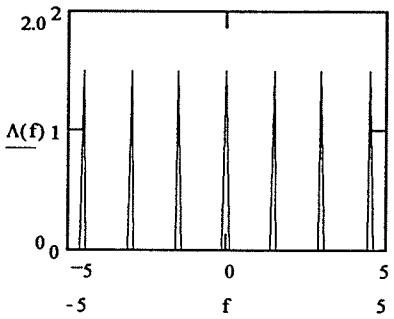

Figure 2.5-(d)

Figure 2.5 Aliased Fourier transform of a waveform sampled at an insufficient rate.

The sampling theorem states that if the Fourier transform of a function $h(t)$ is zero for all frequencies greater than a certain frequency f_c, then the continuous function $h(t)$ can be uniquely determined from a knowledge of its sampled values.

Now it is time to develop the procedure of the fast Fourier transform: time domain sampling, truncation, and frequency domain sampling.

Consider the Fourier transform pair illustrated in Figs 2.6-(a) and (b). To decompose this transform pair it is first necessary to sample the waveform $h(t)$; the sampled waveform can be written as $h(t)\Delta 0(t)$ where $\Delta 0(t)$ is the time domain

sampling function illustrated in Fig. 2.6-(c). The sampling interval is T. The sampled function can be written as

$$h(t)\Delta 0(t) = h(t)\sum_{k=-\infty}^{\infty}\delta(t-kT) = \sum_{k=-\infty}^{\infty}h(kT)\delta(t-kT) \qquad (2.20)$$

The result of this multiplication is illustrated in Figs. 2.6-(e) and (f). Note the aliasing effect which results from the choice of T.

Next, the sampled function is truncated by multiplication with the rectangular function $x(t)$ illustrated in Fig. 2.6-(g):

$$x(t) = 1 \qquad -\frac{T}{2} < t < T_0 - -\frac{T}{2}$$

$$= 0 \qquad \text{otherwise} \qquad (2.21)$$

where T_0 is the duration of the truncation function.

Truncation yields

$$h(t)\Delta 0(t)x(t) = \left[\sum_{k=-\infty}^{\infty}h(kT)\delta(t-kT)\right]x(t) = \left[\sum_{k=-0}^{N-1}h(kT)\delta(t-kT)\right] \qquad (2.22)$$

where it has been assumed that there are N equidistant impulse functions lying within the truncation interval; that is, $N = \frac{T_0}{T}$. The sampled truncated waveform and its Fourier transform are illustrated in Figs. 2.6-(i) and (j). As in the previous example, truncation in the time domain results in rippling in the frequency domain.

The final step in modifying the original Fourier transform pair to a discrete Fourier transform pair is to sample the Fourier Transform of Eq. (2.22). The time domain this product is equivalent of convolving the sampled truncated waveform (2.22) and the time function $\Delta 1(t)$, illustrated in Fig 2.6-(k). Function $\Delta 1(t)$ is given by Fourier transform pair as

$$\Delta 1(t) = T_0\sum_{r=-\infty}^{\infty}\delta(t-rT_0) \qquad (2.23)$$

The desired relationship is $[h(t)\Delta 0(t)x(t)]*\Delta 1(t)$; hence

$$[h(t)\Delta 0(t)x(t)]*\Delta 1(t)=\left[\sum_{k=0}^{N-1}h(kT)\delta(t-kT)\right]*\left[T_0\left[\sum_{r=-\infty}^{\infty}\delta(t-rT)\right]\right]$$

$$=\ldots+T_0\sum_{k=0}^{N-1}h(kT)\delta(t+T_0-kT)+T_0\sum_{k=0}^{N-1}h(kT)\delta(t-kT)$$

$$+T_0\sum_{k=0}^{N-1}h(kT)\delta(t-T_0-kT)+\ldots$$

(2.24)

Note that Eq.(2.24) is periodic with period T_0; in compact notation form the equation can be written as

$$\tilde{h}(t)=T_0\sum_{r=-\infty}^{\infty}\left[\sum_{k=0}^{N-1}h(kT)\delta(t-rT_0-kT)\right] \qquad (2.25)$$

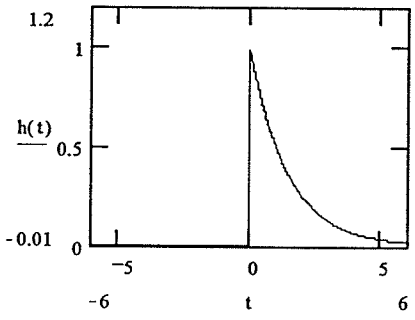

Figure 2.6-(a)

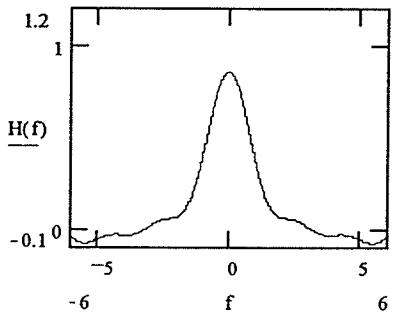

Figure 2.6-(b)

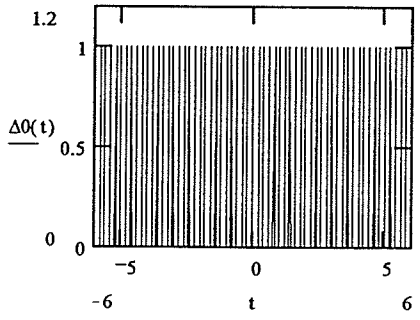

Figure 2.6-(c)

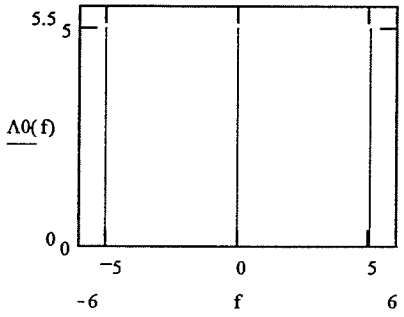

Figure 2.6-(d)

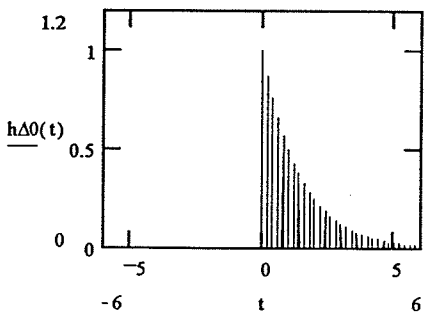

Figure 2.6-(e)

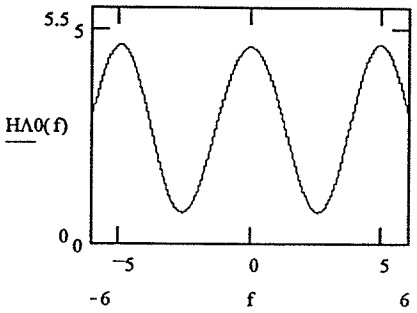

Figure 2.6-(f)

in Figure 2.6-(f) $H\Lambda 0(f) = \left|H(f) * \Lambda 0(f)\right|$

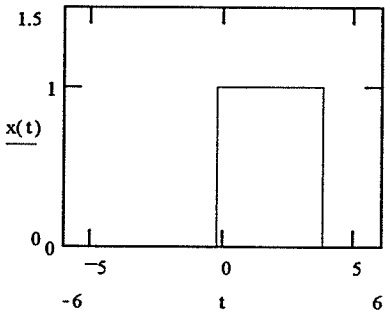

Figure 2.6-(g)

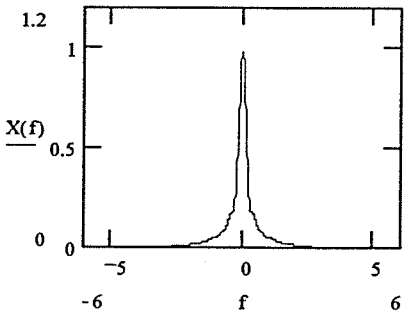

Figure 2.6-(h)

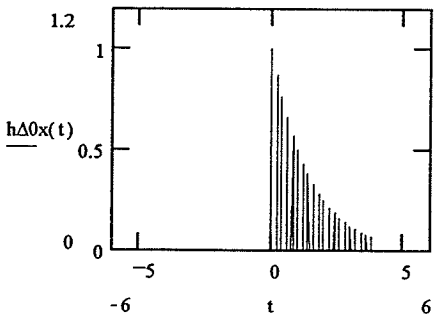

Figure 2.6-(i)

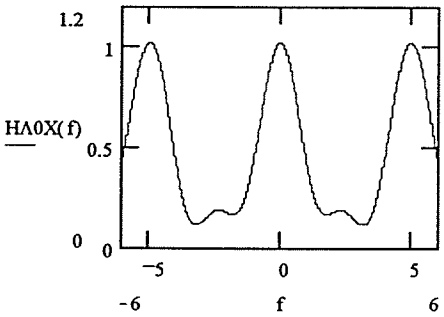

Figure 2.6-(j)

in Figure 2.6-(j) $H\Lambda 0\,X(f) = \left|H(f) * \Lambda 0(f) * X(f)\right|$

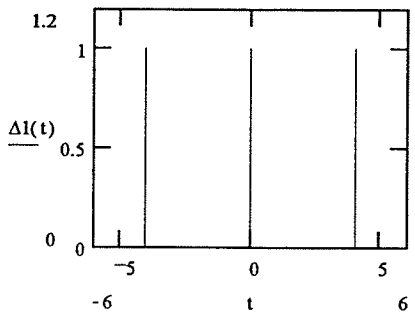

Figure 2.6-(k)

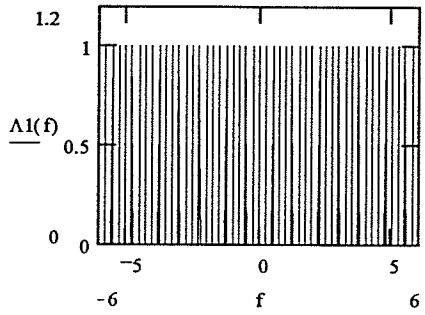

Figure 2.6-(l)

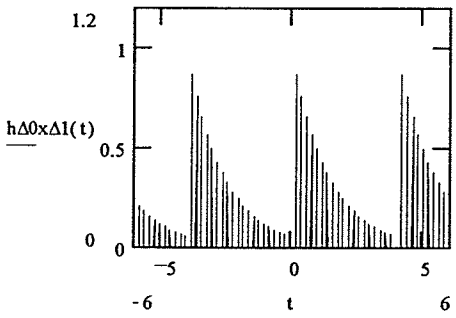

Figure 2.6-(m)

in Figure 2.6-(m) $h\Delta 0 x \Delta 1(t) = \left|[h(t) \cdot \Delta 0(t) x(t)] * \Delta 1(t)\right|$

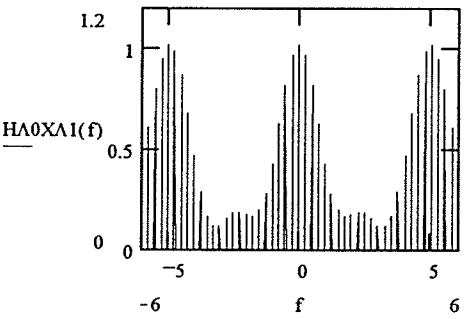

Figure 2.6-(n)

in Figure 2.6-(n) $H\Lambda 0 X \Lambda 1(f) = \left|[H(f) * \Lambda 0(f) * X(f)] \cdot \Delta 1(f)\right|$

Figure 2.6 Graphical derivation of the discrete Fourier transform pair.

Choice of the rectangular function $x(t)$ as described by Eq. (2.23) can now be explained. Note the convolution result of Eq.(2.25) is a periodic function with period T_0

which consists of N samples. If the rectangular function had been chosen such that a sample value coincided with each end point of the rectangular function, the convolution of the rectangular function with impulses spaced at intervals of T_0 would result in time domain aliasing. That is, the Nth point of one period would coincide with and add to the first point of the next period. To insure that time domain aliasing does not occur, it is necessary to choose the truncation interval as illustrated in Fig. 2.6-(g).

To develop the Fourier transform of Eq.(2.25), recall from the discussion on Fourier series. that the Fourier transform of a periodic function $h(t)$ is a sequence of equidistant impulses

$$\tilde{H}\left(\frac{n}{T_0}\right) = \sum_{n=-\infty}^{\infty} \alpha_n \delta(f - nf_0) \quad f_0 = \frac{1}{T_0} \tag{2.26}$$

where

$$\alpha_n = \frac{1}{T_0}\int_{-T/2}^{T_0-T/2} \tilde{h}(t) e^{-i2\pi nt/T_0} dt \qquad n = 0, \pm 1, \pm 2, \ldots \tag{2.27}$$

Substitution of (2.25) in (2.27) yields

$$\alpha_n = \frac{1}{T_0}\int_{-T/2}^{T_0-T/2} T_0 \sum_{r=-\infty}^{\infty} \sum_{k=0}^{N-1} h(kT)\delta(t - kT - rT_0) e^{-i2\pi nt/T_0} dt$$

Integration is only over one period, hence

$$\begin{aligned} \alpha_n &= \int_{-T/2}^{T_0-T/2} \sum_{k=0}^{N-1} h(kT)\delta(t - kT) e^{-i2\pi nt/T_0} dt \\ &= \sum_{k=0}^{N-1} h(kT) \int_{-T/2}^{T_0-T/2} e^{-i2\pi nt/T_0} \delta(t - kT) dt = \sum_{k=0}^{N-1} h(kT) e^{-i2\pi nT/T_0} \end{aligned} \tag{2.28}$$

since $T_0 = NT$, Eq.(2.28) can be rewritten as

$$\alpha_n = \sum_{k=0}^{N-1} h(kT) e^{-i2\pi kn/N} \qquad n = 0, \pm 1, \pm 2, \ldots \tag{2.29}$$

and the Fourier transform of Eq.(2.25) is

$$\tilde{H}\left(\frac{n}{NT}\right) = \sum_{n=-\infty}^{\infty} \sum_{k=0}^{N-1} h(kT) e^{-i2\pi kn/N} \tag{2.30}$$

From a cursory evaluation of (2.30), it is not obvious that the Fourier transform $\tilde{H}\left(\frac{n}{NT}\right)$ is periodic as illustrated in Figs. 2.6-(m) and (n). However, there are only N distinct complex values computable from Eq.(2.30). To establish this fact let $n = r$ where r is an arbitrary integer Eq(2.30) becomes

$$\tilde{H}\left(\frac{r}{NT}\right) = \sum_{k=0}^{N-1} h(kT) e^{-i2\pi kr/N} \qquad (2.31)$$

Now let $n = r + N$; note that

$$e^{-i2\pi k(r+N)/N} = e^{-i2\pi kr/N} e^{-i2\pi k} = e^{-i2\pi kr/N} \qquad (2.32)$$

since $e^{-i2\pi k} = \cos(2\pi k) - i \cdot \sin(2\pi k) = 1$ for k integer valued. Thus for $n = r + N$

$$\begin{aligned} \tilde{H}\left(\frac{r+N}{NT}\right) &= \sum_{k=0}^{N-1} h(kT) e^{-i2\pi k(r+N)/N} \\ &= \sum_{k=0}^{N-1} h(kT) e^{-i2\pi kr/N} = \tilde{H}\left(\frac{r}{NT}\right) \end{aligned} \qquad (2.33)$$

Therefore, there are only N distinct values for which Eq.(2.30) can be evaluated; $\tilde{H}\left(\frac{n}{NT}\right)$ is periodic with a period of N samples. Fourier transform Eq.(2.30) can be expressed

$$\tilde{H}\left(\frac{n}{NT}\right) = \sum_{k=0}^{N-1} h(kT) e^{-i2\pi nk/N} \qquad n = 0, 1, \ldots, N-1 \qquad (2.34)$$

Eq.(2.34) is the desired discrete Fourier transform; the expression relates N samples of time and N samples of frequency by means of the continuous Fourier transform. The discrete Fourier transform is then a special case of the continuous Fourier transform. If it is assumed that the N samples of the original function $h(t)$ are one period of a periodic waveform, the Fourier transform of this periodic function is given by the N samples as computed by Eq.(2.34). Notation $\tilde{H}\left(\frac{n}{NT}\right)$ is used to indicated that the discrete Fourier transform is an approximation to the continuous Fourier transform. Normally, Eq.(2.34) is written as

$$G\left(\frac{n}{NT}\right)=\sum_{k=0}^{N-1}g(kT)e^{-i2\pi nk/N} \qquad n=0,1,\ldots,N-1 \qquad (2.35)$$

since the Fourier transform of the sampled periodic function $g(kT)$ is identically $G\left(\frac{n}{NT}\right)$.

The result of Eq.(2.35) is very important and useful since it tells us that *we only need to calculate one period of positional or momental change of a system to get its vibrational frequency.*

2.6 Dynamical Quantum Mechanics

From quantum mechanics, a function $\Psi(x,t)$ can be expanded as

$$\Psi(x,t)=\sum_{m}\left|\Phi_m(x)\right\rangle\left\langle\Phi_m(x)\right|\Psi\rangle e^{-iE_m t/\hbar} \qquad (2.36)$$

$\sum_{m}\left|\Phi_m(x)\right\rangle\left\langle\Phi_m(x)\right|$ is a complete set of eigenstates, and E_m are the corresponding eigenvalues.

If $\Psi(x,t)$ is a function which is obtained by position-displacing the one of the complete set $\sum_{m}\left|\Phi_m(x)\right\rangle\left\langle\Phi_m(x)\right|$.

$$\Psi(x,t)=\Phi'(x',t)=\Phi(x+\delta x,t) \qquad (2.37)$$

Figure 2.7 shows the relationship among the potential $V(r)$, one of the original state functions $\Phi(x,t)$ and the displaced function $\Phi'(x',t)$ at $t=0$.

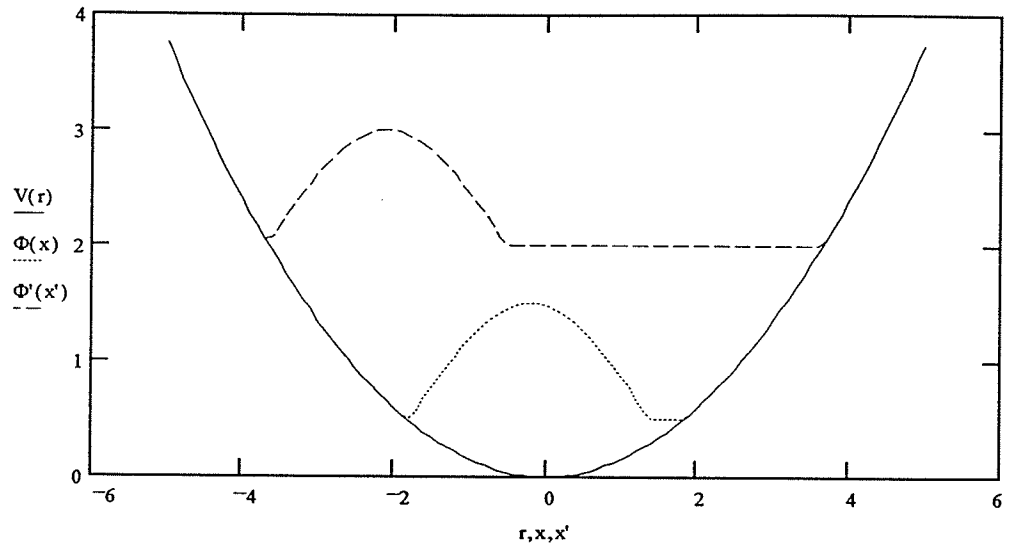

Figure 2.7 Relative position of $\Psi(x,t)$ and $\Phi(x,t)$ when $t = 0$.

When $t = t_1$, the Fig.2.7 evolves as Fig.2.8;

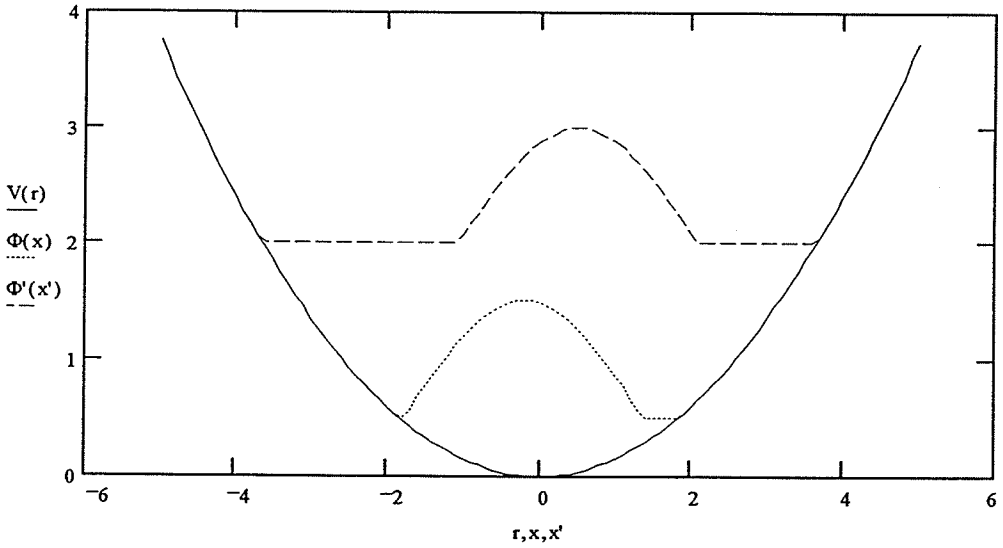

Figure 2.8 Evolution of $\Psi(x,t)$ relative to $\Phi(x,t)$ when $t = t_1$

It is noticed that the wave packet $\Phi'(x',t)$ moves back and forward in the potential well with respect to time; hence the evolution time of the packet can be derived from its motion. Usually the evolution time is the function of the displacement of position

$$t\_evol = f(\delta x) \qquad (38)$$

and sometimes the packet will diffuse with time.

3. Harmonic Potential of HCl Molecule

The potential function is a different function not only for each molecule, but for each electronic state of each molecule. Rather than deal with a different nuclear Schrodinger equation for each molecular electronic state, we seek an approximation that will represent a potential reasonably well for most interactions between two bonded atoms in a molecular system.

The interaction between two covalently bonded atoms is one of the strongest interactions among the atomic interactions in a system. It is reasonable to expect that the nuclei vibrate about the position of minimum potential energy and the nuclear separation doesn't deviate from its equilibrium bond distance very much; therefore, we expand a potential V in a Taylor series about its equilibrium internuclear separation r_e

$$V(r) = V(r_e) + V'(r_e)(r - r_e) + \frac{1}{2!}V''(r_e)(r - r_e)^2 + \frac{1}{3!}V'''(r_e)(r - r_e)^3 + \ldots \quad (3.1)$$

At the position of the equilibrium internuclear separation r_e,, the potential energy is minimum and its first derivative is zero

$$V'(r_e) = 0 \quad (3.2)$$

For the region near r_e, we note that $(r - r_e)^3$ and higher powers of $(r - r_e)$ are small, and can be neglected; we justify this by saying that for small vibrations the internuclear separation will be close to r_e most of the time. Thus Eq.(3.1) becomes

$$V(r) = V(r_e) + \frac{1}{2!}V''(r_e)(r - r_e)^2 \quad (3.3)$$

The $V(r_e)$ is a constant and we can set it as zero; hence Eq.(3.3) becomes

$$V(r) = \frac{1}{2}V''(r_e)(r - r_e)^2 \quad (3.4)$$

For example, the potential of the molecule hydrogen chloride is written as

$$V(r) = \frac{k}{2}(r - r_e)^2 \quad (3.5)$$

in which $r_e = 127.45pm$, and $k = 515.8kg \cdot \sec^{-2}$.

The shape of the potential is a parabolic as shown in Fig.3.1

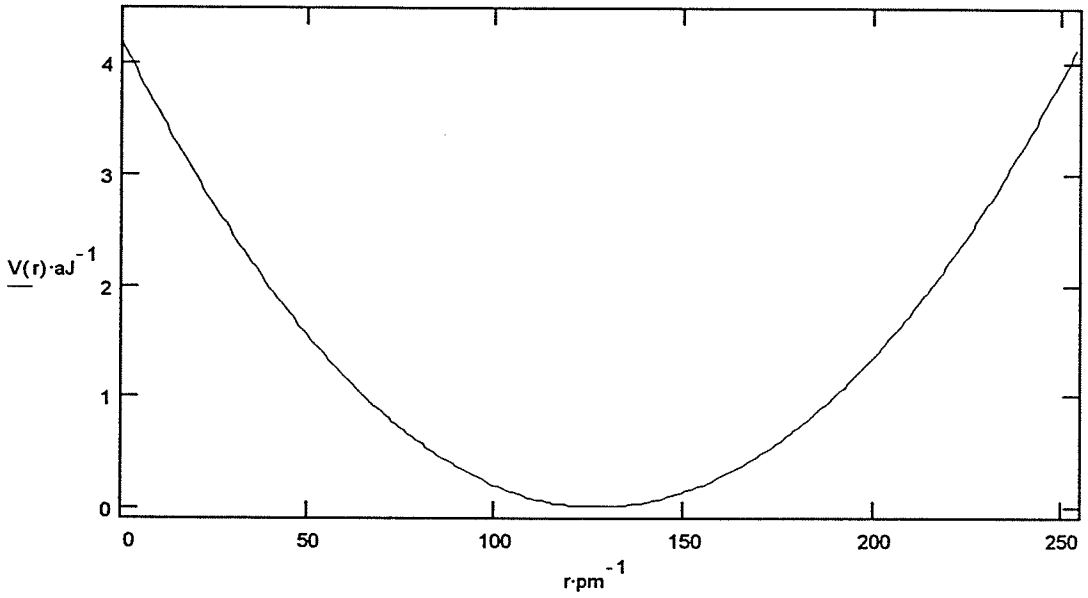

Figure 3.1 The parabolic shape of the HCl molecular harmonic potential

From classical mechanics, the vibration frequency of a particle in the molecule under a harmonic potential interaction is always constant

$$\nu = \frac{1}{2\pi}\sqrt{\frac{k}{\mu}} \qquad \frac{1}{\lambda} = \frac{\nu}{c} = 2991.0cm^{-1} \qquad (3.6)$$

Dealing with this system by quantum mechanics, the energy eigenvalues are obtained by solving Schrodinger equation

$$E_n = \left(n + \frac{1}{2}\right)h\nu \qquad (3.7)$$

The absorption or emission frequency can be calculated from the eigenvalues

$$\frac{1}{\lambda} = \frac{1}{c}\cdot\frac{E_{n+1} - E_n}{h} = 2991.0cm^{-1} \qquad (3.8)$$

Hence for a harmonic potential system, classical mechanics and quantum mechanics approach the same conclusion: the nuclear vibration frequency is independent of the total energy put into the system.

Molecular dynamics simulation computes the position and momentum change with time. From Newtonian mechanics, the acceleration caused by the force exerted on this system is

$$a(r) = -\frac{1}{\mu}\frac{d}{dr}V(r) = -\frac{1}{\mu}\frac{d}{dr}\{\frac{k}{2}\cdot(r-r_e)^2\} \qquad (3.9)$$

From Eq.(3.9) the position and momentum changes with time can be computed by molecular dynamics simulation. In order to start the simulation calculation, the initial conditions are necessary. Set the initial conditions as follows

$$r_{init} = 145pm, \qquad v_{init} = 3000.0m\cdot\sec^{-1} \qquad (3.10)$$

The energy given to the system is contained in the initial conditions

$$E = \frac{1}{2}\cdot\mu\cdot v_{init}^2 + V(r_{init}) = 0.0868aJ \qquad (3.11)$$

The conventional way of portraying energies is to draw the potential energy curve and superimpose the total energy upon this curve. The kinetic energy at any distance is the vertical line between potential and total energy.

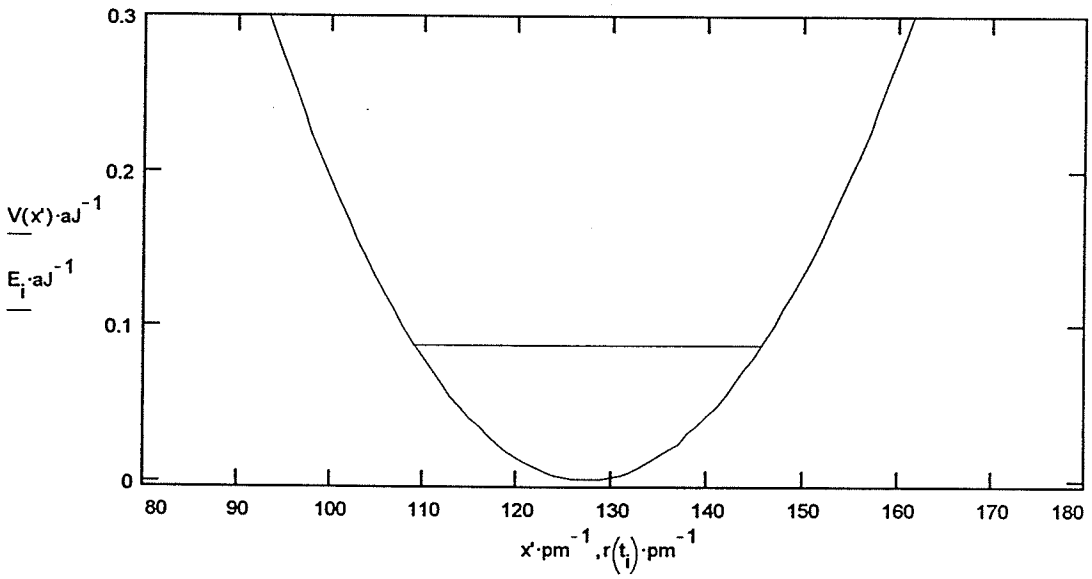

Figure 3.2 The position of total energy $E = 0.0868aJ$ on the harmonic potential surface.

The simulation time array is defined as

$$t = h\cdot i \qquad (3.12)$$

in which

$$h = \frac{t_{max} - t_{min}}{Steps}\cdot\sec^{-1} \qquad i = 1,2,3,.....,Steps \qquad (3.13)$$

From initial conditions set initial X matrix column as

$$X = \begin{pmatrix} r_{init} \cdot m^{-1} \\ v_{init} \cdot m^{-1} \cdot \sec \end{pmatrix} \tag{3.14}$$

and define the derivative column vector as

$$D(t,X) = \begin{bmatrix} X_1 \\ -\frac{1}{\mu} \cdot \frac{d}{dr} V(r)\Big|_{r=X_0} \end{bmatrix} \tag{3.15}$$

From Eqs(3.14) and (3.15) the X is filled with solutions of following equation

$$X^{\langle i \rangle} = X^{\langle i-1 \rangle} + RK\left(t_{i-1}, X^{\langle i-1 \rangle}, D, h\right) \tag{3.16}$$

in which $RK(t,X,D,h)$ is the Runge Kutta integration[10] and is modified as

$$\begin{aligned}
&K1(t,X,D,h) \equiv D(t,X) \\
&K2(t,X,D,h) \equiv D\left(t+\frac{h}{2}, X+\frac{h}{2}\cdot K1(t,X,D,h)\right) \\
&K3(t,X,D,h) \equiv D\left(t+\frac{h}{2}, X+\frac{h}{2}\cdot K2(t,X,D,h)\right) \\
&K4(t,X,D,h) \equiv D(t+h, X+h\cdot K3(t,X,D,h)) \\
&RK(t,X,D,h) \equiv \frac{h}{6}\cdot(K1(t,X,D,h)+2\cdot K2(t,X,D,h)+2\cdot K3(t,X,D,h)+K4(t,X,D,h))
\end{aligned} \tag{3.17}$$

The positional and momental changes with time are obtained from Eq.(3.16)

$$t = t \cdot \sec \qquad r_i = X_{0,i} \cdot m \qquad v_i = X_{1,i} \cdot m \cdot \sec^{-1} \qquad P_i = \mu \cdot v_i \tag{3.18}$$

As shown in Figure 3.3, the bond length oscillates back and forth in a regular periodic fashion between minimum and maximum values. The time spent in the vicinity of the compressed bond turning point is the same as that at the stretched bond turning point.

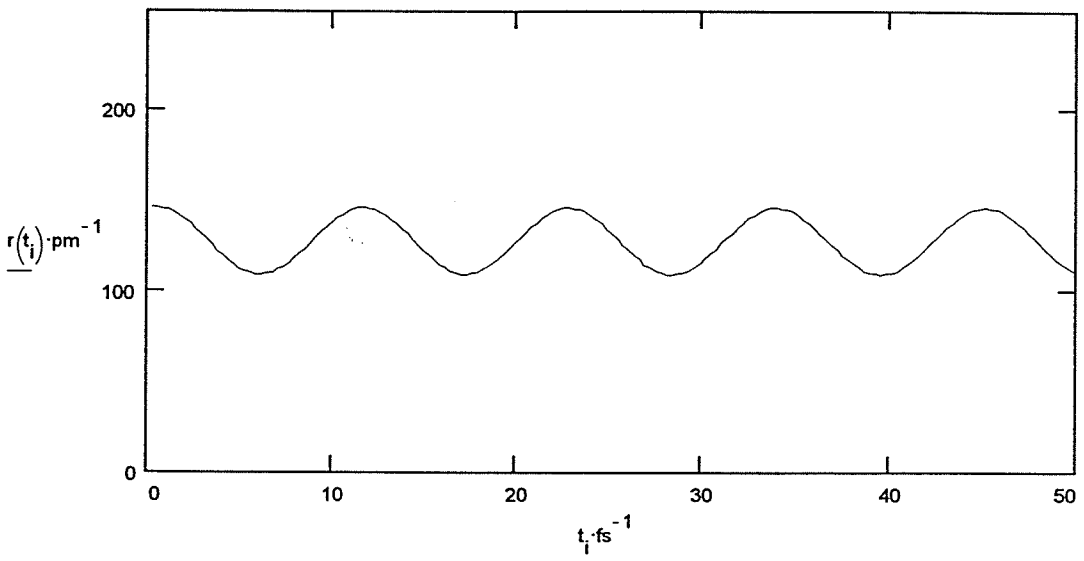

Figure 3.3 The periodic change of the bond length with time when $E = 0.0868aJ$.

However the momentum, although it is periodic, does not behave in the same fashion; between them there exists a phase difference as shown in Fig. 3.4

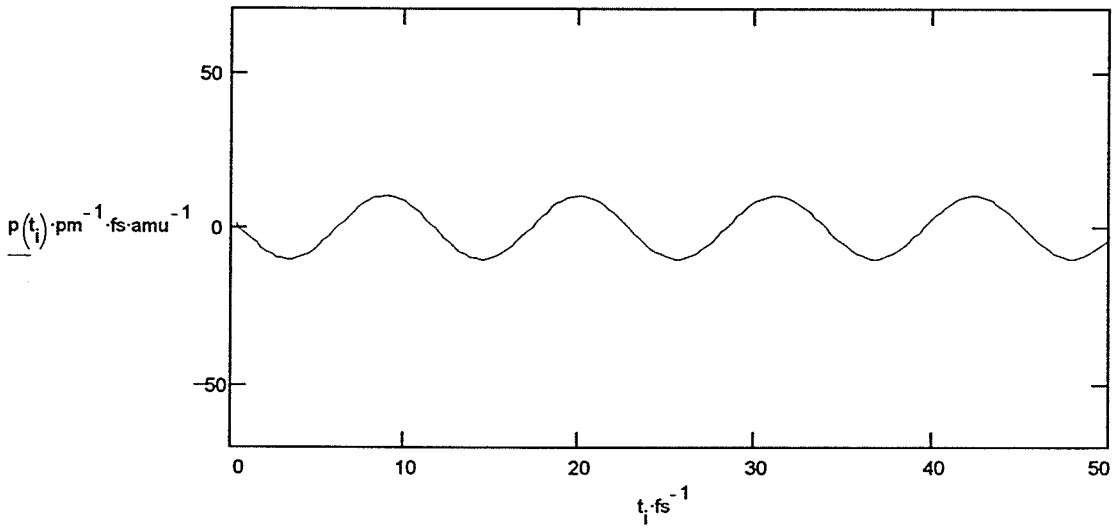

Figure 3.4 The periodic change of the *HCl* molecular nuclear motion momentum with time when $E = 0.0868aJ$.

By the fast Fourier transform, transform the position from the time domain to the frequency domain and get its frequency constituent

$$\sigma\_fft = \frac{1}{\lambda_{fft}} = FFT\left[r(t)\Big|_{E=0.0868aJ}\right] = 2991.0 \cdot cm^{-1} \qquad (3.19)$$

The phase portrait of this system is obtained from molecular dynamics simulation computation as shown in Fig.3.5

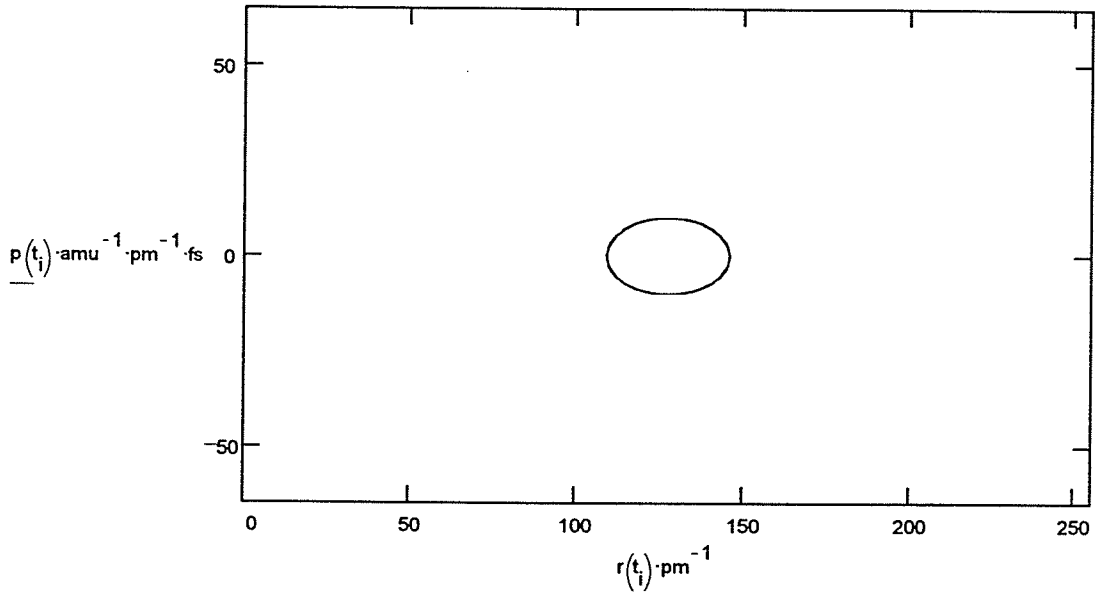

Figure 3.5 The phase portrait of the *HCl* molecular nuclear motion when $E = 0.0868aJ$.

The time taken to complete a cycle defines the period

$$period = 11.15\cdot fs \qquad \frac{1}{\lambda} = \frac{1}{c}\cdot\frac{1}{period} = 2991.0\cdot cm^{-1} \qquad (3.20)$$

It is noticed that the vibrational frequency is independent of initial conditions, i.e., the energy put into the system. For example, change the initial conditions Eqs.(3.10) as following

$$r_{init} = 245pm \qquad v_{init} = 3000.0m\cdot \sec^{-1} \qquad (3.21)$$

The energy given to the system is contained in the initial conditions

$$E = \frac{1}{2}\cdot\mu\cdot v_{init}^2 + V(r_{init}) = 1.365aJ \qquad (3.22)$$

The potential curve and superimposition of total energy are shown in Fig.3.6.

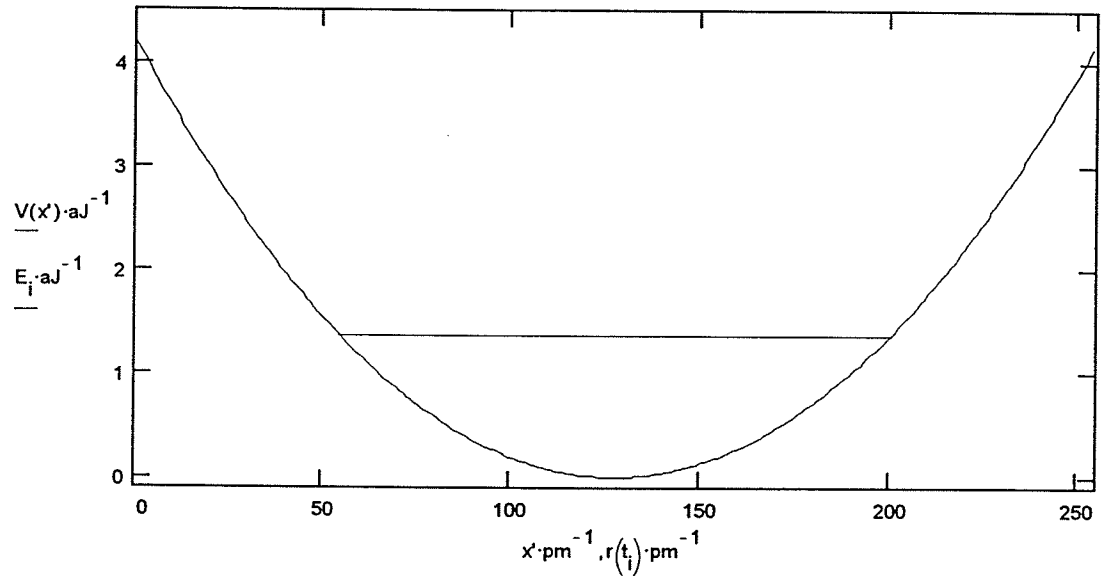

Figure 3.6 The position of total energy $E = 1.3650aJ$ on the harmonic potential surface.

The bond length variation with time under initial conditions Eq.(3.21) is shown in Fig.3.7

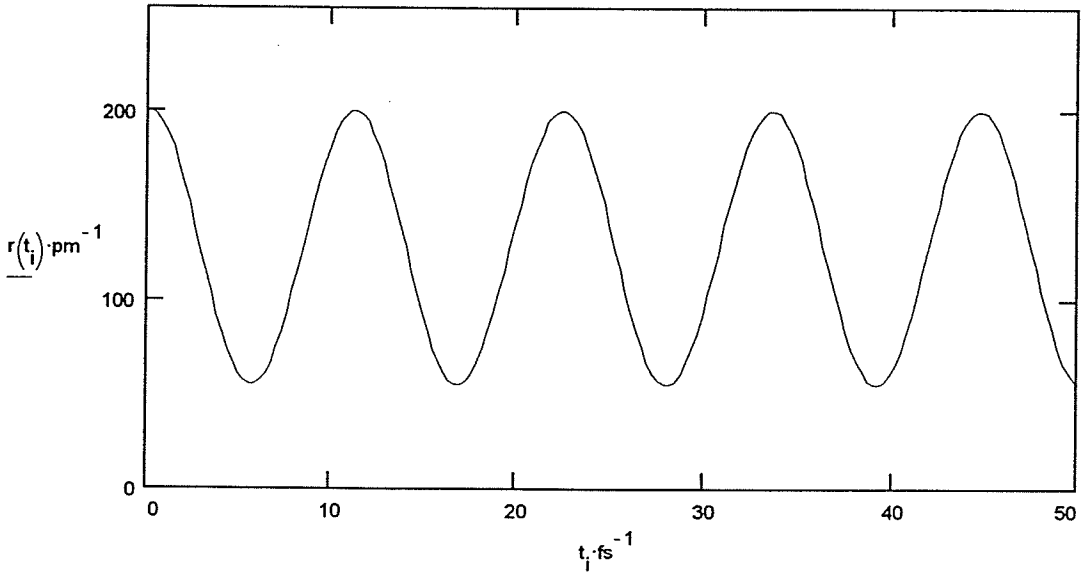

Figure 3.7 The periodic change of the bond length with time when $E = 1.3650aJ$.

The momental variation with respect to time under initial conditions Eq.(3.21) is shown in Fig.3.8

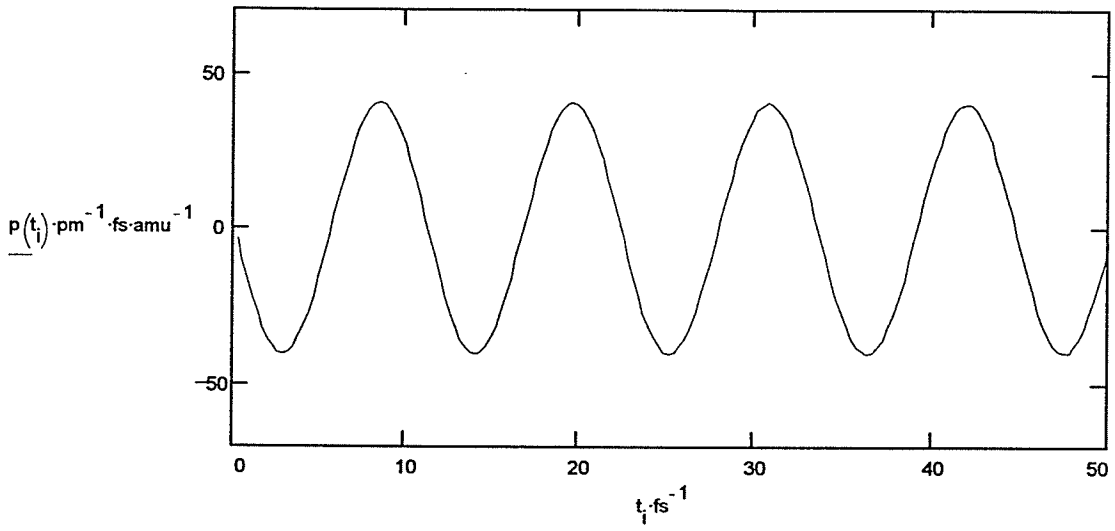

Figure 3.8 The periodic change of the *HCl* molecular nuclear motion momentum with time when $E = 1.3650aJ$.

From the fast Fourier transform of $r(t)$, the frequency of its vibration doesn't change

$$\sigma\_fft = \frac{1}{\lambda_{fft}} = FFT\left[r(t)\Big|_{E=1.365aJ}\right] = 2991.0 \cdot cm^{-1} \qquad (3.23)$$

The phase space portrait under initial conditions Eq(3.21) is shown in Fig.3.9

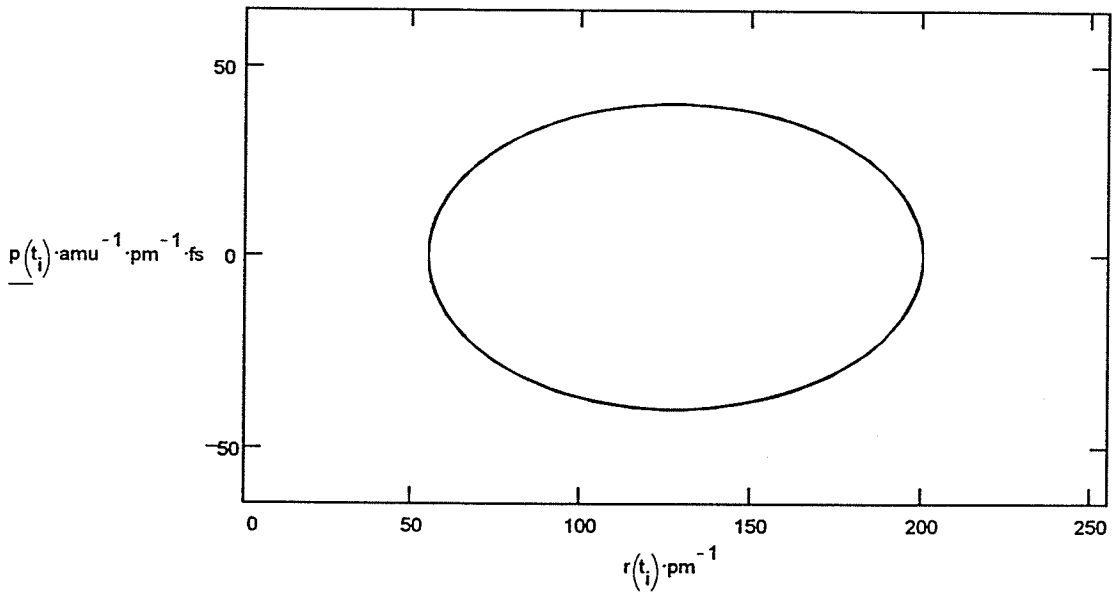

Figure 3.9

Figure 3.9 The phase portrait of the *HCl* molecular nuclear motion when $E = 1.3650aJ$.

From the phase portrait it is shown that the period remains constant. Hence it is demonstrated that the frequency of the bond vibration doesn't change with the energy put into the system.

The Hamiltonian of the harmonic potential of the molecule *HCl* is written as

$$-\frac{\hbar^2}{2\mu}\cdot\frac{d^2}{dr^2}\Phi(x)+\frac{1}{2}k(x-r_e)^2\Phi(x)=E\Phi(x) \qquad (3.24)$$

Substitute $r = x - r_e$ into Eq.(23); Eq.(23) becomes

$$-\frac{\hbar^2}{2\mu}\cdot\frac{d^2}{dr^2}\Phi(r)+\frac{1}{2}\cdot k\cdot r^2\cdot\Phi(r)=E\cdot\Phi(r) \qquad (3.25)$$

Using the Numerov[8] , Eq.(3.24) can be solved to obtain its eigenstate functions $\Phi_n(r)$ and eigenvalues E_n.

$\Phi_n(r)$ is a set of stationary eigenfunctions of Eq.(3.25). For example, the distribution of the probability density of $\Phi_0(r)$, $P(r,t) = \langle \Phi_0(r)\varphi(t) | \Phi_0(r)\varphi(t) \rangle$, doesn't change with respect to time. The contour plot of $P(r,t) = M$ is shown in Fig.3.10.

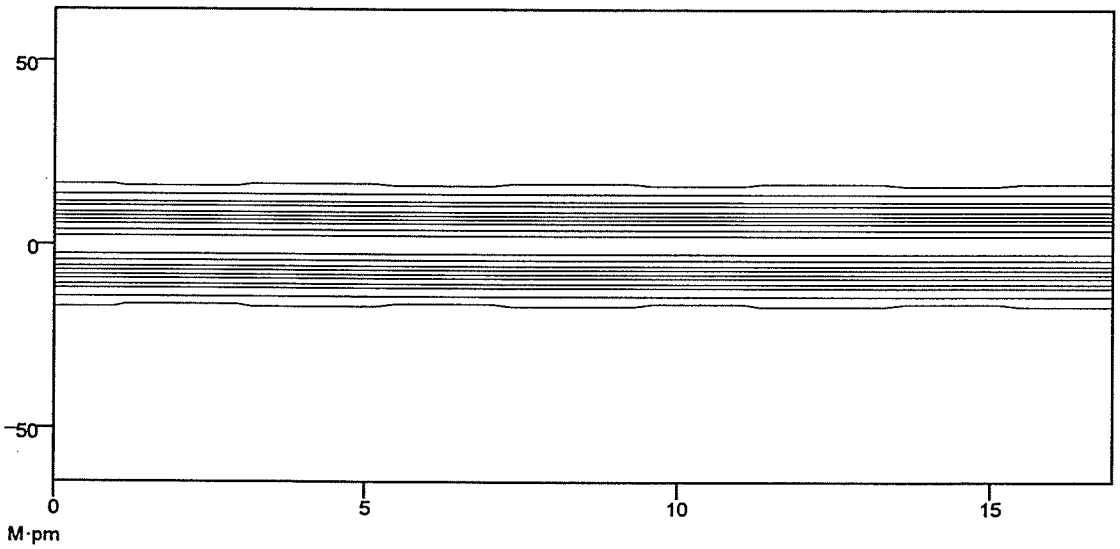

Figure 3.10 The contour plot of the probability density of $\Phi_0(r)$ in which the x axis is t and the y is r.

However, it is possible to get the dynamical properties of the system from the motion of a non stationary state. Usually the non stationary state can be obtained by displacing and reshaping $\Phi_n(r)$

$$\Phi_0'(r',t) = D(\delta r)\left[R(x)\Phi(r)\right]\cdot\varphi_0(t) \qquad (3.26)$$

in which

$$D(\delta r)\Phi(r) = \Phi(r+\delta r) \qquad (3.27)$$

and $R(x)$ means that changes the width of $\Phi_0(r)$ x times.

When

$$D(\delta r) = D(0) \text{ and } R(x) = R(2) \qquad (3.28)$$

the relationship between $\Phi_0(r)$ and $\Phi_0'(r')$ is shown in Fig.3.11.

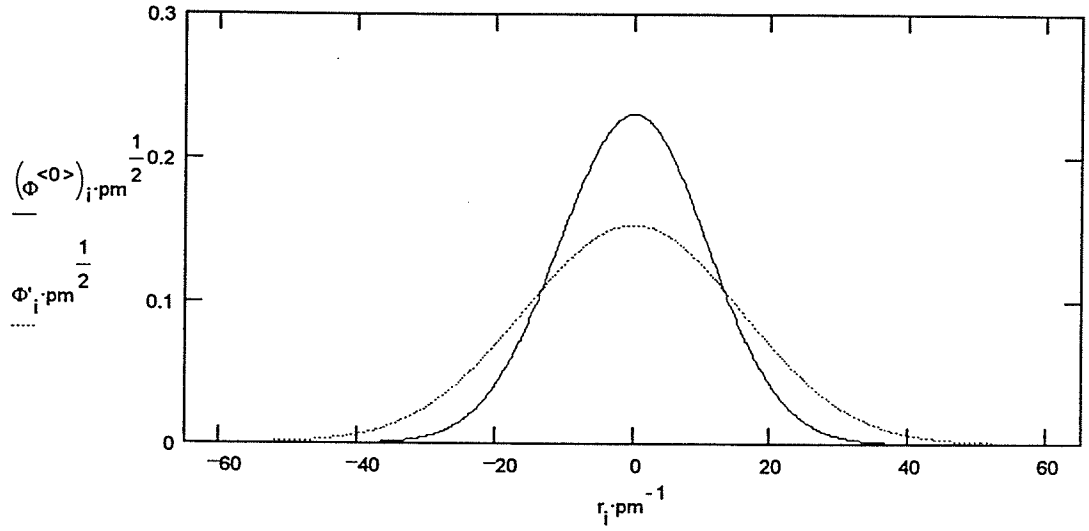

Figure 3.11 The shape and position of $\Phi'_0(r',0) = D(0)\left[R(2)\Phi_0(r)\right]\cdot\varphi_0(0)$ relative to $\Phi_0(r,0)$.

The wave packet movement of $\Phi'_0(r',t)$ with respect to time can be demonstrated by the motion of its probability density with time.

$$\boldsymbol{Prob}(\mathbf{x},\mathbf{t}) = \Phi'_0(r',t)\cdot\left[\Phi'_0(r',t)\right]^* \qquad (3.29)$$

The change of the probability density $\boldsymbol{Prob}(\mathbf{x},\mathbf{t}) = \mathbf{M}$ distribution is shown in Fig.3.12.

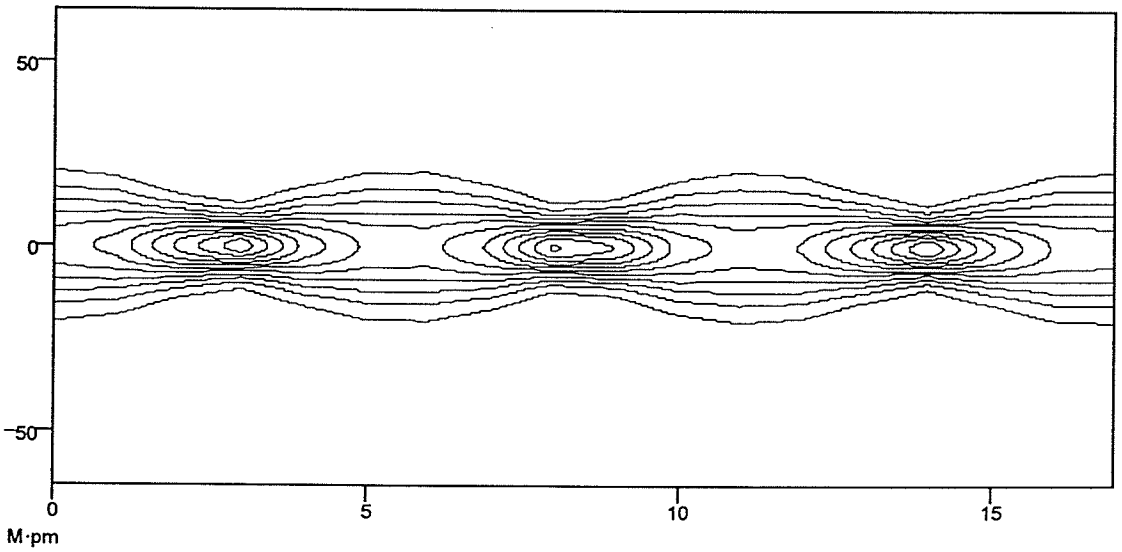

Figure 3.12 The contour plot of the probability density of $D(0)\left[R(2)\Phi(r)\right]\cdot\varphi_0(t)$ in which the x axis is t and the y axis is r.

It is known that the average energy of $\Phi_0'(r',t)$ depends on both δr of $D(\delta r)$ and x of $R(x)$

$$\overline{E}(\delta r, x) = \left\langle \Phi_0'(r',t) \middle| \hat{H} \middle| \Phi_0'(r',t) \right\rangle \qquad (3.30)$$

From the Fig. 3.12 the evolution time of the wave package movement is estimated as

$$t\_evol(\overline{E})\Big|_{\overline{E}(0,2)=0.1378aJ} = 11.15fs \qquad (3.31)$$

When $D(\delta r) = D(30)$ and $R(x) = R(1)$, the relationship between $\Phi_0(r)$ and $\Phi_0'(r')$ is shown in Fig.3.13

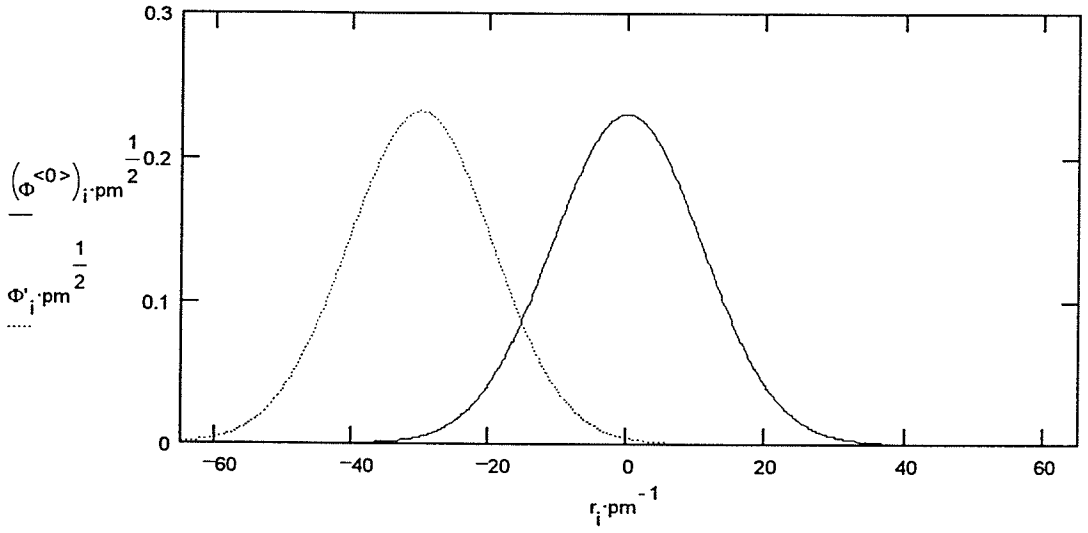

Figure 3.13 The shape and position of $\Phi_0'(r',0) = D(30)\left[R(1)\Phi_0(r)\right] \cdot \varphi_0(0)$ relative to $\Phi_0(r,0)$

The change of the probability density $\boldsymbol{Prob(x,t) = M}$ distribution is shown in Fig.3.14.

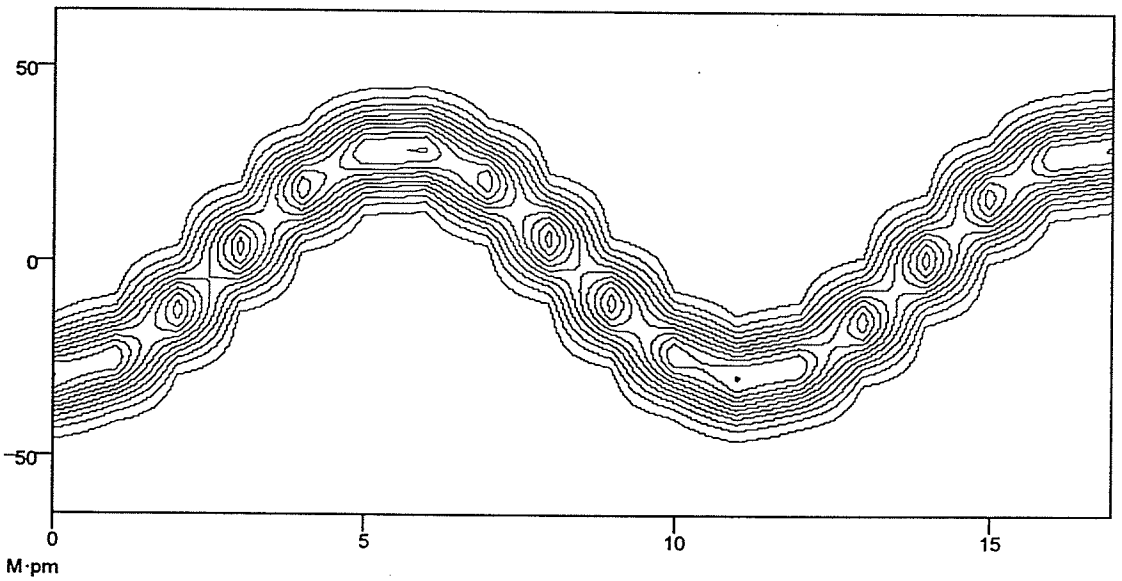

Figure 3.14 The contour plot of the probability density of $D(30)\left[R(1)\Phi(r)\right]\cdot\varphi_0(t)$ in which the x axis is t and the y axis is r.

From the Fig. 3.12 the evolution time of the wave packet movement is estimated as

$$t\_evol(\bar{E})\Big|_{\bar{E}(30,1)=0.2621aJ} = 11.15fs \qquad (3.32)$$

The bumps shown in the figure are because the packet movement diffuses with the time.

When $D(\delta r) = D(15)$ and $R(x) = R(2)$, the relationship between $\Phi_0(r)$ and $\Phi_0'(r')$ is shown in Fig.3.15.

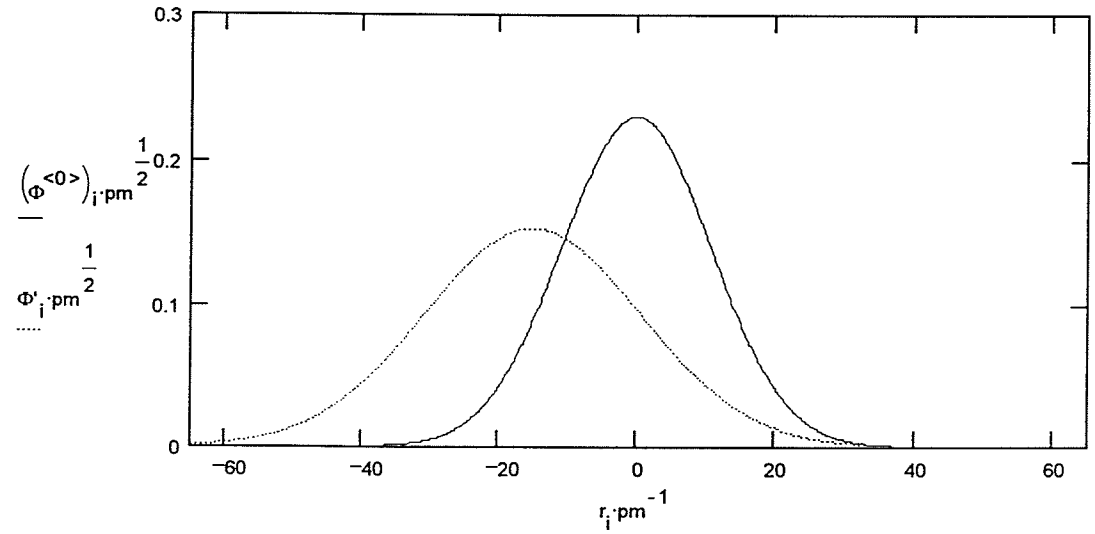

Figure 3.15 The shape and position of $\Phi_0'(r',0) = D(15)\left[R(2)\Phi_0(r)\right]\cdot\varphi_0(0)$ relative to $\Phi_0(r,0)$.

The change of the probability density ***Prob*(x,t) = M** distribution is shown in Fig.3.16.

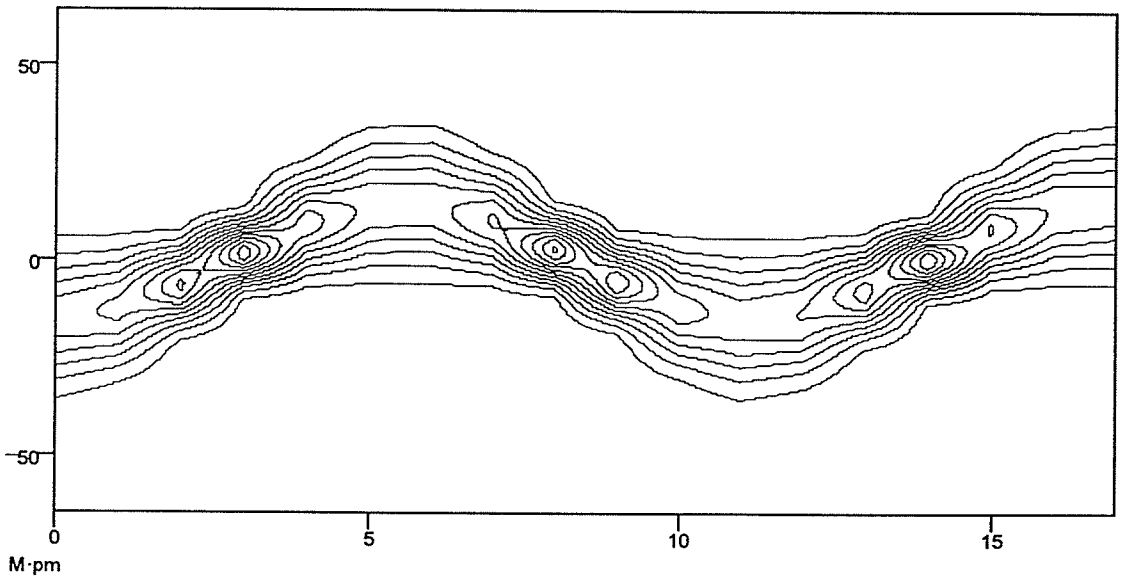

Figure 3.16 The contour plot of the probability density of $D(15)\left[R(2)\Phi(r)\right]\cdot\varphi_0(t)$ in which the x axis is t and the y axis is r.

From the Fig. 15 the evolution time of the wave package movement is estimated as

$$t\_evol(\bar{E})\Big|_{\bar{E}(15,2)=0.3354aJ} = 11.15fs \qquad (3.33)$$

When $D(\delta r) = D(0)$ and $R(x) = R(0.35)$, the relationship between $\Phi_0(r)$ and $\Phi_0'(r')$ is shown in Fig.3.17.

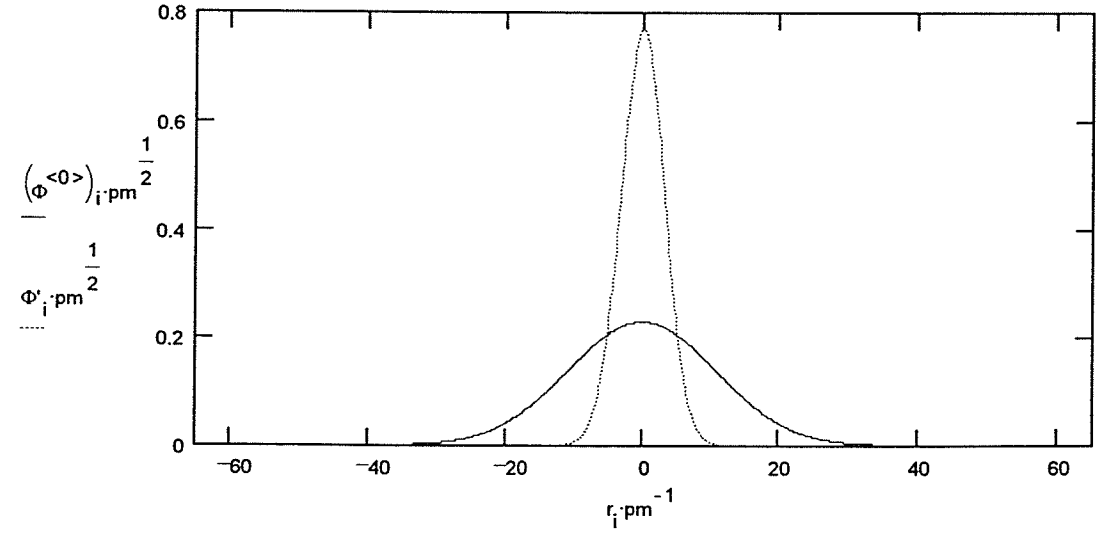

Figure 3.17 The shape and position of $\Phi_0'(r',0) = D(0)\left[R(0.35)\Phi_0(r)\right]\cdot\varphi_0(0)$ relative to $\Phi_0(r,0)$.

The change of the probability density ***Prob*(x,t) = M** distribution is shown in Fig.3.18

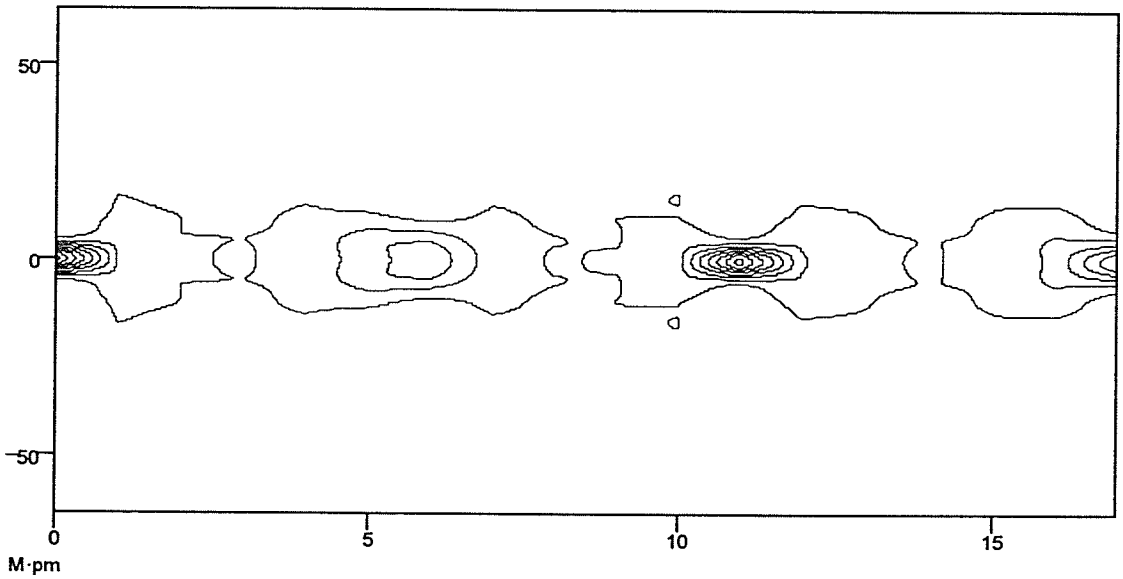

Figure 3.18 The contour plot of the probability density of $D(0)\left[R(0.35)\Phi(r)\right]\cdot\varphi_0(t)$ in which the x axis is t and the y axis is r.

From the Fig. 3.18 the evolution time of the wave packet movement is estimated as

$$t\_evol(\bar{E})\big|_{\bar{E}(0,0.35)=0.0479aJ} = 11.15fs \qquad (3.34)$$

When $D(\delta r) = D(45)$ and $R(x) = R(0.35)$, the relationship between $\Phi_0(r)$ and $\Phi_0'(r')$ is shown in Fig.3.19.

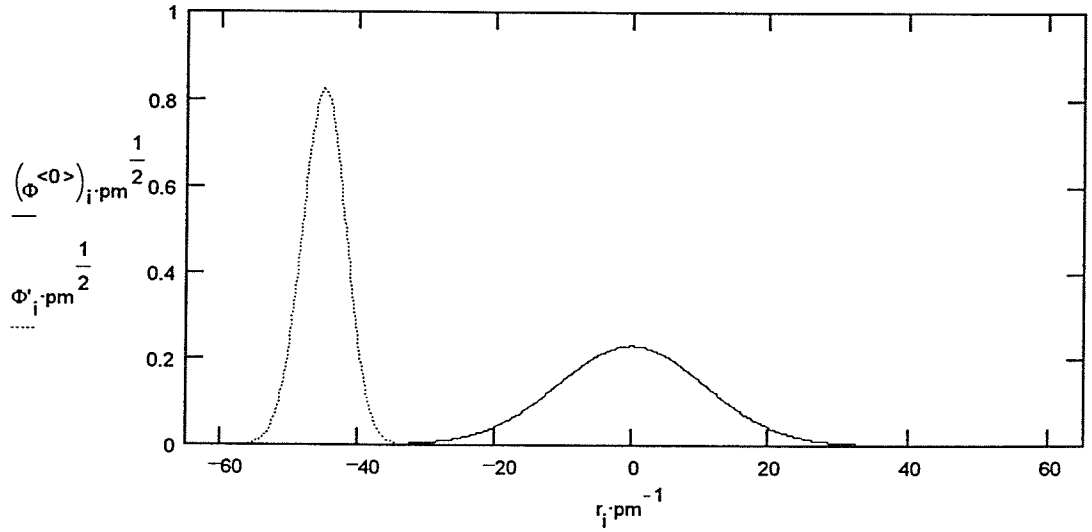

Figure 3.19 The shape and position of $\Phi_0'(r',0) = D(45)\left[R(0.35)\Phi_0(r)\right]\cdot\varphi_0(0)$ relative to $\Phi_0(r,0)$.

The change of the probability density ***Prob*(x, t) = M** distribution is shown in Fig.3.20

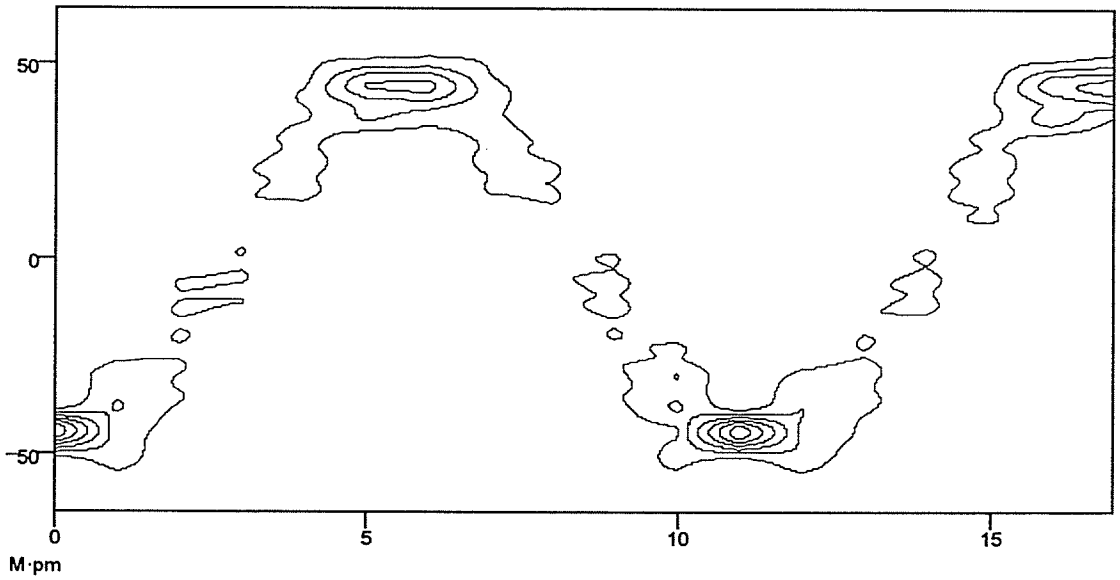

Figure 3.20 The contour plot of the probability density of $D(45)\left[R(0.35)\Phi(r)\right]\cdot\varphi_0(t)$ in which the x axis is t and the y axis is r.

From the Fig. 20 the evolution time of the wave package movement is estimated as

$$t\_evol(\bar{E})\big|_{\bar{E}(45,0.35)=0.1829aJ} = 11.15fs \qquad (3.35)$$

From the above discussion, it is clearly shown for a harmonic potential system that classical, stationary and dynamical quantum mechanics give the same results which is that the frequency of the bond vibration doesn't change with respect to the energy put into the system. However this potential is good only a small vibration range; that is , when a system's total energy is much smaller than its dissociation energy, the harmonic potential is an ideal potential approximation. When a system's total energy is near to its dissociation energy, the vibration range is not small enough for the harmonic potential approximation and looking for other potential forms are required.

4. Morse Potential of HCl Molecule

From the above discussion we know that the harmonic oscillator does not reflect a real interaction between the bonded atoms in a molecule and does not fit to large amplitude vibration. The Morse potential provides a more accurate description of the interaction on stretching vibrations than the harmonic oscillator does since the Morse potential describes dissociation of the bond. However the bottom of the Morse potential well is similar in shape to the harmonic well, it can be predicted for really small vibrations about the equilibrium that both of them would yield similar dynamical motion pictures. The Morse oscillator is better for a greater degree of excitation than harmonic oscillator.

The form of the Morse potential is written as

$$V(r) = De\left[1 - e^{-a(r-r_e)}\right]^2 \qquad (4.1)$$

For the HCl molecule, dissociation energy De and the parameter a are as follows

$$De = 0.71aJ$$

$$a = \left(\frac{k}{2De}\right)^{1/2}$$

$$k = 4\pi^2 c^2 \left(\frac{1}{\lambda}\right)^2 \mu$$

$$\frac{1}{\lambda} = 2991cm^{-1} \qquad \mu = \frac{m_H m_{Cl}}{m_H + m_{Cl}}$$

The shape of the Morse potential curve is shown in Fig 4.1

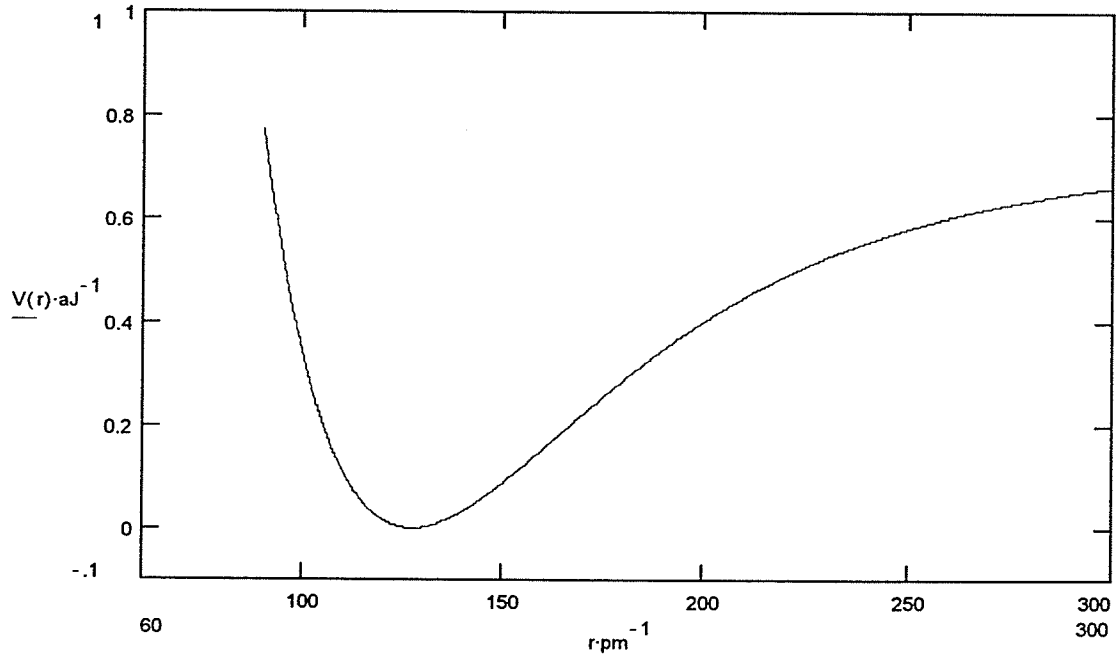

Figure 4.1 The shape of the HCl molecular Morse potential.

It is seen that at the bottom of the well near the equilibrium internuclear separation of the HCl molecule the shape of the Morse potential is similar to that of the harmonic potential. Further up we see how the potential flattens out for a large internuclear separation as the dissociation energy is reached.

From Newtonian mechanics, the acceleration corresponding to the Morse potential is

$$a(r) = -\frac{1}{\mu}\frac{d}{dr}V(r) = -\frac{1}{\mu}\frac{d}{dr}\left\{De\left[1-e^{-a(r-r_e)}\right]^2\right\} \qquad (4.2)$$

From Eq.(4.2) the position and momental changes with respect to time can be obtained by molecular dynamic simulation calculation. The motion of the system and the results of dynamical simulation computation depend on the total energy put into the system. For example, with initial conditions

$$r_{init} = 1.1 \cdot r_e, \qquad v_{init} = 100.0 \cdot m \cdot \sec^{-1} \qquad (4.3)$$

the energy given to the system is contained in the initial conditions

$$E = \frac{1}{2}\mu v_{init}^2 + V(r_{init}) = 0.033aJ \qquad (4.4)$$

The energies are shown in Fig.4.2 by a conventional way that draws the potential energy curve and superimposes the total energy upon this curve. The kinetic energy at any distance is the vertical line between potential and total energy.

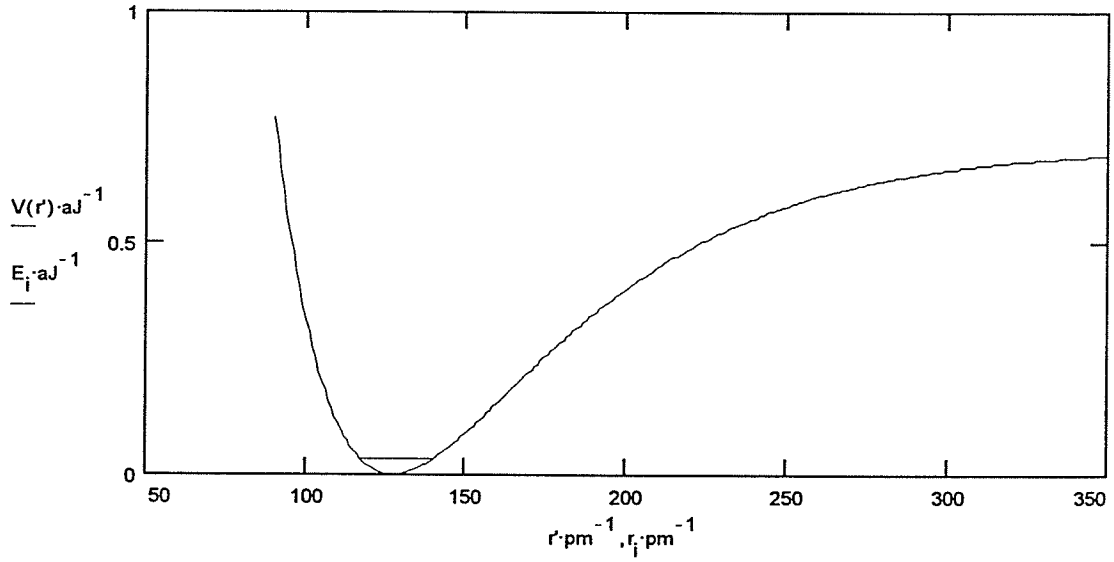

Figure 4.2 The position of total energy $E = 0.033aJ$ on the Morse potential surface.

The simulation time array t is defined as

$$t_i = h \cdot i \qquad i = 1, 2, \ldots, Steps \qquad (4.5)$$

in which

$$h = \frac{t_{\max} - t_{\min}}{Steps} \qquad (4.6)$$

From initial conditions, set initial X matrix column as

$$X^{(0)} = \begin{pmatrix} r_{init} \cdot m^{-1} \\ v_{init} \cdot m^{-1} \cdot \sec \end{pmatrix} \qquad (4.7)$$

and define the derivative column vector as

$$D(t,x)=\begin{bmatrix} X_1 \\ -\frac{1}{\mu}\frac{d}{dr}V(r)\Big|_{r=X_0} \end{bmatrix} \qquad (4.8)$$

From Eqs (4.7) and (4.8) we can fill the X matrix with solutions by following equation.

$$X^{\langle i\rangle} := X^{\langle i-1\rangle} + RK\left(t_{i-1}, X^{\langle i-1\rangle}, D, h\right) \qquad (4.9)$$

in which $RK(t, X, D, h)$ is Runge Kutta integration[10] and is written as

$$K1(t,X,D,h) \equiv D(t,X)$$

$$K2(t,X,D,h) \equiv D\left(t+\frac{h}{2}, X+\frac{h}{2}\cdot K1(t,X,D,h)\right)$$

$$K3(t,X,D,h) \equiv D\left(t+\frac{h}{2}, X+\frac{h}{2}\cdot K2(t,X,D,h)\right)$$

$$K4(t,X,D,h) \equiv D(t+h, X+h\cdot K3(t,X,D,h))$$

$$RK(t,X,D,h) \equiv \frac{h}{6}\cdot(K1(t,X,D,h)+2\cdot K2(t,X,D,h)+2\cdot K3(t,X,D,h)+K4(t,X,D,h)) \qquad (4.10)$$

From Eq.(4.9) the particle's position and momentum change with time

$$t = t\cdot \sec \qquad r_i = X_{0,i}\cdot m \qquad v_i = X_{1,i}\cdot m\cdot \sec^{-1} \qquad p_i = \mu\cdot v_i \qquad (4.11)$$

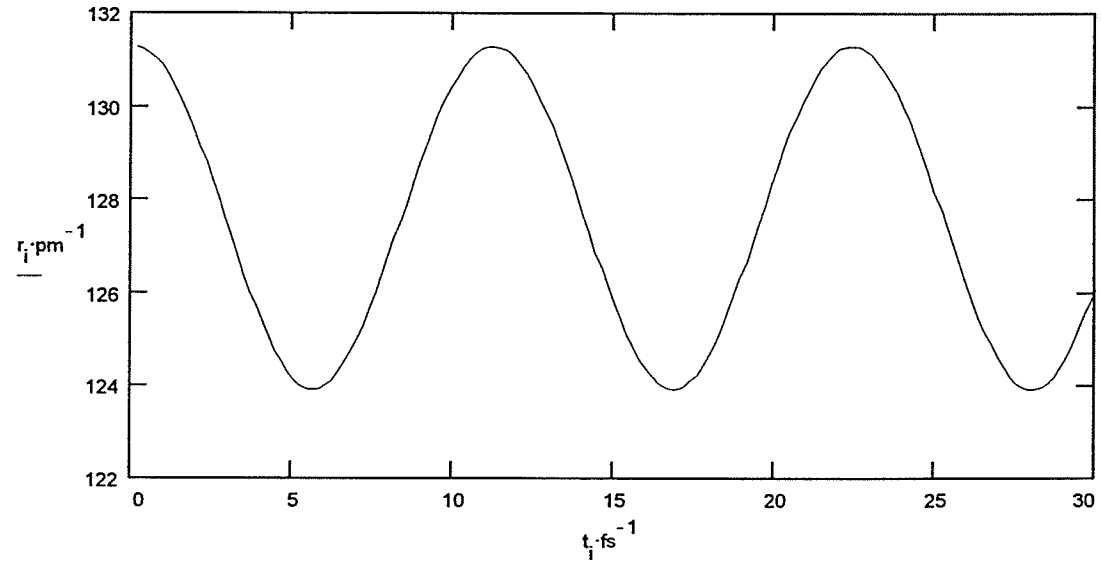

Figure 4.3 The periodic change of the bond length with time when $E = 0.033aJ$.

As shown in Fig. 4.3 the bond length oscillates periodically as the harmonic oscillator does. From the positional change with respect to time the bond vibration frequency can be gotten by the fast Fourier transform;

$$\sigma\_fft(E)\big|_{E=0.033aJ} = \frac{1}{\lambda_{fft}} = FFT\left[r(t)\big|_{E=0.033aJ}\right] = 2900.0cm^{-1} \qquad (4.12)$$

The phase portrait of the system under initial conditions (4.3) is shown in Fig. 4.4

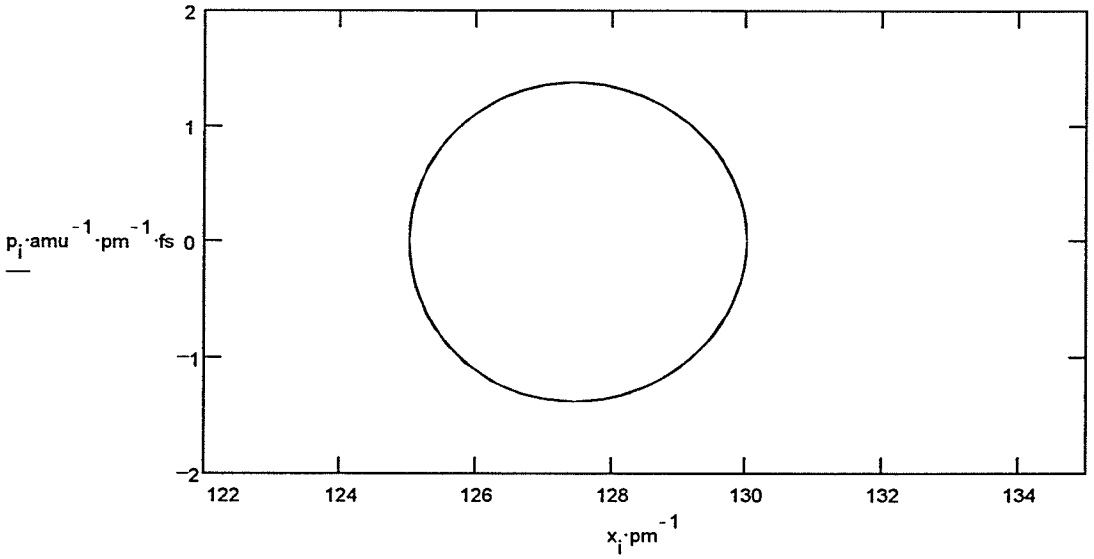

Figure 4.4 The phase portrait of the *HCl* molecular nuclear motion when $E = 0.0868aJ$.

From the phase portrait we can get its period, the time taken to complete one cycle of the phase portrait

$$period(E)\big|_{E=0.033aJ} = 11.437 \cdot fs \qquad (4.13)$$

Its corresponding frequency, the number of periods executed per second, is the reciprocal of the period

$$\nu\_period(E)\big|_{E=0.033aJ} = \frac{1}{period(E)\big|_{E=0.033aJ}} \qquad (4.14)$$

$$\sigma\_period(E)\big|_{E=0.033aJ} = \frac{1}{\lambda_{period}} = \frac{\nu\_period(E)\big|_{E=0.033aJ}}{c} = 2917.4cm^{-1} \qquad (4.15)$$

The dynamical properties of this system depend on the energy put into the system. For example, when the energy put into the system is near its dissociation energy with initial conditions

$$r_{init} = 2.8 \cdot r_e, \qquad v_{init} = 1500.0 \cdot m \cdot \sec^{-1} \tag{4.16}$$

the energy given to the system is contained in the initial conditions

$$E = \frac{1}{2}\mu v_{init}^2 + V(r_{init}) = 0.6944aJ \tag{4.17}$$

The energies shown in Fig.4.2 by a conventional way that draw the potential energy curve and superimpose the total energy upon this curve are changed as in Fig. 4.5.

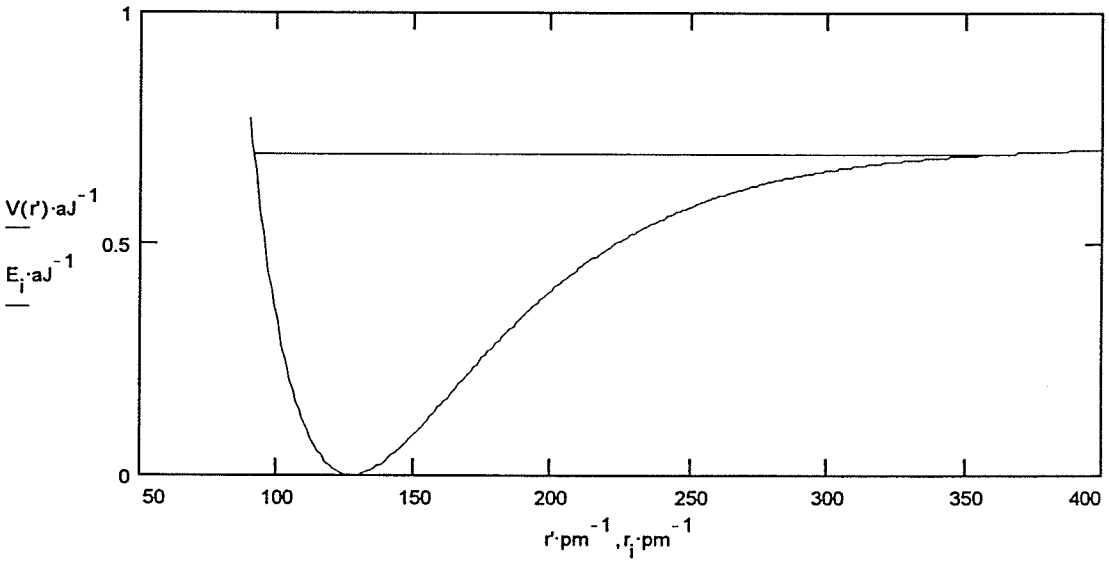

Figure 4.5 The position of total energy $E = 0.6944aJ$ on the Morse potential surface.

Under the initial conditions (4.16), the positional and momental changes with time are obtained from Eqs. (4.9) and (4.10).

It is noticed that the bond length oscillates back and forth in a regular periodic fashion between minimum and maximum values--the turning points. The time spent in the vicinity of the compressed bond turning point is less than at the stretched bond turning point since the force exerted on the particles in the vicinity of the compressed

bond turning point is much larger than that near the vicinity at the stretched bond turning point.

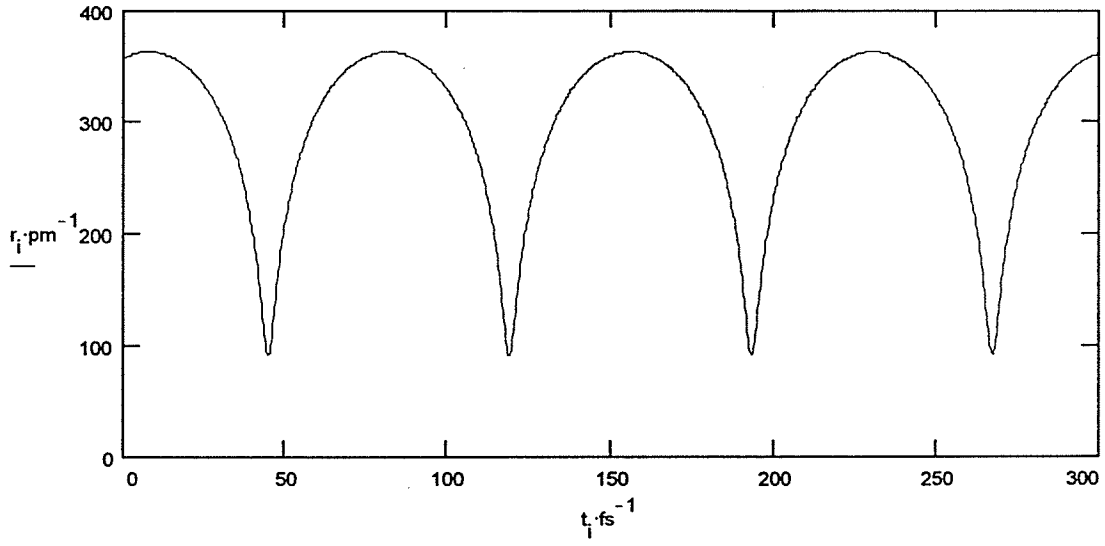

Figure 4.6 The periodic change of the bond length with time when $E = 0.6944aJ$.

From the positional change with time we can get the bond vibration frequency by the fast Fourier transform;

$$\sigma\_fft(E)\big|_{E=0.6944aJ} = \frac{1}{\lambda_{fft}} = FFT\left[r(t)\big|_{E=0.6944aJ}\right] = 463.11cm^{-1} \qquad (4.18)$$

σ_fft is a function of the energy put into the system since $r(t)$ is dependent on system's total energy. The relationship between σ_fft and the energy E is shown in Fig. 4.7.

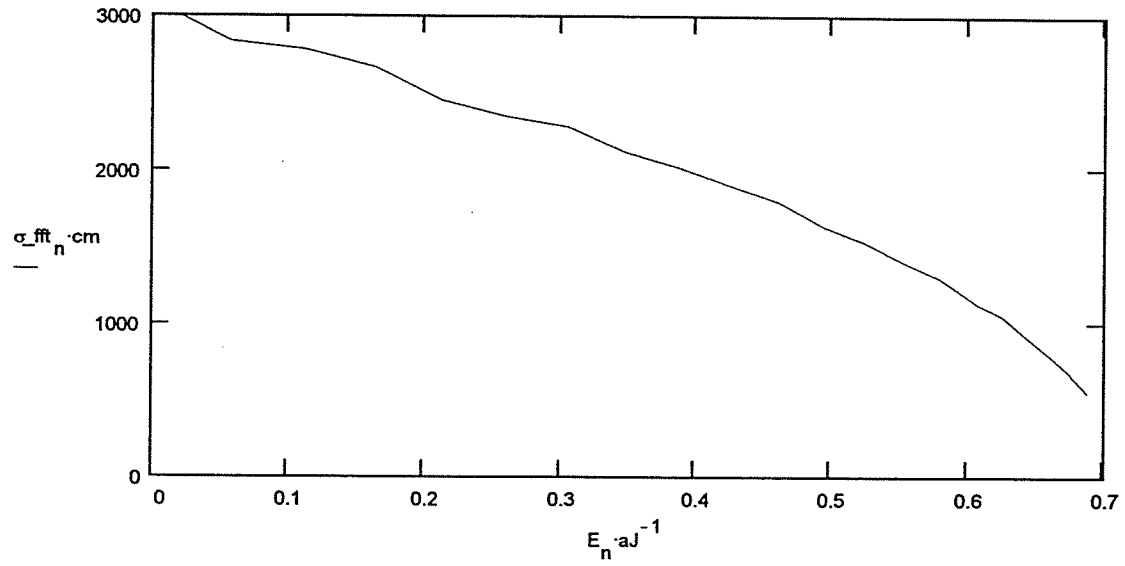

Figure 4.7 The relationship between the fast Fourier transform vibrational frequencies and total energy put into the Morse potential system.

However the momentum shown in Fig.4.8, while periodic in time, does not behave in the same fashion during the bond compression as during the bond stretching because the potential is not symmetric about the equilibrium bond distance.

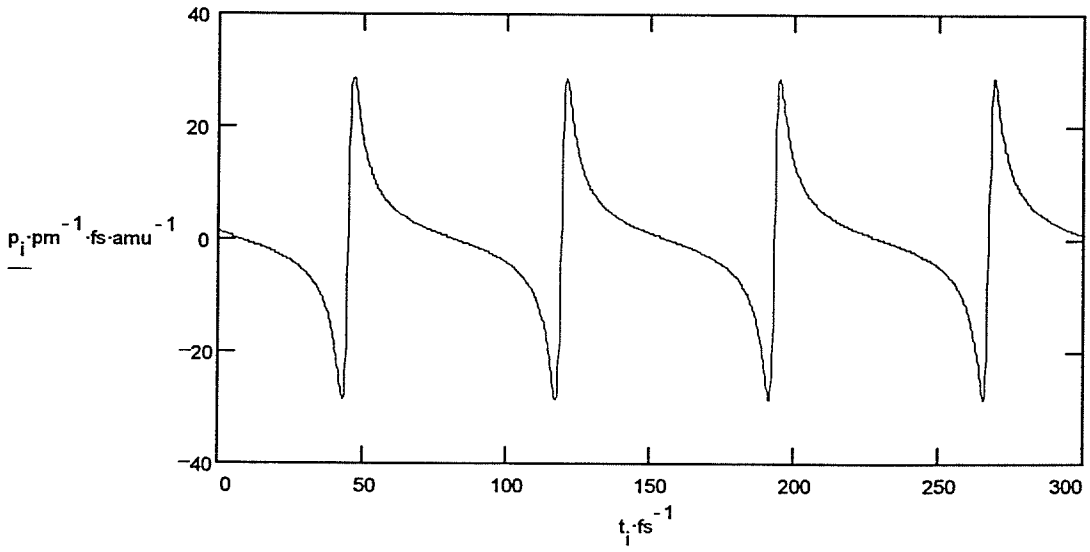

Figure 4.8 The periodic change of the *HCl* molecular nuclear motion momentum with time when $E = 0.6944aJ$.

The phase portrait of the system is dependent on that how much energy is put into the system and is not an ellipse as for the harmonic oscillator. Under initial conditions (16) it looks like a kind of stretched egg shaped ellipse since the oscillator extends further beyond the equilibrium distance when stretched than when compressed.

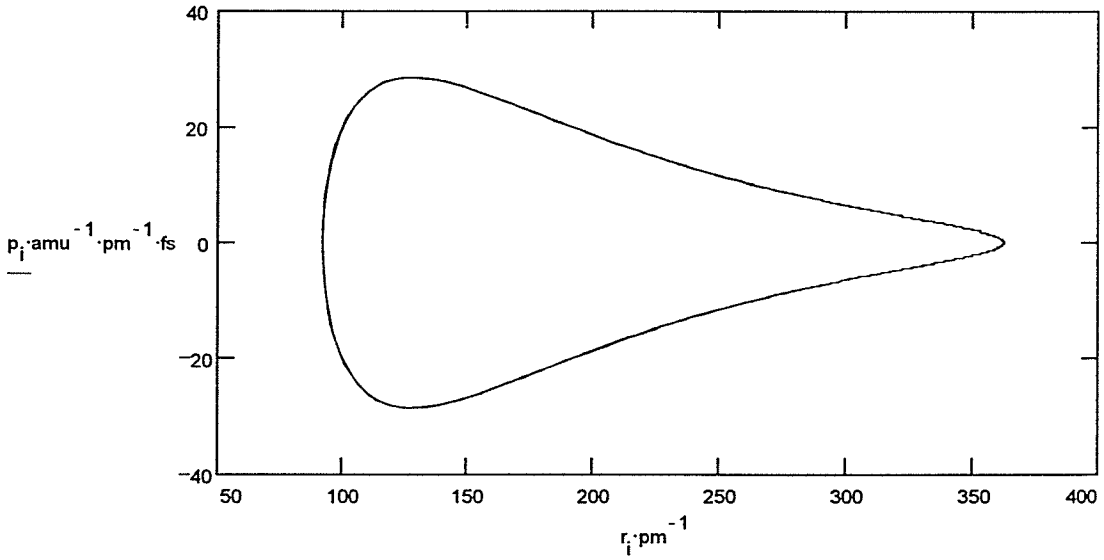

Figure 4.9 The phase portrait of the *HCl* molecular nuclear motion when $E = 0.6944 aJ$.

From the phase portrait we can get its period, the time taken to complete one cycle of the phase portrait

$$period(E)\big|_{E=0.6944\,aJ} = 74.133 \cdot fs \qquad (4.19)$$

Its corresponding frequency, the number of periods executed per second, is the reciprocal of the period

$$v\_period(E)\big|_{E=0.6944\,aJ} = \frac{1}{period(E)\big|_{E=0.6944\,aJ}} \qquad (4.20)$$

$$\sigma\_period(E)\big|_{E=0.6944\,aJ} = \frac{1}{\lambda_{period}} = \frac{v\_period(E)\big|_{E=0.6944\,aJ}}{c} = 450.09 cm^{-1} \qquad (4.21)$$

It is obvious that the shape of the phase portrait depends on the energy put into the system; consequently, σ_period depends on its total energy too. The change of σ_period with the energy E is shown in Fig.4.10.

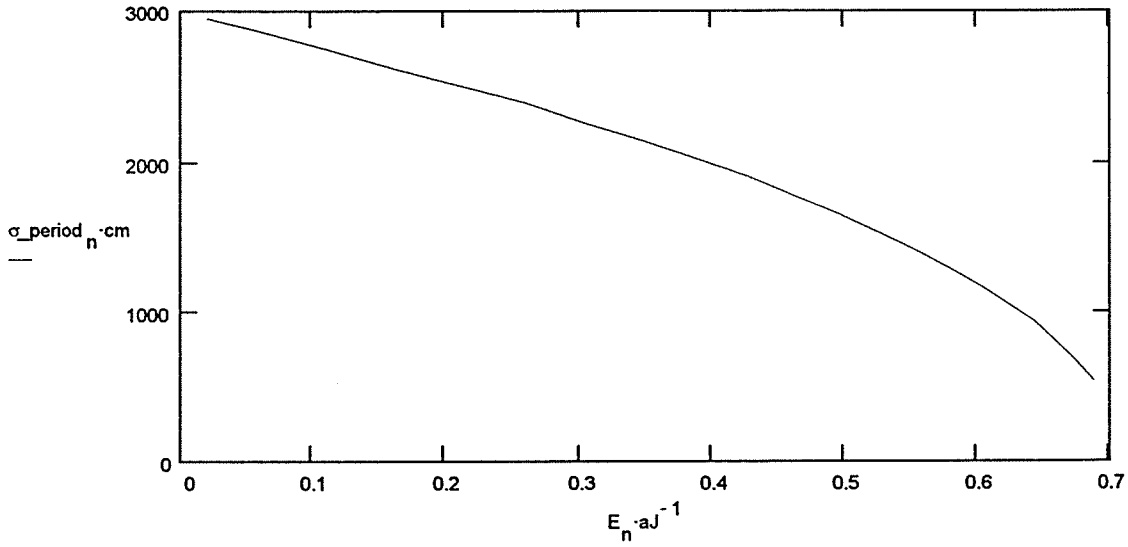

Figure 4.10 The relationship between the phase vibrational frequencies and total energy put into the Morse potential system.

The potential energy has alternating short and long time periods between its zeroes at the equilibrium distance. The short periods correspond to bond compression on a relatively repulsive potential, the long periods being for bond extension during which it takes longer for the stretch to slow down and turn around.

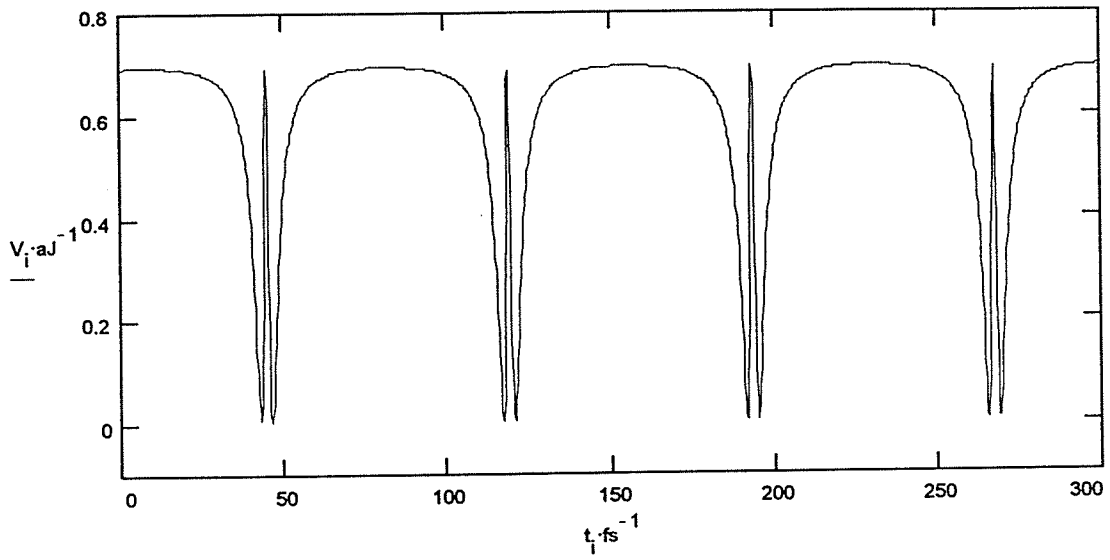

Figure 4.11 The potential change with time when total energy $E = 0.6944aJ$.

The kinetic energy mirrors the behavior of the potential energy and its shape can be explained ups and downs of particle speed.

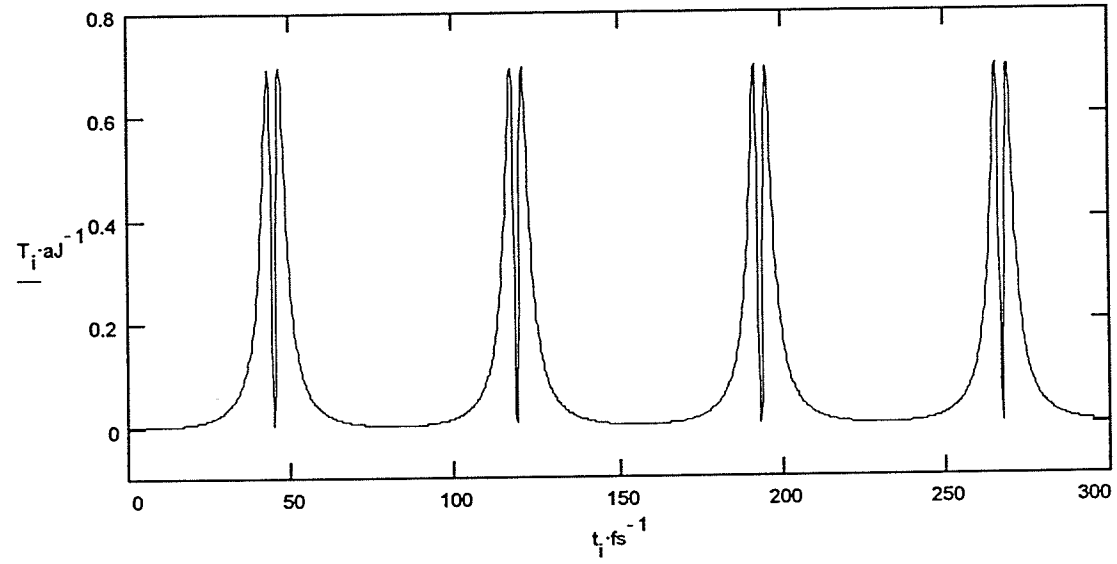

Figure 4.12 The kinetic energy change with time when total energy $E = 0.6944aJ$.

In spite of the ups and downs of separate kinetic and potential energies, the sum of the two, the overall energy, turns out to be constant, i.e., the total energy is a constant of the motion, $E = T + V = 0.6944aJ$.

It is known that both of σ_fft and σ_period are functions of system's total energy. The higher the system's total energy, the lower the frequency of vibration; when the total energy is larger than dissociation energy, the frequency is zero; it means that the bond is broken. Hence the Morse potential is better than the harmonic potential surface for describing molecular motion behavior near dissociation.

For the diatomic Morse potential system, the Hamiltonian is written as

$$-\frac{\hbar^2}{2\mu}\frac{d^2}{dx}\psi + De\left[1-e^{-a(x-req)}\right]^2\psi = Eig\psi \qquad (4.22)$$

Eq.(4.5) can be solved by analytical quantum mechanics or quantum numerical method. The energy eigenvalues obtained by analytical quantum mechanics[7] are

$$Eig_n = De - A^{-2}\left[K-\left(n+\frac{1}{2}\right)\right]^2 \qquad (4.23)$$

in which

$$A = \frac{(2\mu)^{\frac{1}{2}}}{a\hbar}$$

$$K = ADe^{\frac{1}{2}}$$

We see that the absorption or emission frequency $Eig_{n+1} - Eig_n$ is dependent on quantum number n, i.e., the system's total energy. The absorption or emission frequency can be expressed as

$$\sigma\_anal_n = \frac{Eig_{n+1} - Eig_n}{hc} \qquad n = 0,1,2,... \qquad (4.24)$$

In figure 4.13 we plot the analytical frequency as a function of the total energy. In order to have a continuous carve, we artificially define energy mid-points between quantum energy levels as

$$E_n = Eig_n + \frac{Eig_{n+1} - Eig_n}{2} \qquad n = 0,1,2,... \qquad (4.25)$$

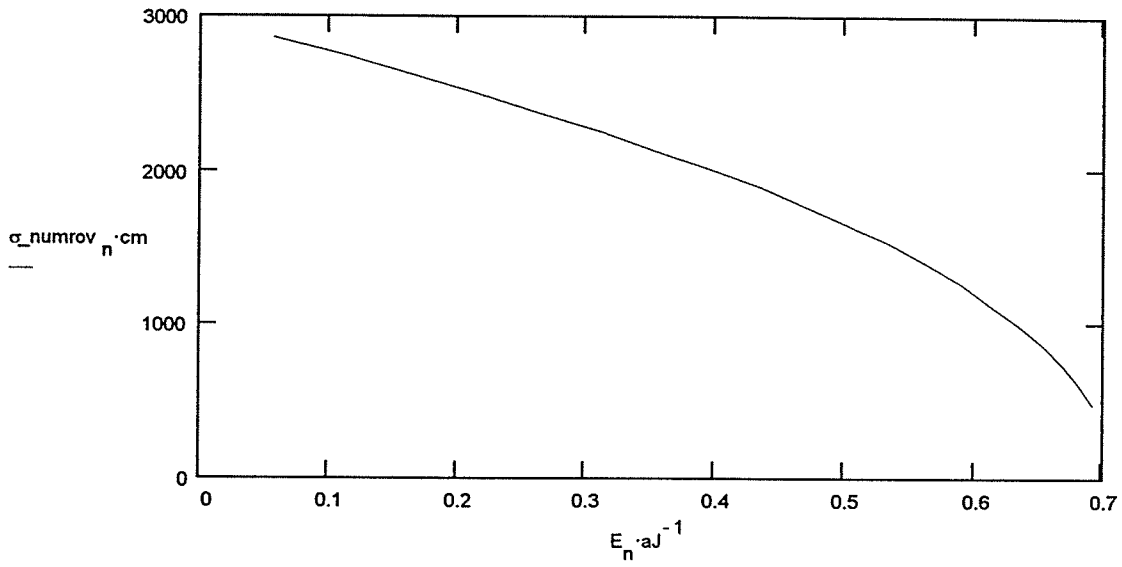

Figure 4.13 The relationship between the analytical frequencies and total energy put into the Morse potential system.

Because we ultimately want to express the eigenfunction as a set of discrete values over a set of points in position space, it is more convenient to solve Eq.(4.22) numerically First we convert it as non-unit equation by the following parameter conversion

$$r = r' \cdot pm \tag{4.26}$$

Eq (22) becomes

$$-\frac{\hbar^2}{2\mu}\frac{1}{pm^2}\frac{d^2}{dr'^2}\psi + De\left[1-e^{-a\cdot pm\left(r'-r_e'\right)}\right]^2\psi = Eig\cdot\psi \tag{4.27}$$

Then we standardize Eq (27) according[8]

$$\left[A\frac{d^2}{dx^2}+B\frac{d}{dx}+V(x)\right]\psi = E\cdot\psi \tag{4.28}$$

in which $A = 1$

$B = 0$

$$V(x) = -\frac{2\mu}{\hbar^2}\cdot pm^2\cdot De\left[1-e^{-a\cdot pm\left(r'-r_e'\right)}\right]^2$$

$$E = -\frac{2\mu}{\hbar^2} \cdot pm^2 \cdot Eig \qquad (4.29)$$

Eq.(4.28) is then solved using the Numrov program written in the Fortran language, we obtain dimensionless eigenvalues E and their corresponding eigenfunctions. From E we get Eig; hence we can calculate the absorption or emission frequency

$$\sigma\_numrov = \frac{Eig_{n+1} - Eig_n}{hc} \quad n = 0,1,2,... \qquad (4.30)$$

Artificially set the energy corresponding to every frequency as

$$E_n = Eig_n + \frac{Eig_{n+1} - Eig_n}{2} \quad n = 0,1,2,... \qquad (4.31)$$

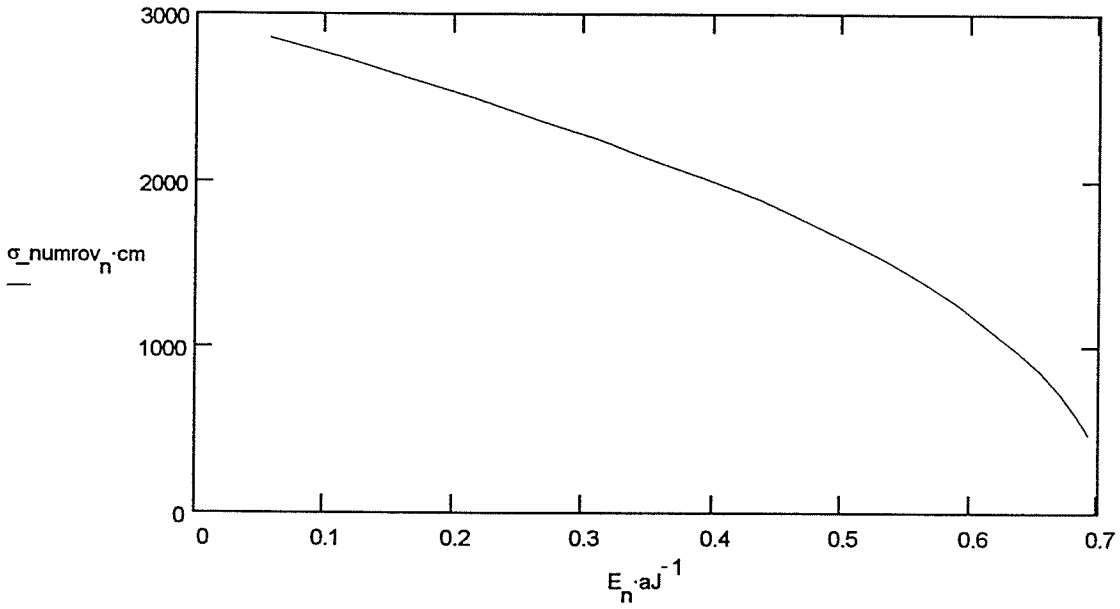

Figure 4.14 The relationship between the numerical calculated frequencies and total energy put into the Morse potential system.

The complete solution set $\psi_n(r)$ of stationary eigenstate functions of Eq. (4.22) and corresponding eigenvalues E_n can be obtained by the normalized numerical method. However, it is possible to get the dynamical properties of the system from the motion of a non stationary eigenfunction. Usually the non stationary eigenfunction can be obtained by displacing and reshaping $\psi_n(r)$

$$\psi_m'(r',t) = D(\delta r)\left[R(x)\,\psi_m(r)\right] \cdot \varphi_m(t) \qquad (4.32)$$

in which

$$D(\delta r)\psi_m(r) = \psi_m(r + \delta r) \qquad (4.33)$$

and $R(x)$ means that changes the width of $\psi_0(r)$ x times. $\psi'_m(r',t)$ will move back and forward through original function $\psi_m(r)$.

When $D(\delta r) = D(2.5pm)$ and $R(x) = R(1)$, the relative position between $\psi'_0(r',0)$ and $\psi_0(r)\cdot\varphi_m(0)$ is shown in Fig.4.15

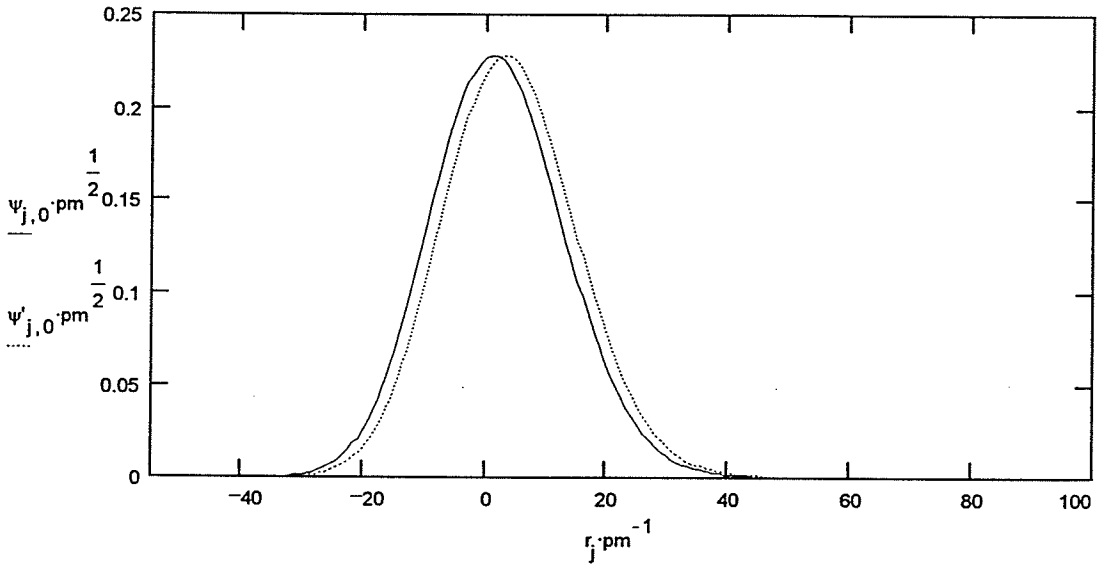

Figure 4.15 The shape and position of $\psi'_0(r',0) = D(2.5pm)\left[R(1)\psi_0(r)\right]\cdot\varphi_0(0)$ relative to $\psi_0(r,0)$.

Demonstrate the motion of $\psi'_0(r',0)$ with respect to time as the change of its probability density with respect to time

$$\textbf{\textit{Prob}}(r,t) = \psi'_0(r',0)\cdot\left[\psi'_0(r',0)\right]^* \qquad (4.34)$$

and the movement is shown in Figs.16 and 17

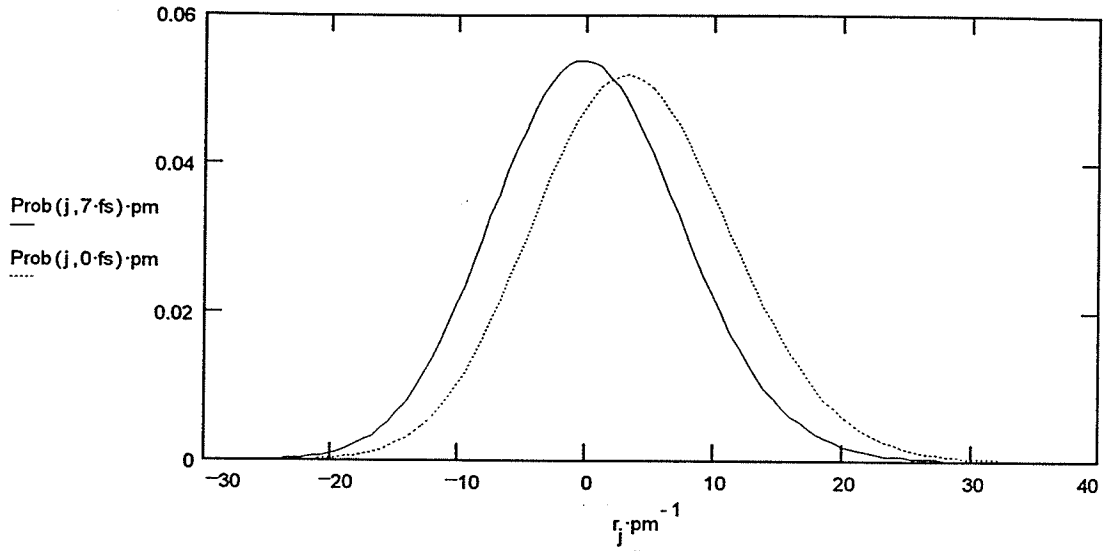

Figure 4.16 The probability of $D(2.5\,pm)\left[R(1)\,\psi_0(r)\right]\cdot\varphi_0(t)$

when $t=0$ and $t=7\,fs$.

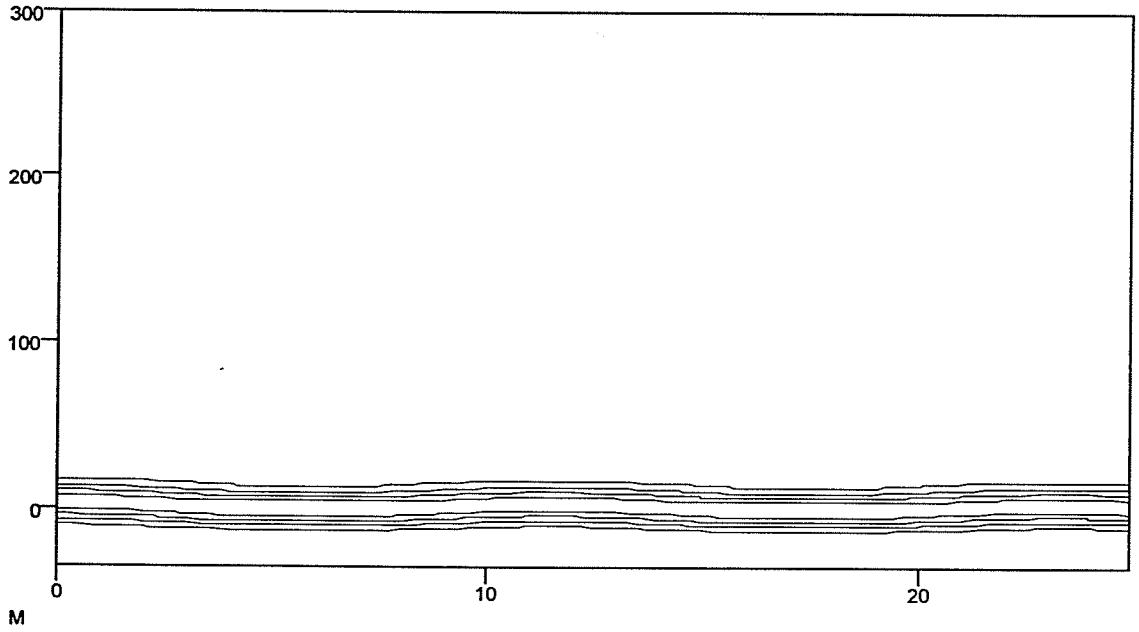

Figure 4.17 The contour plot of the probability density of $D(2.5\,pm)\left[R(1)\,\psi_0(r)\right]\cdot\varphi_0(t)$ in which the x axis is t and the y axis is r.

From the motion of the wave package with respect time shown in Fig.4.17 the evolution time is estimated as

$$t\_evol(\delta r)\big|_{\delta r=2.5pm} = 11.2 \cdot fs \qquad (4.35)$$

It is seen that when $\delta r = 2.5pm$, the movement of the wave packet is a periodical motion without diffusion.

However when δr becomes larger, although the movement of the wave package is periodical, it diffuses with respect to time or position. For example, when $D(\delta r) = D(230pm)$ and $R(x) = R(1)$, the relative position between $\psi_0'(r',0)$ and $\psi_0(r) \cdot \varphi_m(0)$ is shown in Fig.4.18

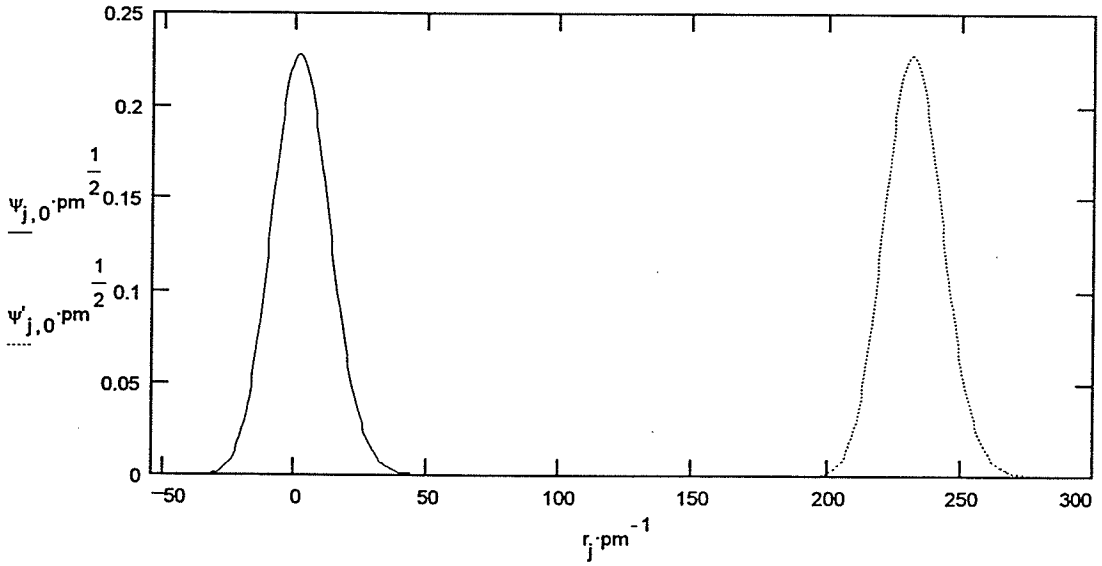

Figure 4.18 The shape and position of $\psi_0'(r',0) = D(230pm)\left[R(1)\psi_0(r)\right] \cdot \varphi_0(0)$ relative to $\psi_0(r,0)$.

Demonstrate the motion of $\psi_0'(r',0)$ with respect to time as the change of its probability density distribution in Fig.4.19

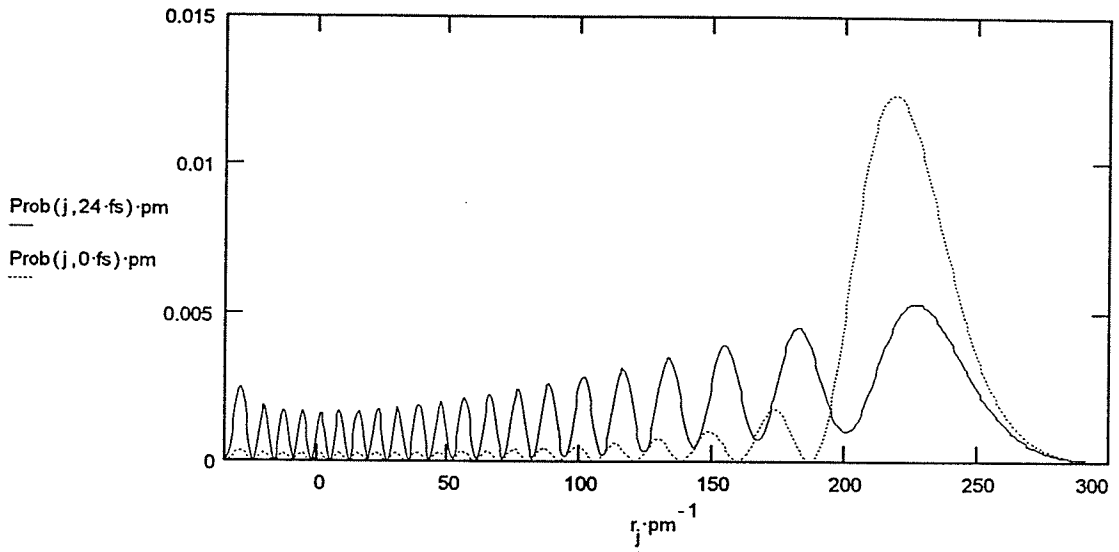

Figure 4.19 The probability of $D(230\,pm)\left[R(1)\,\psi_0(r)\right]\cdot\varphi_0(t)$

when $t=0$ and $t=24\,fs$.

The above picture shows that the wave packet of $\psi_0'(r',0)$ diffuses with respect to time. However the movement of the wave packet or the change of the probability density distribution with respect to time is still a periodical motion as shown in Fig.4.20

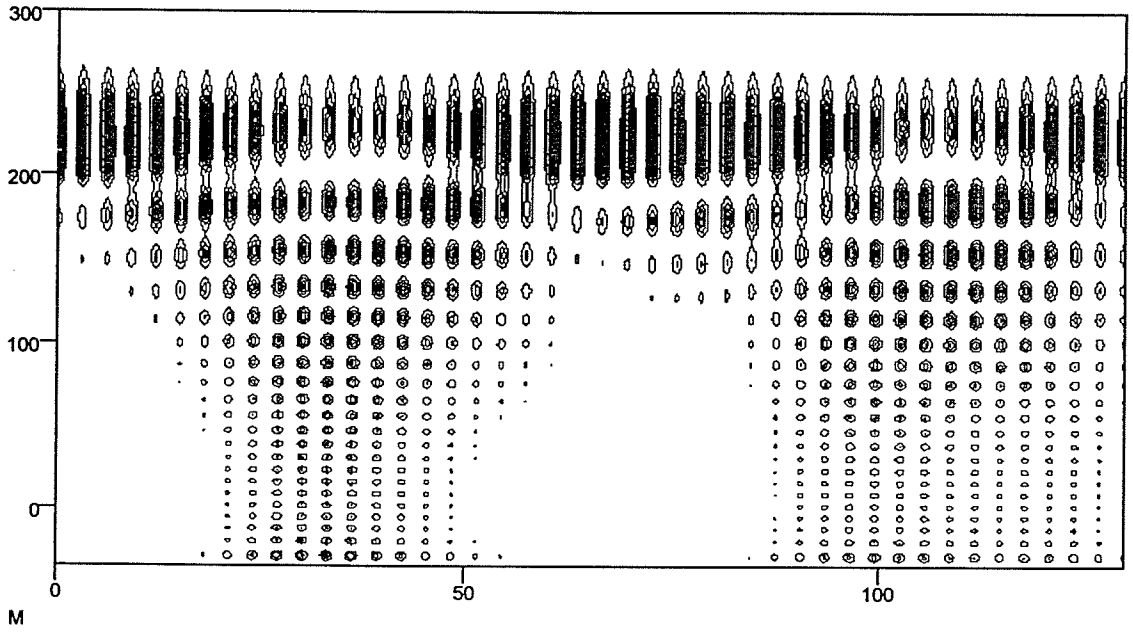

Figure 4.20 The contour plot of the probability density of $D(230\,pm)\left[R(1)\,\psi_0(r)\right]\cdot\varphi_0(t)$ in which the x axis is t and the y axis is r.

Therefore it is possible to get the evolution time of the wave packet movement

$$t\_evol(\delta r)\big|_{\delta r=230\,pm} = 65.00 \cdot fs \qquad (4.36)$$

The change of $t\_evol(\delta r)$ with δr is shown in Fig.4.21

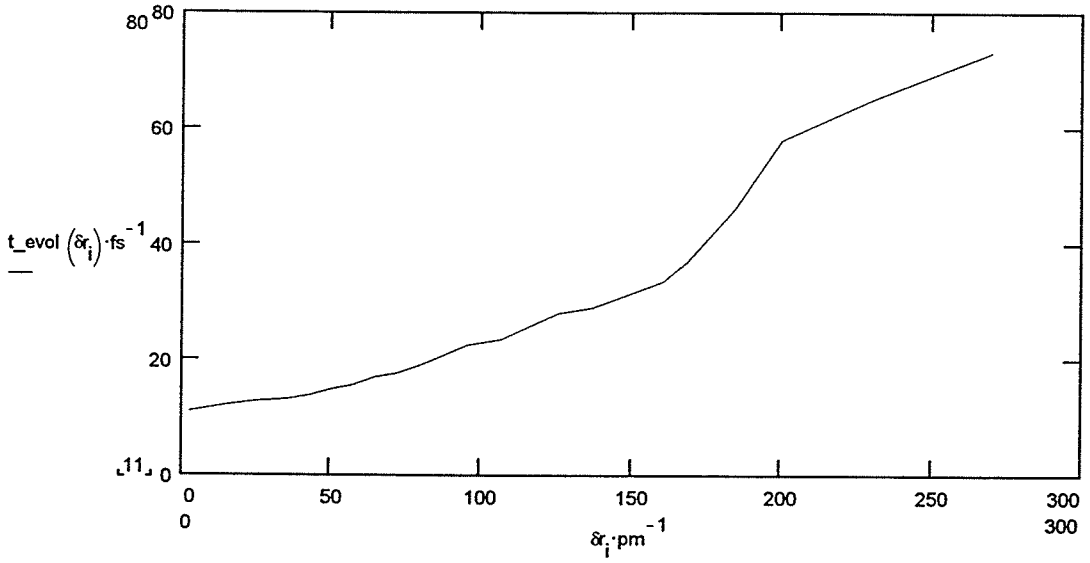

Figure 4.21 The evolution time change with respect to the position displacement.

From the evolution time of the motion, the motion frequency can be gotten as

$$\sigma\_pbd(\delta r) = \frac{1}{\lambda(\delta r)} = \frac{1}{c \cdot t\_evol(\delta r)} \qquad (4.37)$$

Since $\psi_0'(r',0)$ is the transformation of $\psi_0(r)\cdot\varphi_0(t)$ with the positional displacement δr and the variation range of $\psi_0'(r',0)$ is restricted in the potential well, the energy corresponding to $\psi_0'(r',0)$ can be roughly correlated to δr and expressed as

$$E'(\delta r) = E_0 + V\left(\left\langle \psi_0(r)\middle|r\middle|\psi_0(r)\right\rangle + \delta r\right) \qquad (4.38)$$

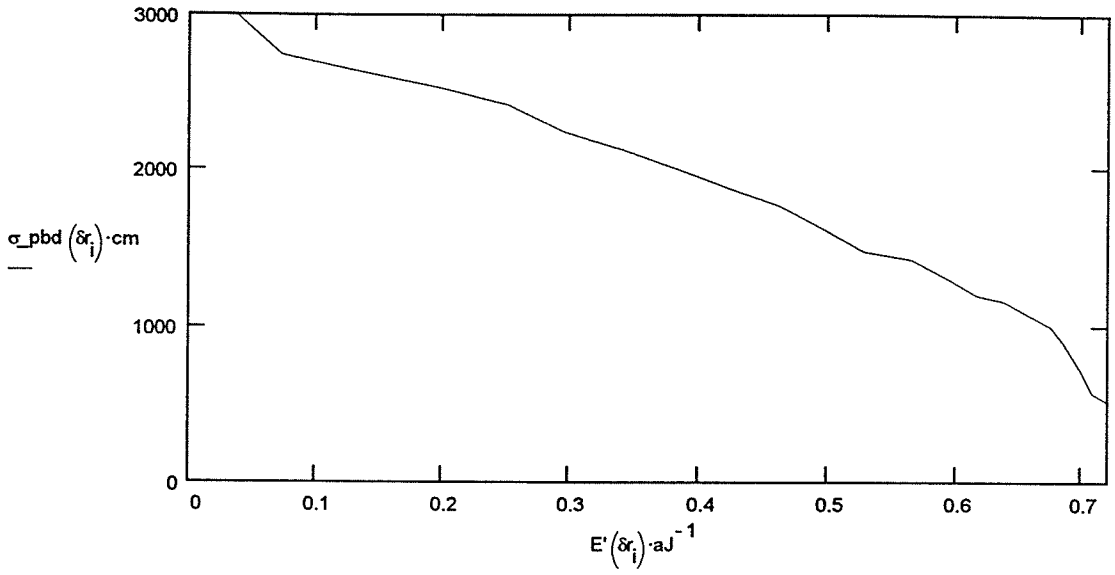

Figure 4.22 The relationship between the dynamical quantum frequencies and total energy put into the Morse potential system.

The evolution time of the above wave packet movement is dependent on the position displacement δr which determines the energy. It is known that the energy $E'(\delta r)$ of Eq.(4.37) is different from the average energy $\overline{E}$ of $\psi'(r')$

$$\overline{E} = \langle \psi'(r',t) | \hat{H} | \psi'(r',t) \rangle \qquad (4.39)$$

if $R(x) \neq R(1)$ in Eq.(4.32). Precisely the evolution time of a wave packet movement depends on the average energy $\overline{E}$ defined in Eq.(4.39).

When $\psi_0'(r',0) = D(80 \cdot pm) \cdot R(1) \cdot \psi_0(r) \cdot \varphi_0(t)$, both $\psi_0'(r')$ and $\psi_0(r)$ are shown in Fig.4.23

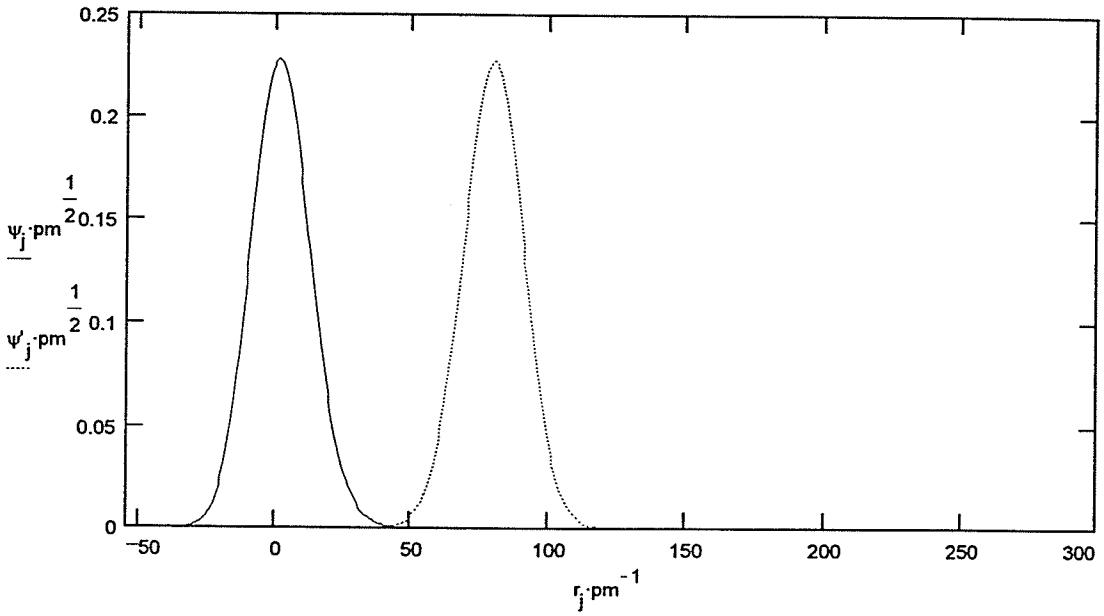

Figure 4.23 The shape and position of
$\psi'_0(r',0) = D(80pm)\left[R(1)\psi_0(r)\right]\cdot\varphi_0(0)$ relative to $\psi_0(r,0)$.

$$\overline{E} = \left\langle \psi'(r',t)\middle|\hat{H}\middle|\psi'(r',t)\right\rangle = 0.4615aJ \qquad (4.40)$$

The motion of the wave packet is shown in Fig. 4.24

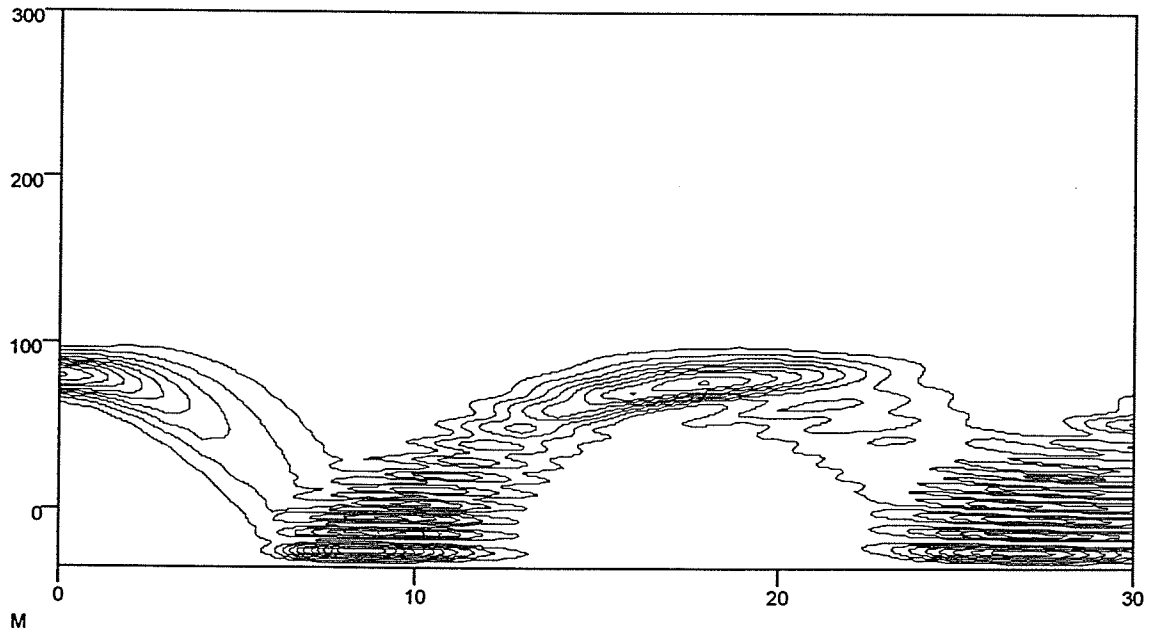

Figure 4.24 The contour plot of the probability density of
$D(80pm)\left[R(1)\psi_0(r)\right]\cdot\varphi_0(t)$ in which the x axis is t and the y axis is r.

$$t\_evol(\delta r, x)\big|_{\delta r=80\,pm,x=1} = 18.30 \cdot fs \qquad (4.41)$$

When $\psi'_0(r',0) = D(42.2 \cdot pm) \cdot R(2) \cdot \psi_0(r) \cdot \varphi_0(t)$, both $\psi'_0(r')$ and $\psi_0(r)$ are shown in Fig.4.25

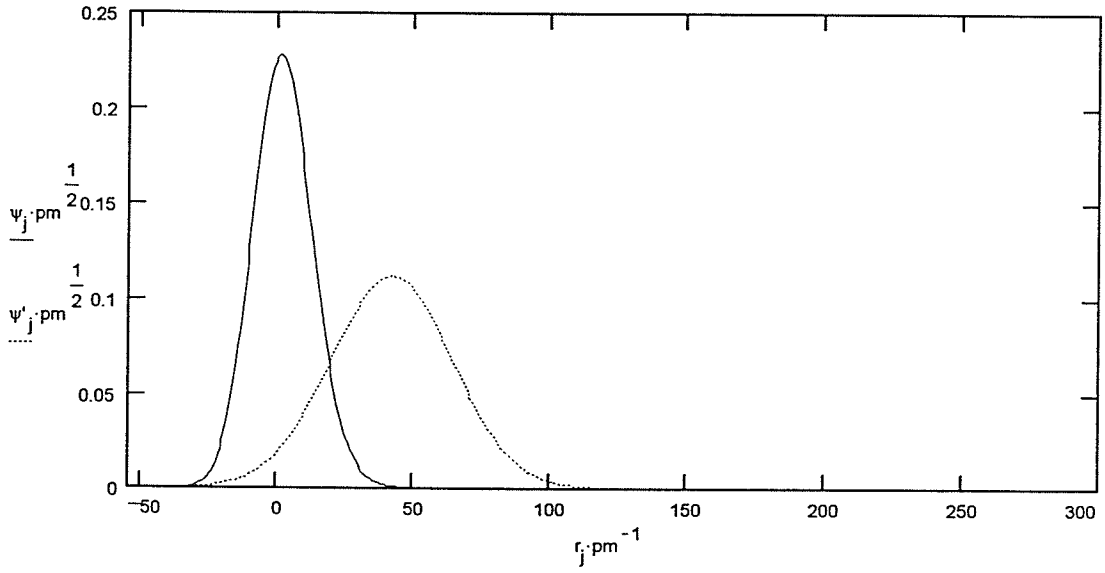

Figure 4.25 The shape and position of $\psi'_0(r',0) = D(42.2\,pm)\left[R(2)\,\psi_0(r)\right] \cdot \varphi_0(0)$ relative to $\psi_0(r,0)$.

$$\overline{E} = \left\langle \psi'(r',t) \middle| \hat{H} \middle| \psi'(r',t) \right\rangle = 0.1985aJ \qquad (4.42)$$

The motion of the wave packet is shown in Fig. 4.26

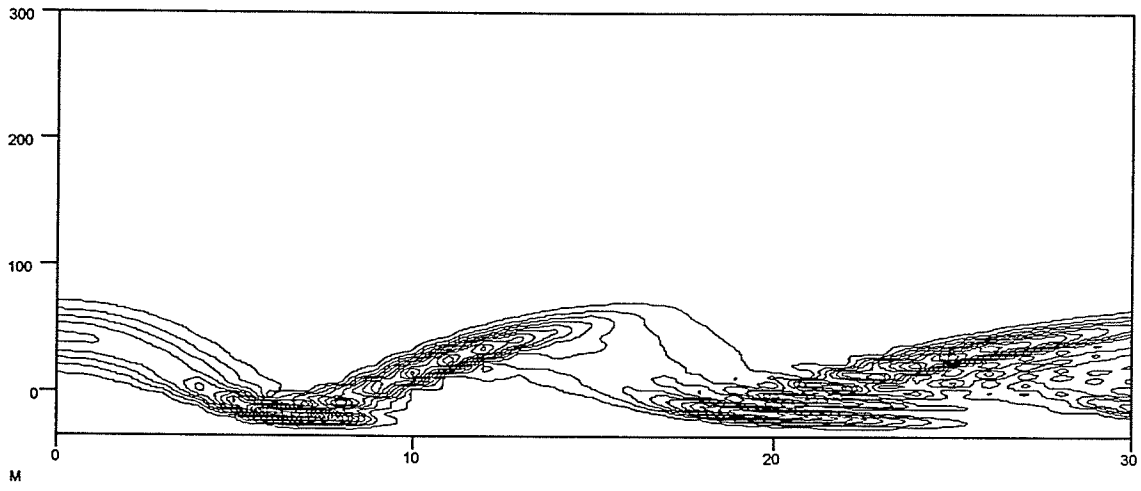

Figure 4.26 The contour plot of the probability density of $D(42.2\,pm)\left[R(2)\,\psi_0(r)\right] \cdot \varphi_0(t)$ in which the x axis is t and the y axis is r.

$$t\_evol(\delta r, x)\big|_{\delta r=42.2\,pm,x=2} = 13.10 \cdot fs \qquad (4.43)$$

When $\psi'_0(r',0) = D(152 \cdot pm) \cdot R(0.5) \cdot \psi_0(r) \cdot \varphi_0(t)$, both $\psi'_0(r')$ and $\psi_0(r)$ are shown in Fig.4.27

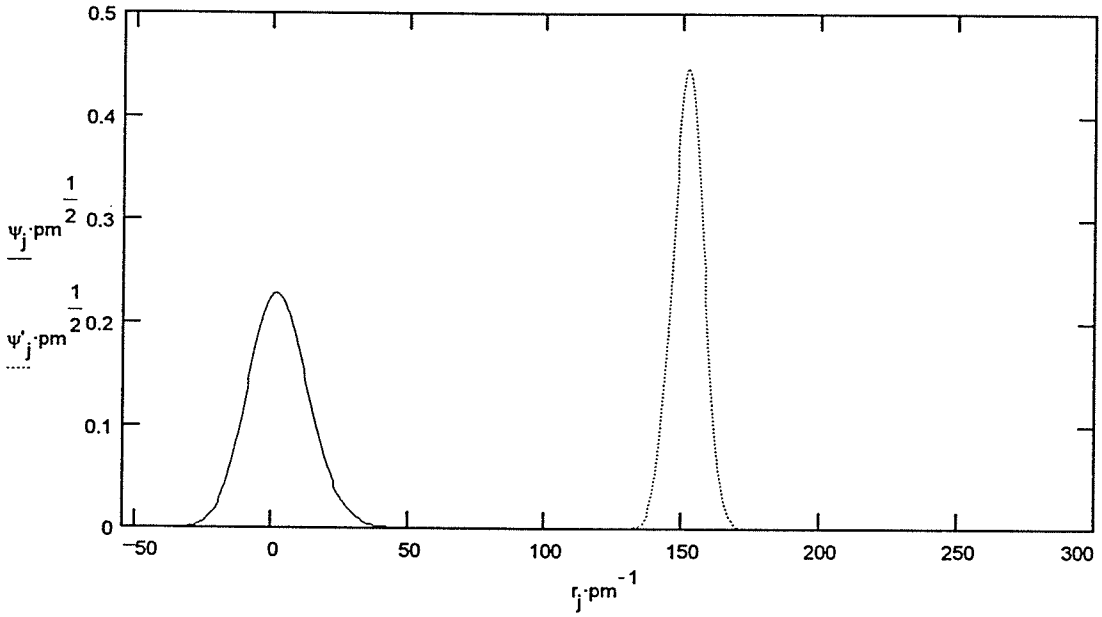

Figure 4.27 The shape and position of $\psi'_0(r',0) = D(152\,pm)\left[R(0.5)\,\psi_0(r)\right] \cdot \varphi_0(0)$ relative to $\psi_0(r,0)$.

$$\overline{E} = \left\langle \psi'(r',t) \middle| \hat{H} \middle| \psi'(r',t) \right\rangle = 0.6938aJ \qquad (4.44)$$

The motion of the wave packet is shown in Fig. 4.28

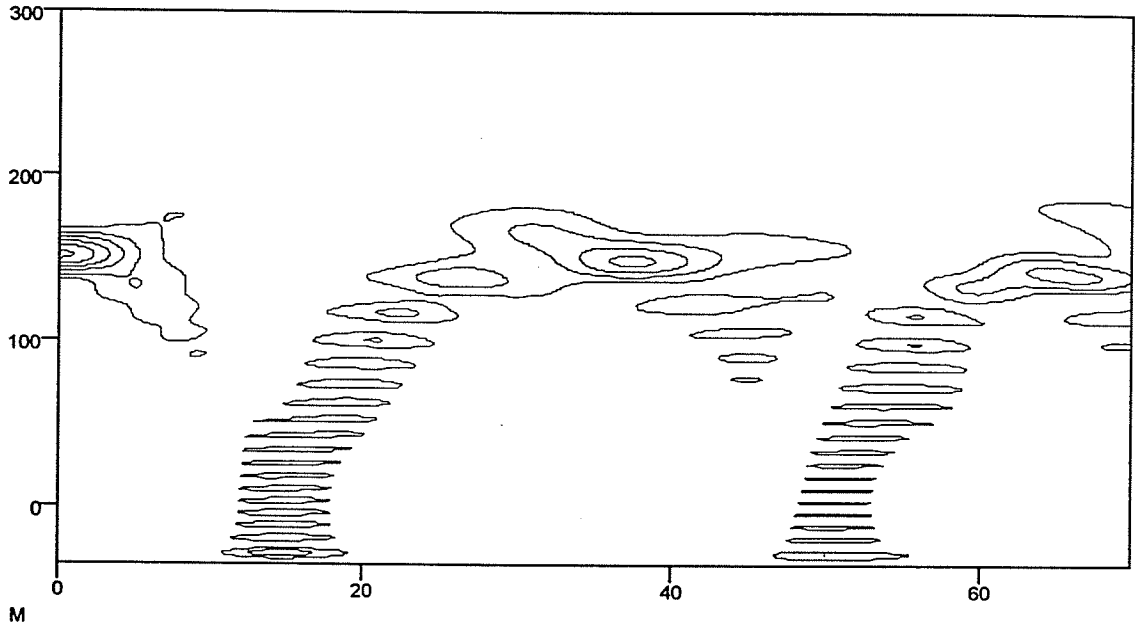

Figure 4.28 The contour plot of the probability density of $D(152\,pm)\left[R(0.5)\,\psi_0(r)\right]\cdot\varphi_0(t)$ in which the x axis is t and the y axis is r.

$$t\_evol(\delta r, x)\big|_{\delta r=152\,pm, x=0.5} = 36.65\cdot fs \qquad (4.45)$$

It is clear that the evolution time of a wave packet movement only depends on the average energy of its state.

We have obtained five different frequencies for a Morse potential system by five different methods: the fast Fourier transform, the phase portrait, analytical quantum calculation, numerical quantum calculation and dynamical quantum calculation; their results are very close.

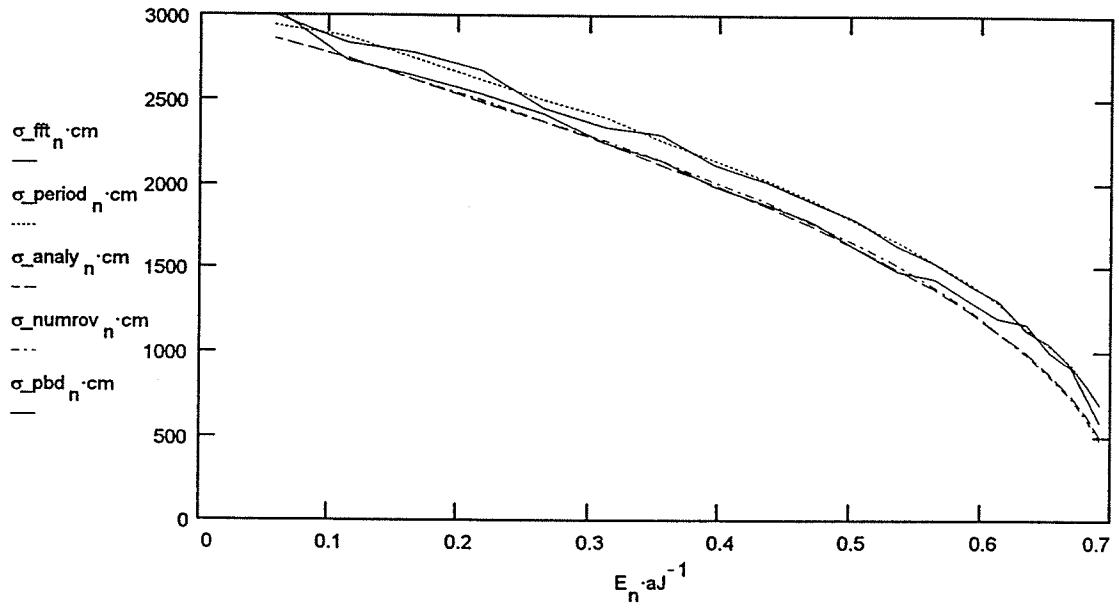

Figure 4.29 The comparison of vibrational frequencies obtained by different methods.

Hence for Morse potential system, we can get the same dynamical properties by different methods.

5. Internal Rotation of the n-Butane Molecule

In a molecule there exists another important interaction, the rotational potential resulting from interactions between nonbonded atoms, like the van der Waals interaction, and the hydrogen bond interaction. The rotational potential is different from other bond interactions in form, such as harmonic or Morse potential. Usually the former is weak and the latter is strong; another property is that a rotational potential usually is characterized by more than one potential minimum. For example, the rotation interaction of the 1,4-methyl groups of the n-butane molecule is expressed as

$$V(\theta) = h_1\left[1+\cos(3\cdot\theta)\right]+h_2\left[1+\cos(\theta)\right] \qquad (5.1)$$

in which

$$h_1 = 0.0139\cdot aJ$$

$$h_2 = 0.0063\cdot aJ$$

The shape of the rotational potential curve is shown in Fig. 5.1

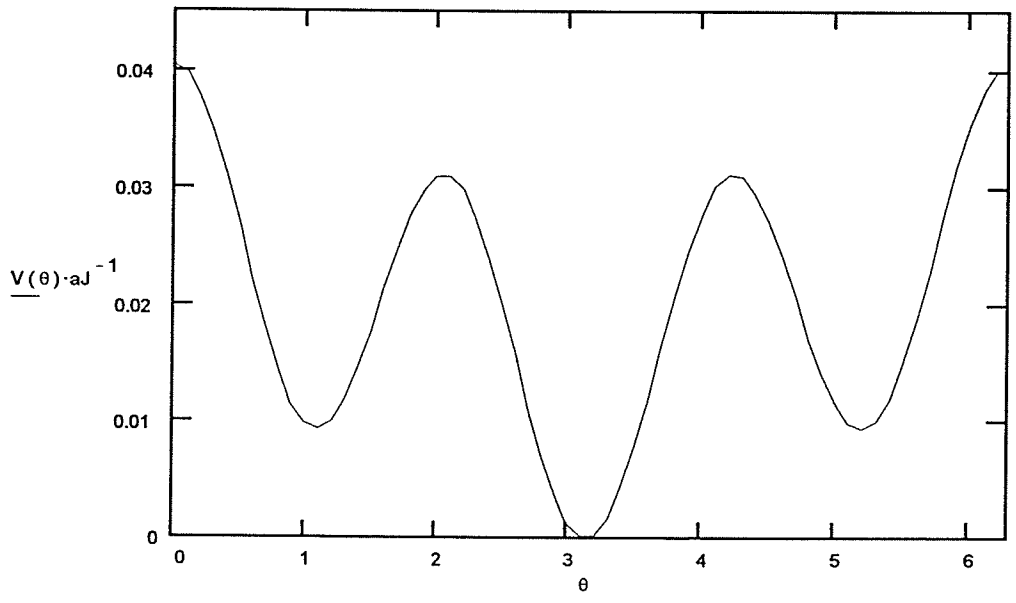

Figure 5.1 The rotational potential shape of the 1,4-methyl groups of the n−butane.

It is seen that the barriers of the potential are not high and there are three minimum potential points. It can be predicted that the molecule can easily overcome these barriers and continuously rotate.

From Newtonian mechanics, the acceleration caused by the force exerted on this system is

$$a = -\frac{1}{\mu}\frac{d}{dx}V(x) = -\frac{1}{\mu}\frac{1}{r_e^2}\frac{d}{d\theta}V(\theta) = -\frac{1}{\mu}\frac{1}{r_e^2}\frac{d}{d\theta}\left\{h_1\left[1+\cos(3\cdot\theta)\right]+h_2\left[1+\cos(\theta)\right]\right\} \tag{5.2}$$

in which

$$\mu = 15\cdot amu$$

$$r_e = 145.2\cdot pm$$

From Eq.(2) we can get the angle and its corresponding momentum changes with respect to time by a molecular dynamic simulation calculation. However, the molecular dynamical properties depend not only on the total energy put into the system, but on initial position. For example, we put $0.025\cdot aJ$ into the system and set up initial conditions

$$\theta_{init} = 1.00, \qquad v_{init} = 7.61\cdot 10^{12}\cdot \sec^{-1} \tag{5.3}$$

The energy given to the system is contained in the initial conditions

$$E = \frac{1}{2}\mu\cdot r_e^2\cdot v_{init}^2 + V(\theta_{init}) = 0.025\cdot aJ \tag{5.4}$$

The simulation time array t is defined as

$$t_i = h*i \tag{5.5}$$

in which

$$h = \frac{t_{\max} - t_{\min}}{Steps} \qquad i = 1,2,3,\ldots,Steps \tag{5.6}$$

From initial conditions, set initial X matrix column as

$$X^{\langle 0\rangle} = \begin{pmatrix} \theta_{init} \\ v_{init} \cdot \sec \end{pmatrix} \tag{5.7}$$

and define the derivative column vector as

$$D(t,x) = \begin{bmatrix} X_1 \\ -\frac{1}{\mu}\frac{1}{r_e^2}\frac{d}{d\theta}V(\theta)\Big|_{\theta=X_0} \end{bmatrix} \tag{5.8}$$

From Eqs (7) and (8) we can fill the X matrix with solutions by following equation.

$$X^{\langle i\rangle} := X^{\langle i-1\rangle} + RK\left(t_{i-1}, X^{\langle i-1\rangle}, D, h\right) \tag{5.9}$$

in which $RK(t, X, D, h)$ is Runge Kutta integration[10] and is written as

$$K1(t,X,D,h) \equiv D(t,X)$$

$$K2(t,X,D,h) \equiv D\left(t+\frac{h}{2}, X+\frac{h}{2}\cdot K1(t,X,D,h)\right)$$

$$K3(t,X,D,h) \equiv D\left(t+\frac{h}{2}, X+\frac{h}{2}\cdot K2(t,X,D,h)\right)$$

$$K4(t,X,D,h) \equiv D(t+h, X+h\cdot K3(t,X,D,h))$$

$$RK(t,X,D,h) \equiv \frac{h}{6}\cdot(K1(t,X,D,h)+2\cdot K2(t,X,D,h)+2\cdot K3(t,X,D,h)+K4(t,X,D,h)) \tag{5.10}$$

From Eq.(9) the particle's position and momentum change with time

$$t = t\cdot\sec \qquad \theta_i = X_{0,i} \qquad v_i = X_{1,i}\cdot\sec^{-1} \qquad p_i = \mu\cdot r_e\cdot v_i \tag{5.11}$$

In spite of the distribution and redistribution of separate kinetic and potential energies, the sum of the two, the overall energy, turns out to be constant, i.e., the total energy is a constant of the motion, $E = T+V = 0.025aJ$ as shown in Fig. 5.2.

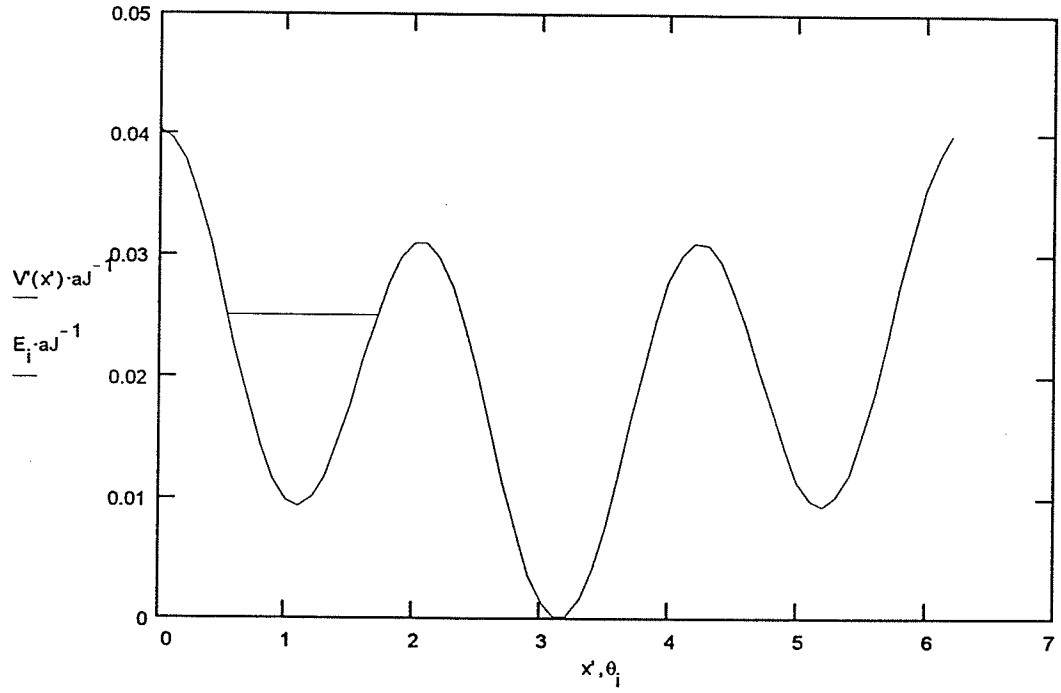

Figure 5.2 The position of total energy $E = 0.025aJ$ on the rotational potential surface of the 1,4-methyl groups of the n-butane when the initial starting point is in the middle well.

It is noticed as in Fig. 5.3 that the methyl group CH_3 oscillates back and forth in a regular periodic fashion between minimum and maximum values--the turning points.

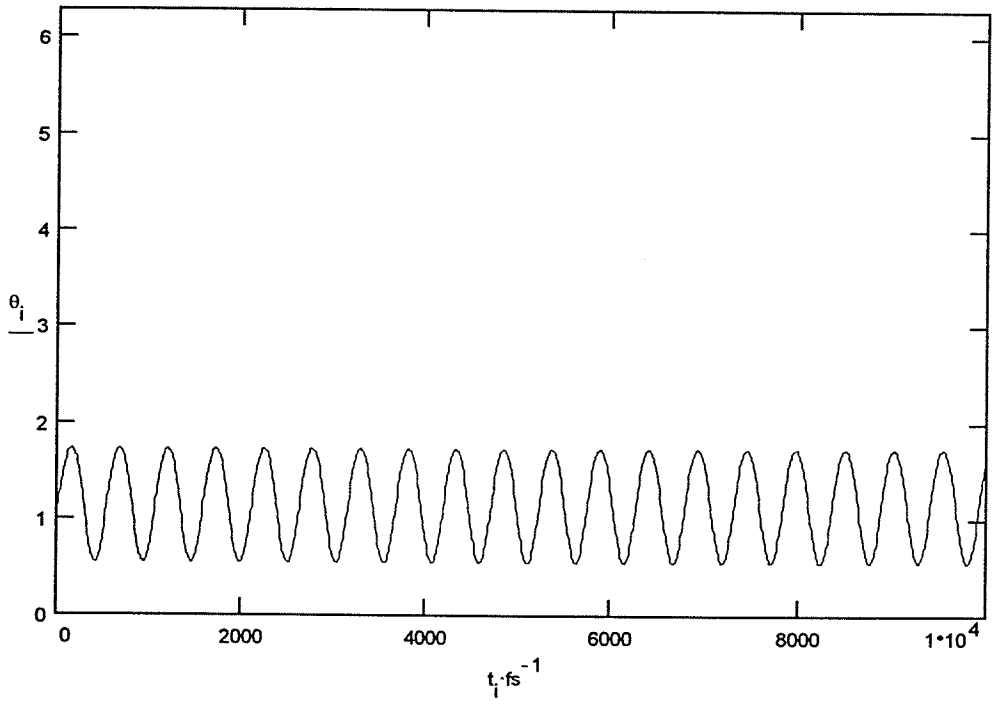

Figure 5.3 The periodic change of the angle with time in the left well of the rotational potential surface of the 1,4-methyl groups of the n-butane when $E = 0.025aJ$.

From the angle change with time we can get its bond vibration frequency by the fast Fourier transform;

$$\sigma\_L_{fft} = \frac{1}{\lambda\_L_{fft}} = FFT\left[r(t)\Big|_{E=0.025aJ}\right] \qquad (5.12)$$

σ_L_{fft} shown in Fig.5.4 is a function of the energy put into the system since $r(t)$ is dependent on system's total energy.

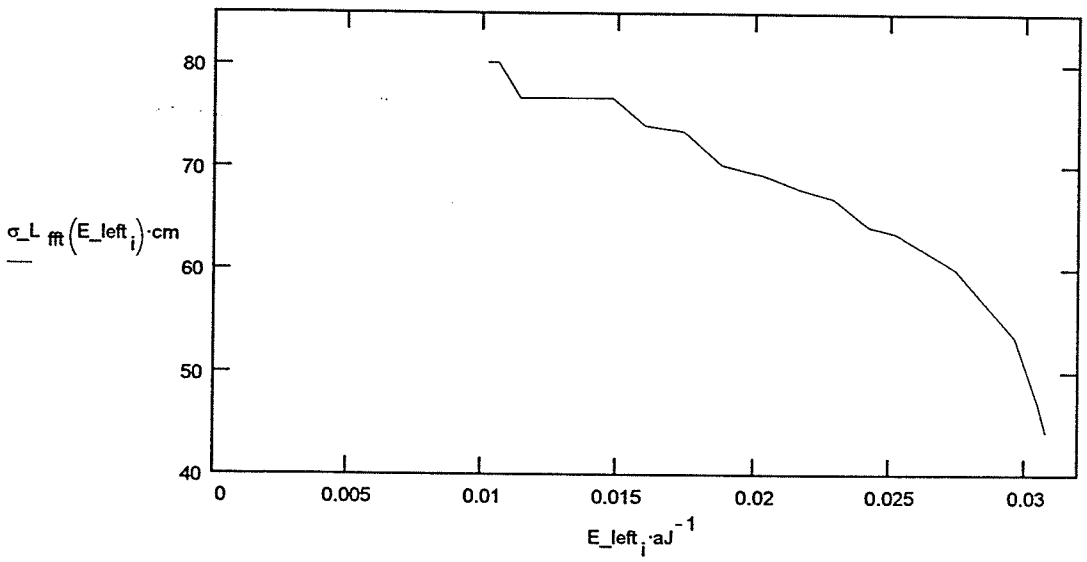

Figure 5.4 The relationship between the fast Fourier transform vibrational frequencies and total energy put into the left well of the rotational potential surface of the 1,4-methyl groups of the n-butane.

The phase portrait of the system is dependent both on that how much energy is put into the system and its initial simulation calculation conditions. For initial conditions (5.3) and total energy (5.4), the phase portrait is as in Fig. 5.5.

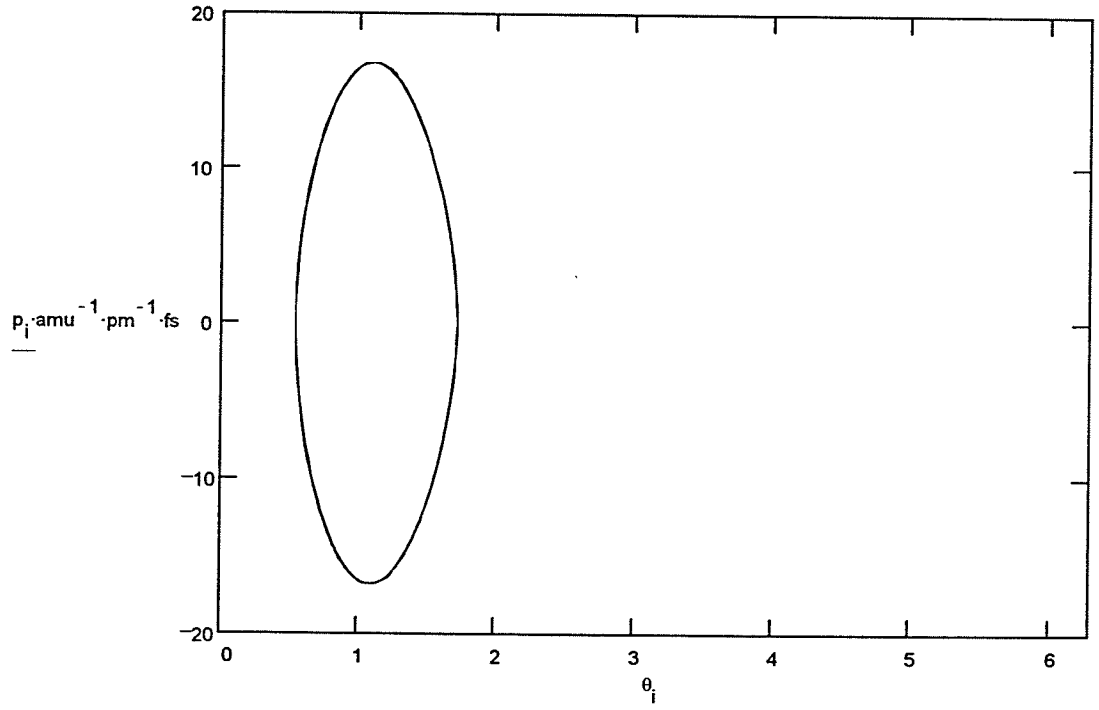

Figure 5.5 The phase portrait of the relative methyl rotation in the left well of the rotational potential surface of the 1,4-methyl groups of the n-butane when $E = 0.025aJ$.

From the phase portrait we can get its period, the time taken to complete one cycle of the phase portrait

$$period\_L = 518.08 \cdot fs \qquad (5.13)$$

Its corresponding frequency, the number of periods executed per second, is the reciprocal of the period

$$\nu\_L_{period} = \frac{1}{period\_L} \qquad (5.14)$$

$$\sigma_{period\_L} = \frac{1}{\lambda_{period\_L}} = \frac{\nu_{period\_L}}{c} \qquad (5.15)$$

The change of σ_{period_L} with respect to the energy put into the system is shown in Fig. 5.6.

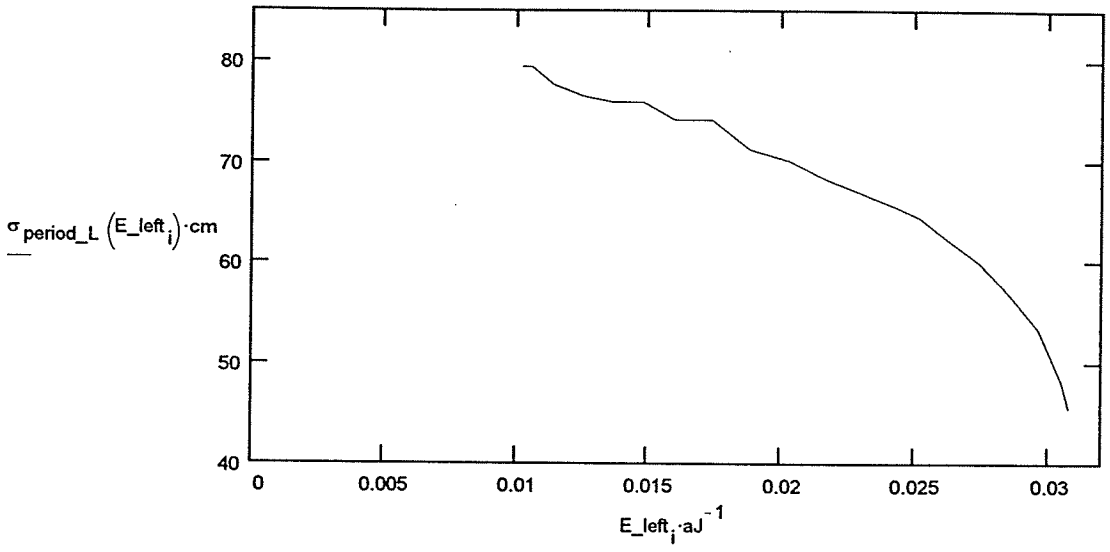

Figure 5.6 The relationship between the phase portrait vibrational frequencies and total energy put into the left well of the rotational potential surface of the 1,4-methyl groups of the n-butane.

Even we put the same energy into the system, the different initial positional condition gives rise to different results. For example, set up initial conditions as

$$\theta_{init} = 3.50 \qquad v_{init} = 8.12 \cdot 10^{12} \cdot \sec^{-1}$$

$$E = \frac{1}{2}\mu \cdot r_e^2 \cdot v_{init}^2 + V(\theta_{init}) = 0.025 \cdot aJ \qquad (5.16)$$

The particle oscillates in the middle well as shown in Fig. 5.7.

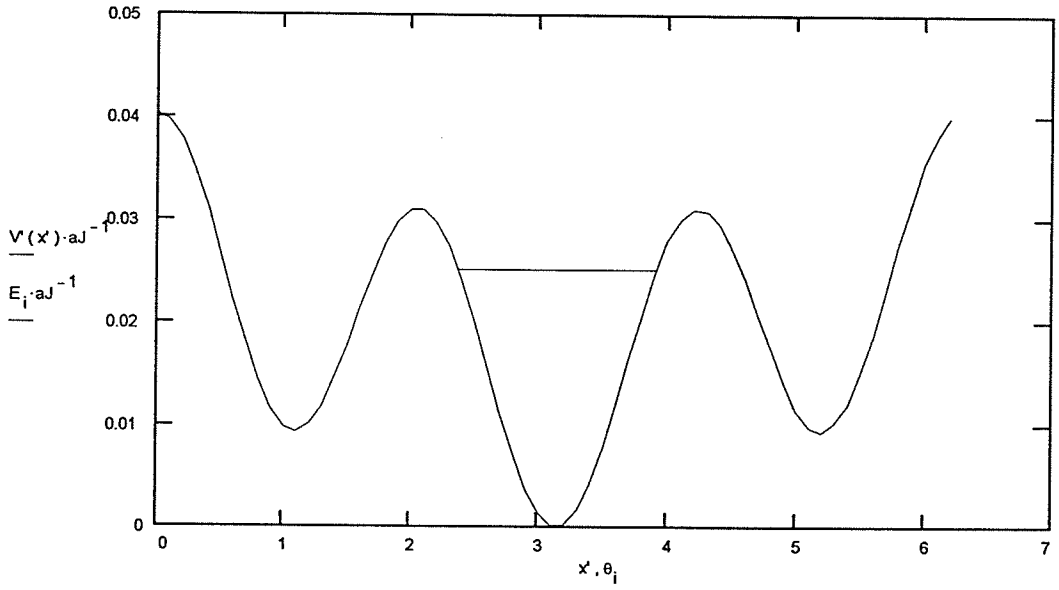

Figure 5.7 The position of total energy $E = 0.025aJ$ on the rotational potential surface of the 1,4-methyl groups of the n-butane when the initial starting point is in the middle well.

The angle change with time is as in Fig. 5.8

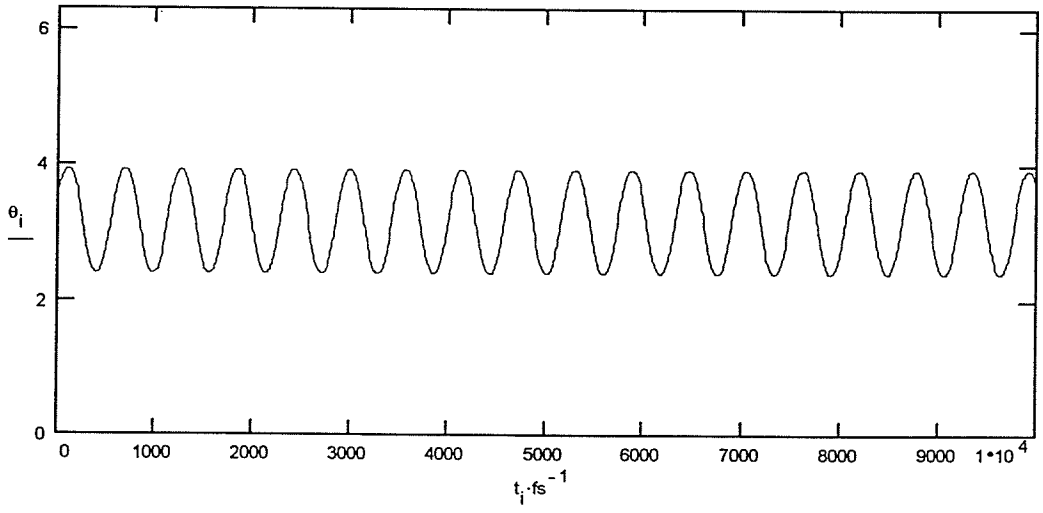

Figure 5.8 The periodic change of the angle with time in the middle well of the rotational potential surface of the 1,4-methyl groups of the n-butane when $E = 0.025aJ$.

From the angle change with respect to time we can get its bond vibration frequency by the fast Fourier transform;

$$\sigma\_M_{fft} = \frac{1}{\lambda\_M_{fft}} = FFT\left[r(t)\Big|_{E=0.025aJ}\right] \qquad (5.17)$$

σ_M_{fft} is a function of the energy put into the system too since $r(t)$ is dependent on system's total energy; its changes with the total energy is shown in Fig.5.9

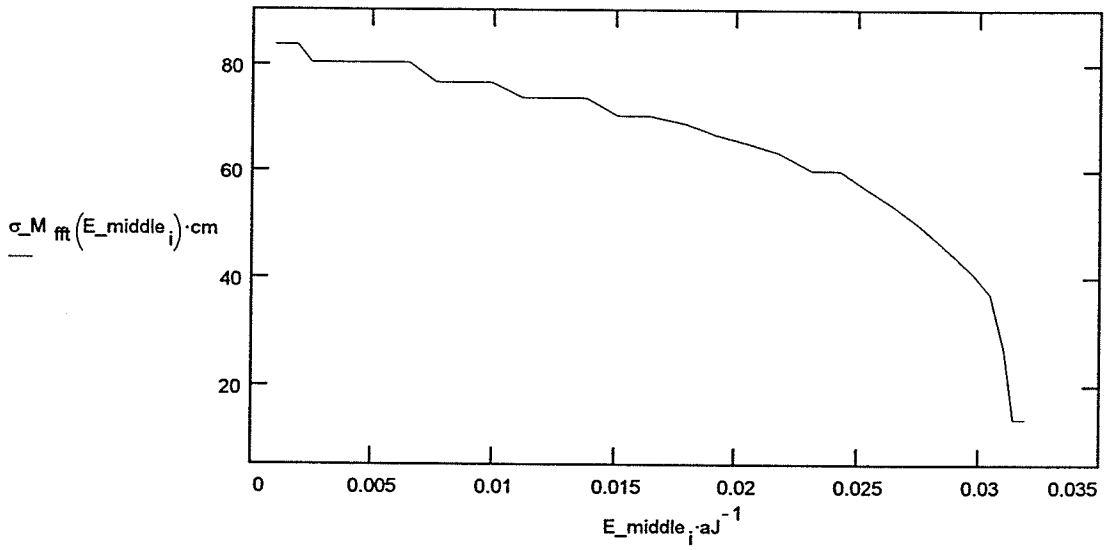

Figure 5.9 The relationship between the fast Fourier transform vibrational frequencies and total energy put into the middle well of the rotational potential surface of the 1,4-methyl groups of the n-butane.

The phase portrait under conditions (5.16) is given in Figure 5.10

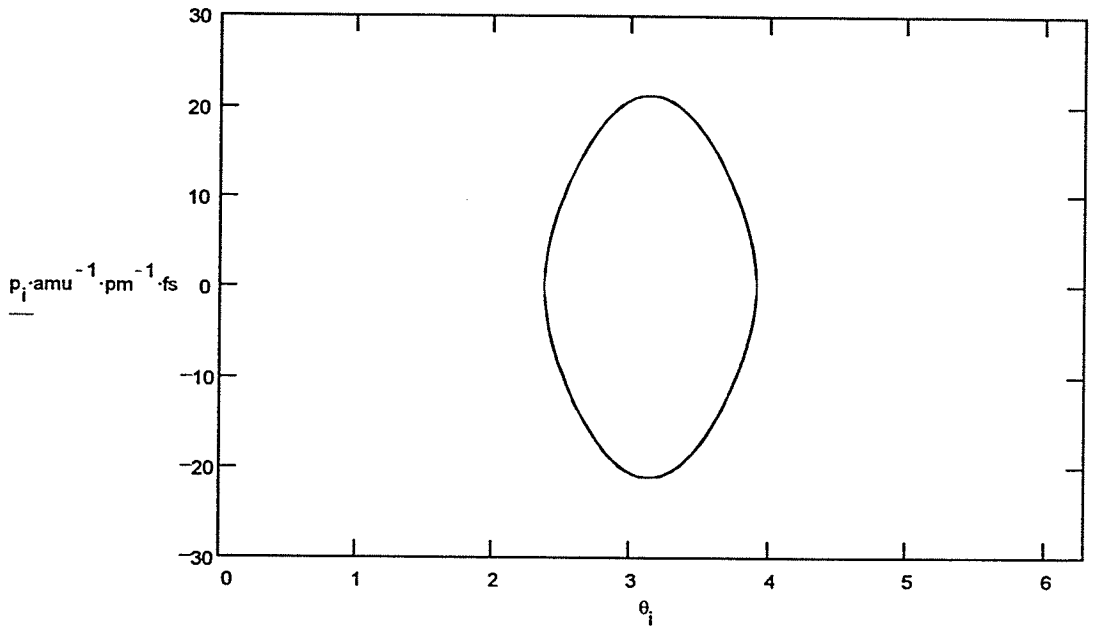

Figure 5.10 The phase portrait of the relative methyl rotation in the middle well of the rotational potential surface of the 1,4-methyl groups of the n-butane when $E = 0.025aJ$.

From the phase portrait we can get its period, the time taken to complete one cycle of the phase portrait

$$period\_M = 576.74 \cdot fs \qquad (5.18)$$

Its corresponding frequency, the number of periods executed per second, is the reciprocal of the period

$$\nu\_M_{period} = \frac{1}{period\_M} \qquad (5.19)$$

$$\sigma_{period\_M} = \frac{1}{\lambda_{period\_M}} = \frac{\nu_{period\_M}}{c} \qquad (5.20)$$

The change of σ_{period_M} with respect to the energy put into the system is shown in Fig.5.11

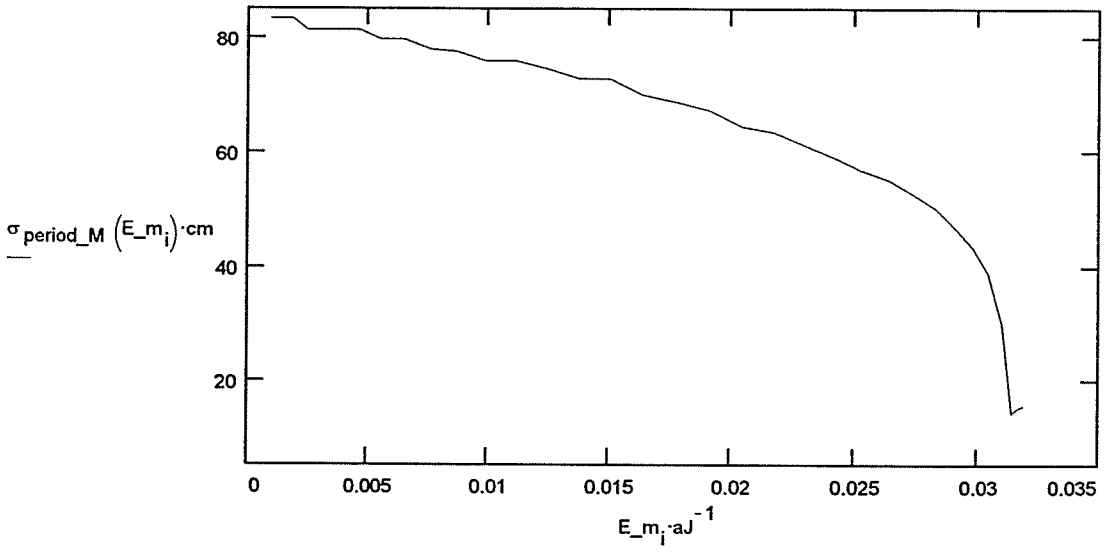

Figure 5.11 The relationship between the phase portrait vibrational frequencies and total energy put into the middle well of the rotational potential surface of the 1,4-methyl groups of the n-butane.

If we put the same energy into the system and set up initial conditions as

$$\theta_{init} = 5.00 \qquad v_{init} = 7.20 \cdot 10^{12} \cdot \sec^{-1}$$

$$E = \frac{1}{2}\mu \cdot r_e^2 \cdot v_{init}^2 + V(\theta_{init}) = 0.025 \cdot aJ \qquad (5.21)$$

the particle oscillates in the left well as shown in Fig. 5.12.

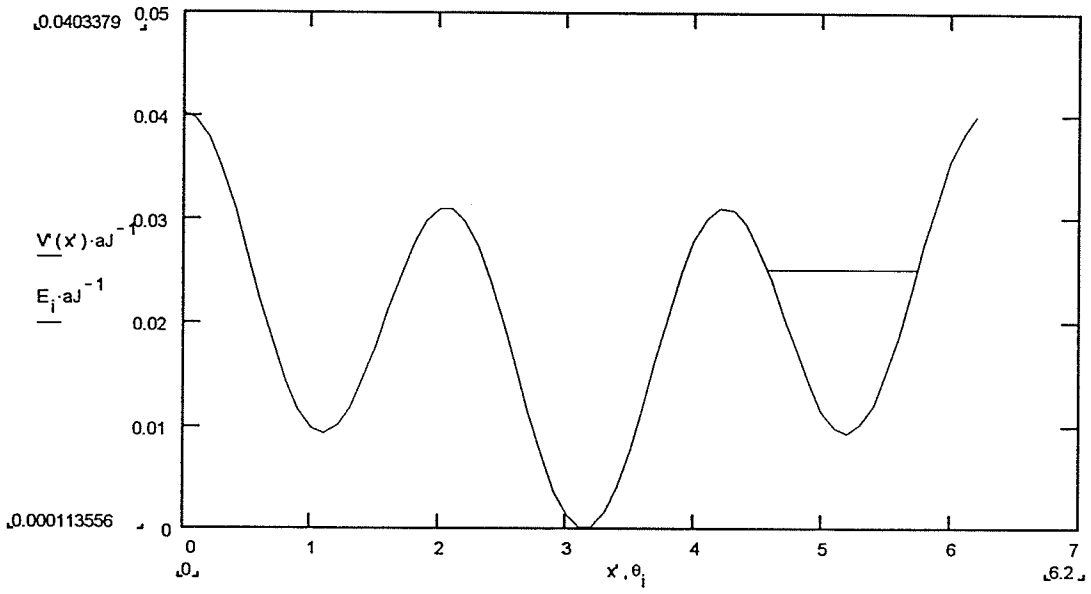

Figure 5.12 The position of total energy $E = 0.025aJ$ on the rotational potential surface of the 1,4-methyl groups of the n-butane when the initial starting point is in the left well.

Under this initial conditions, we get its angle and momentum changes with time as in Fig. 5.13:

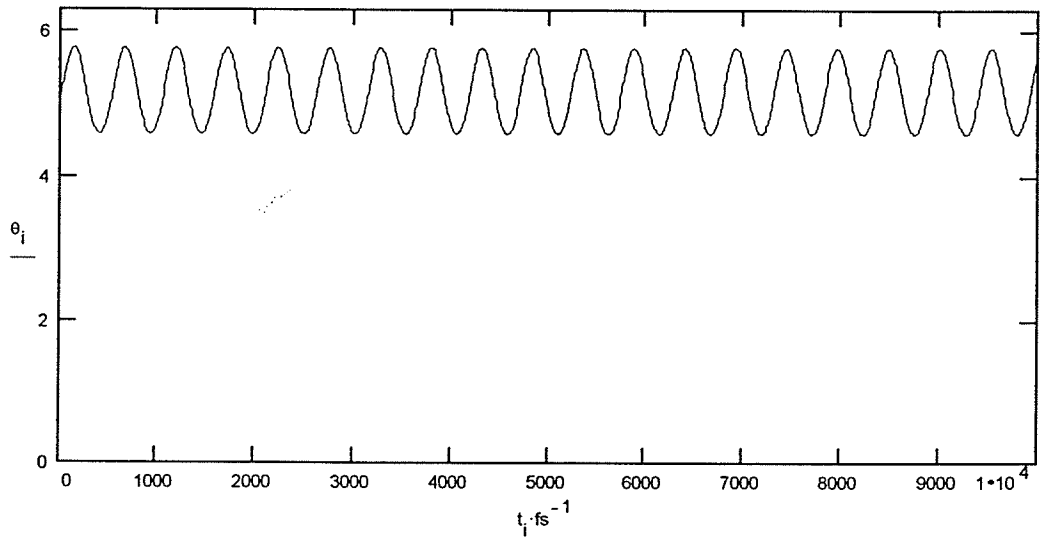

Figure 5.13 The periodic change of the angle with time in the right well of the rotational potential surface of the 1,4-methyl groups of the n-butane when $E = 0.025aJ$.

From the angle change with time we can get its bond vibration frequency by fast Fourier transform;

$$\sigma\_R_{fft} = \frac{1}{\lambda\_R_{fft}} = FFT[r(t)] \qquad (5.22)$$

σ_R_{fft} is a function of the energy put into the system since $r(t)$ is dependent on system's total energy; however it is the same as σ_L_{fft}..

The phase portrait under conditions (5.21) is given in Figure 5.14

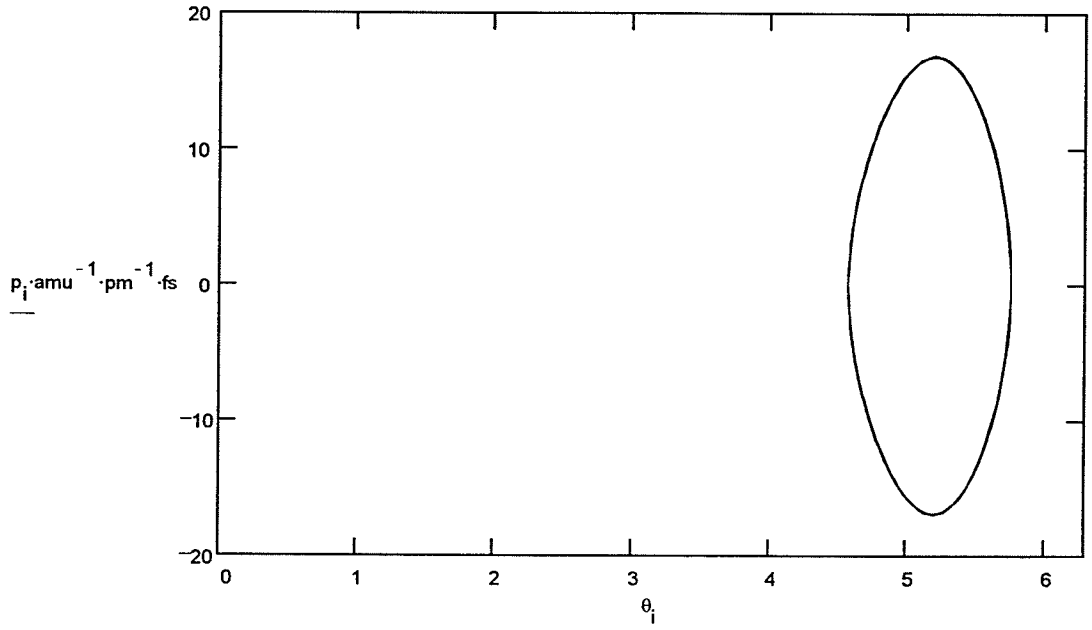

Figure 5.14 The phase portrait of the relative methyl rotation in the right well of the rotational potential surface of the 1,4-methyl groups of the n-butane when $E = 0.025aJ$.

From the phase portrait we can get its period, the time taken to complete one cycle of the phase portrait

$$period\_R = 518.08 \cdot fs \qquad (5.23)$$

Its corresponding frequency, the number of periods executed per second, is the reciprocal of the period

$$\nu\_R_{period} = \frac{1}{period\_R} \tag{5.24}$$

$$\sigma_{period\_R} = \frac{1}{\lambda_{period\_R}} = \frac{\nu_{period\_R}}{c} \tag{5.25}$$

The σ_{period_R} is the same as σ_{period_L}

If more energy is put into the system, for example, the initial conditions are changed to

$$\theta_{init} = 3.50 \qquad \nu_{init} = 1.00 \cdot 10^{13} \cdot \sec^{-1}$$

$$E = \frac{1}{2}\mu \cdot r_e^2 \cdot \nu_{init}^2 + V(\theta_{init}) = 0.0339 \cdot aJ \tag{5.26}$$

Although the particle oscillates, its motion now does not depend on initial positional conditions; we find that it only depends on the energy put into the system.

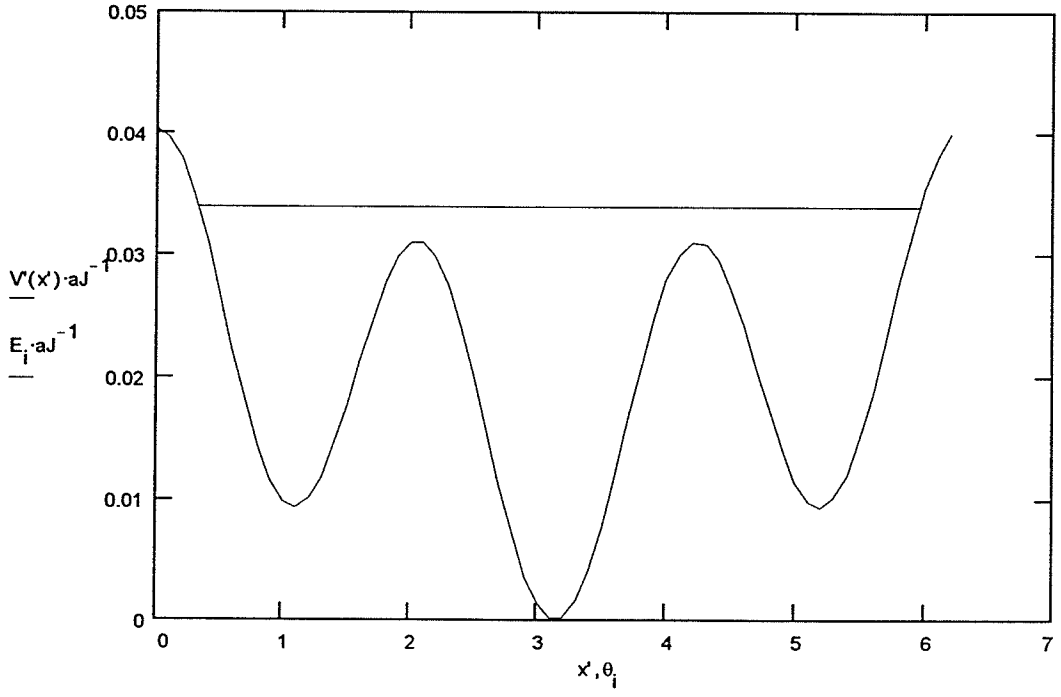

Figure 5.15 The position of total energy $E = 0.0339aJ$ on the rotational potential surface of the 1,4-methyl groups of the n-butane.

The angle changes with time as shown in Fig. 5.16

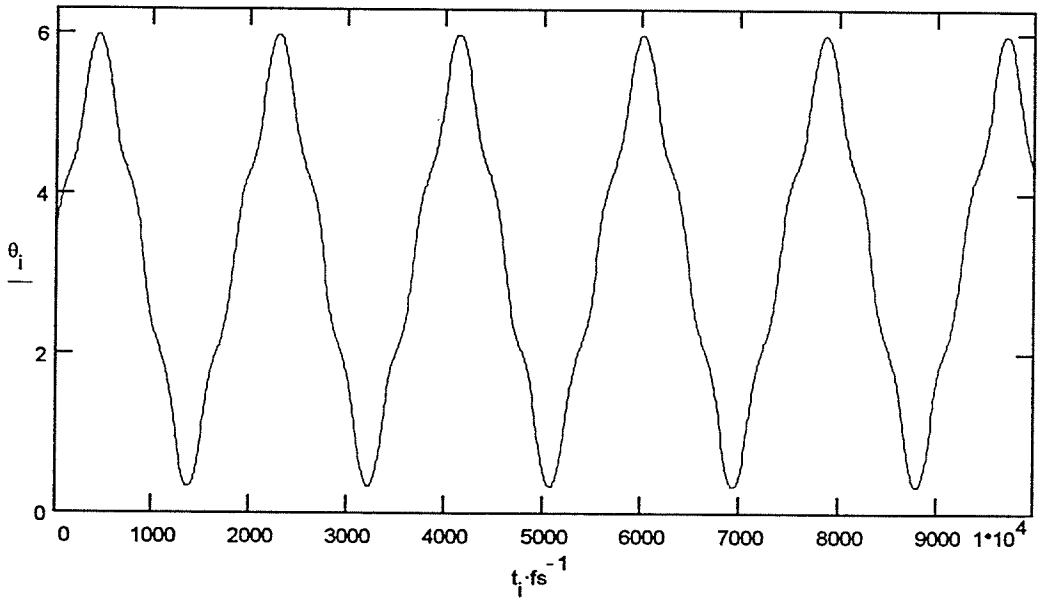

Figure 5.16 The periodic change of the angle with time on the higher part of the rotational potential surface of the 1,4-methyl groups of the n-butane when $E = 0.0339aJ$.

From the angle change with time we can get its bond vibration frequency by fast Fourier transform;

$$\sigma\_upper_{fft} = \frac{1}{\lambda\_upper_{fft}} = FFT\left[r(t)\Big|_{E=0.0339aJ}\right] \qquad (5.27)$$

σ_upper_{fft} is a function of the energy put into the system since $r(t)$ depends on system's total energy. However σ_upper_{fft} is different from σ_L_{fft} and σ_M_{fft}. σ_L_{fft} and σ_M_{fft} are single value functions of the energy put into the system, i.e., we only can get one frequency of each σ_L_{fft} and σ_M_{fft} for every corresponding energy. We can get two frequencies of σ_upper_{fft} for its corresponding energy and define them as σ_upperH_{fft} and σ_upperL_{fft} respectively; their changes with the energy are shown in Fig.5.17

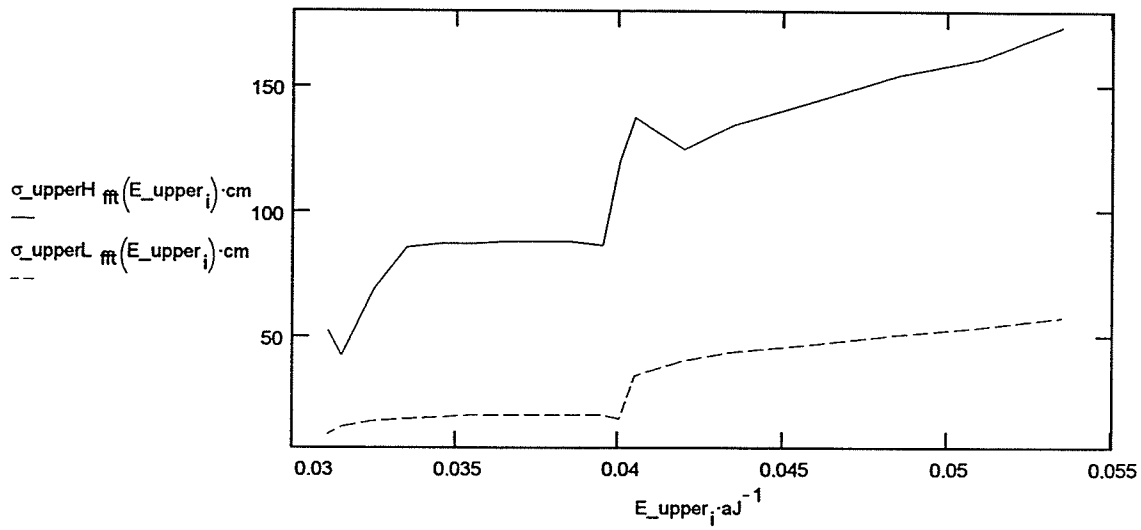

Figure 5.17 The relationship between the fast Fourier transform vibrational frequencies and total energy put on the higher part of the rotational potential surface of the 1,4-methyl groups of the n-butane.

The phase portrait under conditions (5.26) is shown in Fig.5.18

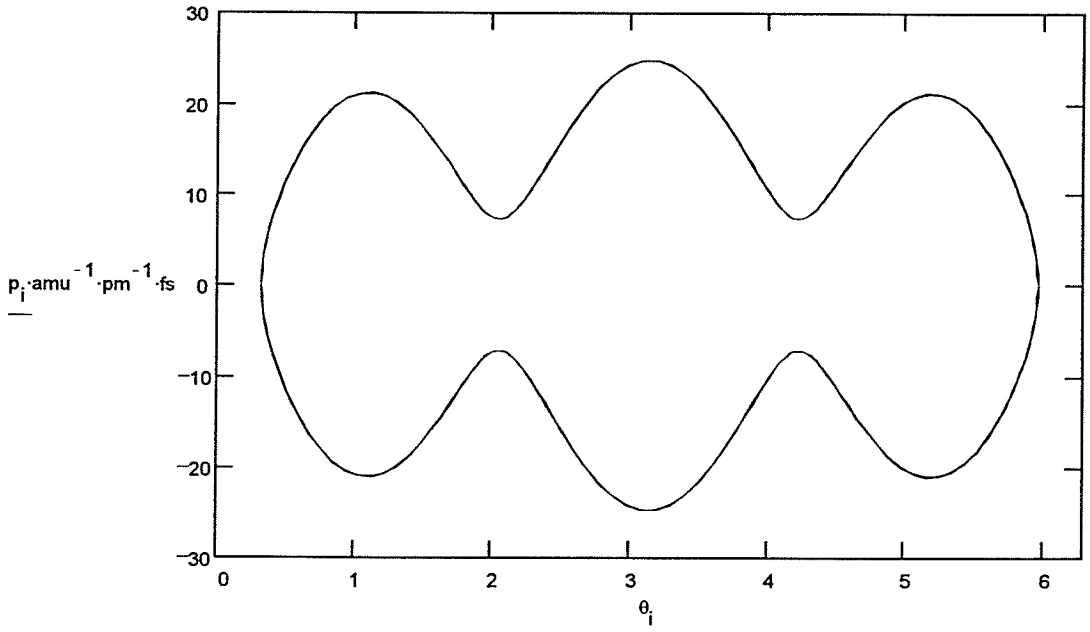

Figure 5.18 The phase portrait of the relative methyl rotation on the higher part of the rotational potential surface of the 1,4-methyl groups of the n-butane when $E = 0.0339aJ$.

From the phase portrait we can get its period, the time taken to complete one cycle of the phase portrait

$$period\_upper = 1857.3 \cdot fs \qquad (5.28)$$

Its corresponding frequency, the number of periods executed per second, is the reciprocal of the period

$$v\_upper_{period} = \frac{1}{period\_upper} \qquad (5.29)$$

$$\sigma_{period\_upper} = \frac{1}{\lambda_{period\_upper}} = \frac{v_{period\_upper}}{c} \qquad (5.30)$$

The change of σ_{period_upper} with respect to time is shown in Fig. 5.19

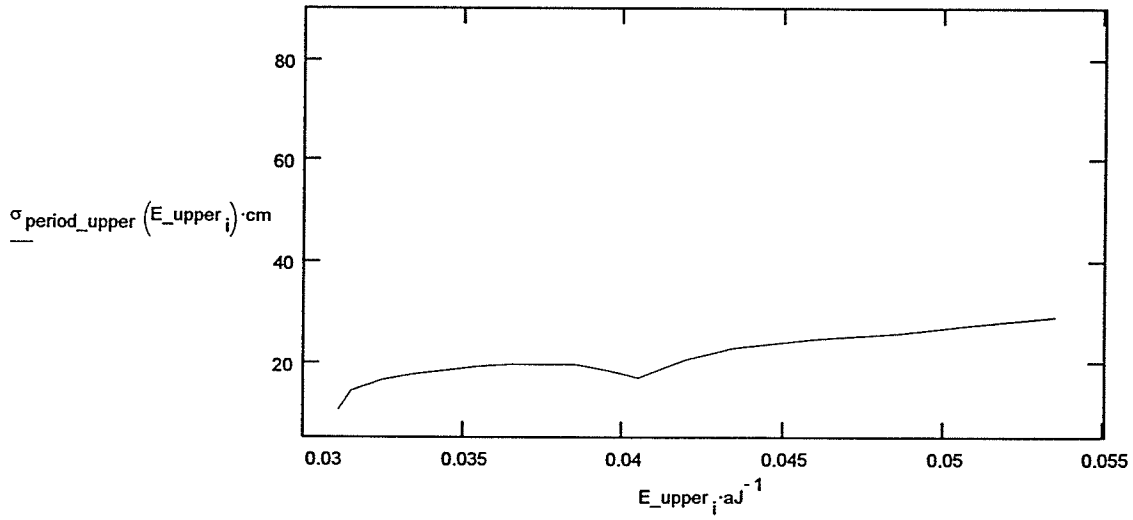

Figure 5.19 The relationship between the phase portrait vibrational frequencies and total energy put on the higher part of the rotational potential surface of the 1,4-methyl groups of the n-butane.

For the rotational potential, the Hamiltonian is written as

$$-\frac{\hbar^2}{2\mu}\frac{d^2}{dx^2}\psi(x) + V(x)\psi(x) = Eig \cdot \psi(x) \qquad (5.31)$$

The variable x is the position parameter describing the change of the position; for convenience, x is replaced by an angular variable θ defined by

$$x = r_e \cdot \theta \tag{5.32}$$

and Eq.(5.31) changes as follows

$$-\frac{\hbar^2}{2\mu}\frac{1}{r_e^2}\frac{d^2}{d\theta^2}\psi(\theta)+V(\theta)\psi(\theta)=E\cdot\psi(\theta) \tag{5.33}$$

in which $V(\theta)$ is Eq.(5.1).

Standardize Eq.(5.33) according to the renormalized Numerov method[9]

$$\left[A\cdot\frac{d^2}{d\theta^2}+B\cdot\frac{d}{d\theta}+V'(\theta)\right]\psi = eig\cdot\psi \tag{5.34}$$

in which

$$A = 1$$

$$B = 0$$

$$V'(\theta) = -\left(\frac{\hbar^2}{2\mu}\frac{1}{r_e^2}\right)^{-1}\cdot\left[h_1\cdot\cos(3\cdot\theta)+h_2\cdot\cos(\theta)\right]$$

$$= 1312.0\cdot\cos(3\cdot\theta)+590.0\cdot\cos(\theta)$$

$$eig = -\left(\frac{\hbar^2}{2\mu}\frac{1}{r_e^2}\right)^{-1}\cdot\left(E-h_1-h_2\right) \tag{5.35}$$

Solving Eq.(5.34) with a Numerov program, we obtain eigenvalues *eig* and their corresponding eigenfunctions. From *eig* we can get E; hence the absorption or emission frequency can be calculated from E.

$$\sigma\_numrov = \frac{E_{n+1}-E_n}{h\cdot c} \qquad n = 0,1,2,..... \tag{5.36}$$

The energy corresponding to every frequency can be set up as

$$E_n = E_n + \frac{E_{n+1}-E_n}{2} \qquad n = 0,1,2,..... \tag{5.37}$$

The change of frequency with respect to energy put into the system is shown in Fig.5.20.

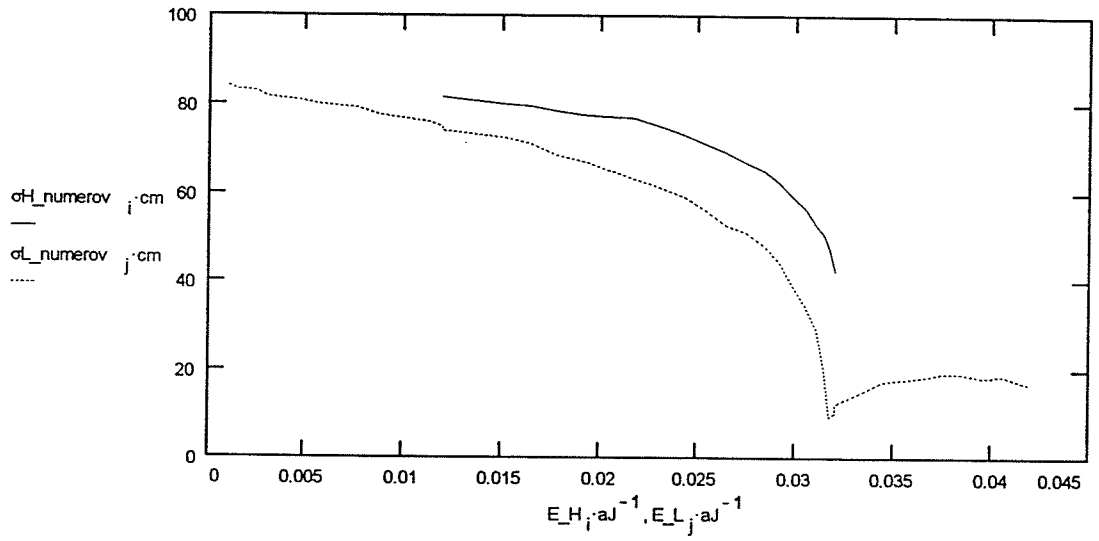

Figure 5.20 The relationship between the quantum numerical calculated frequencies and total energy put on the system of the rotational potential surface of the 1,4-methyl groups of the n-butane.

Putting all these results together, the frequencies change with time as follows:

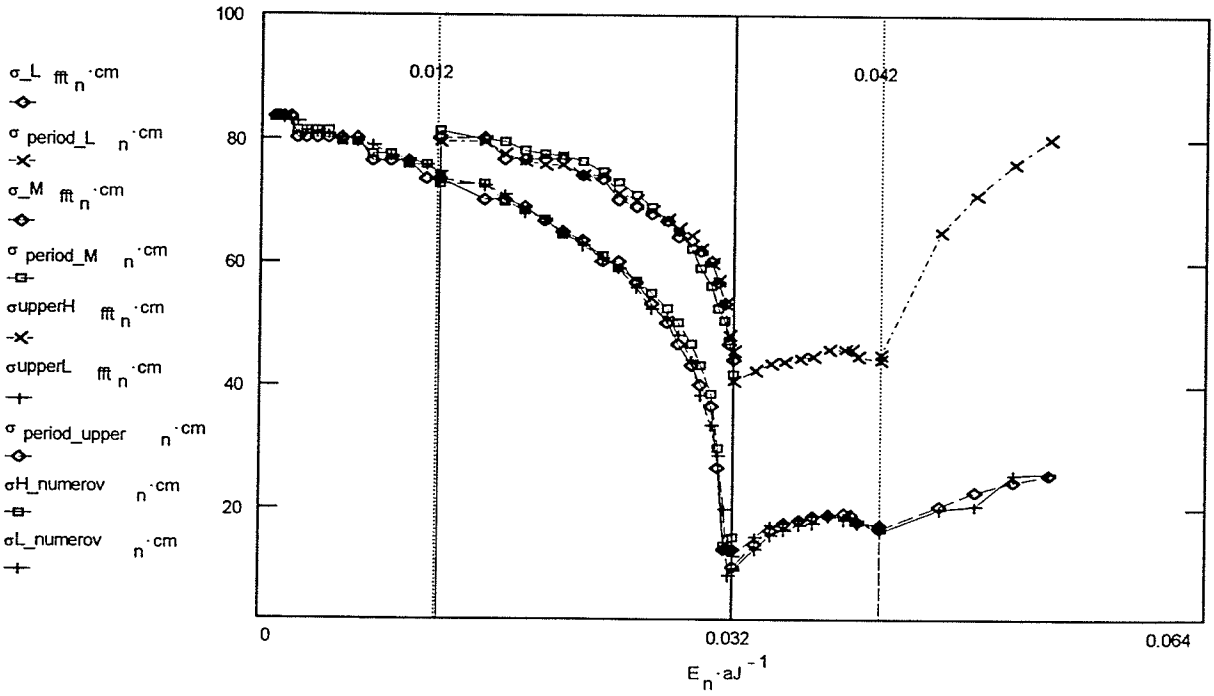

Figure 5.21. The comparison of the frequencies calculated by different methods.

6. Conclusion

It is recognized that vibrational spectroscopy has played a very important role in the development of potential functions and the studies of molecular mechanics. As seen, the classical and quantum mechanical methods have been used for calculating the vibrational frequencies of various potential molecular systems. The comparisons between molecular dynamics simulations and quantum mechanical calculation results have proved that the molecular dynamics simulations give results as precise as quantum mechanical calculations do. It is noticed that once a molecular dynamics simulation has generated a phase space portrait, the portrait serves as the raw materials for obtaining the time average of properties and dynamical pictures of molecular motion. It is reasonable to deduce that the molecular dynamics simulation, and the approach to the evolution of vibrational spectra as shown above, detailed dynamical information of macromolecular systems can be obtained.

7. References

[1] Trygve Helgaker, J. Phys. Chem., Vol. 95, 4618(1991).

[2] Cooley, J.W., and J. W. Tukey, 'An algorithm for the machine calculation of complex Fourier series,' Mathematics of Computation(1965), Vol. 19, No.90, pp.297-301.

[3] Hao Bai-Lin, Ed., Chaos, World Scientific, Singapore, 1984, Chapter 2.

[4] J. L. Lebowitz and O. Penrose, "Modern Ergodic Theory," Phys. Today, 26(2), 23(1973)

[5] J. L. Lebowitz and O. Penrose, "Modern Ergodic Theory," Phys. Today, 26(2), 23(1973).

[6] R. Kuth, Axiomatics of Classical Statistical Mechanics, Pergamon, Oxford, 1960.

[7] R. Wallace, Analytical Quantum Mechanics of the Morse Oscillator, Chem. Phys. Lett., Vol. 37, Number. 1, 115, 1976.

[8] J.P. Leroy and R. Wallace, Renormalized Numerov Method Applied to Eigenvalue Equations. J. Phys. Chem. 1985, 89, 1928

[9] J.P. Leroy and R. Wallace, 'Renormalized Numerov Method Applied to Eigenvalue Equations: Extension to Include Single Derivative Terms and a Variety of Boundary Conditions"; J. Phys. Chem. 1985, 89, 1928-1932.

[10] Harry G. Hecht, Mathematics in Chemistry, pp.190-191, Prentice Hall Inc., New Jersey, 1990.